Sources of Air Pollution Relevant for the Austrian Biosphere Reserve Wienerwald

Petra Seibert
Sabine Radanovics
Bernd C. Krüger

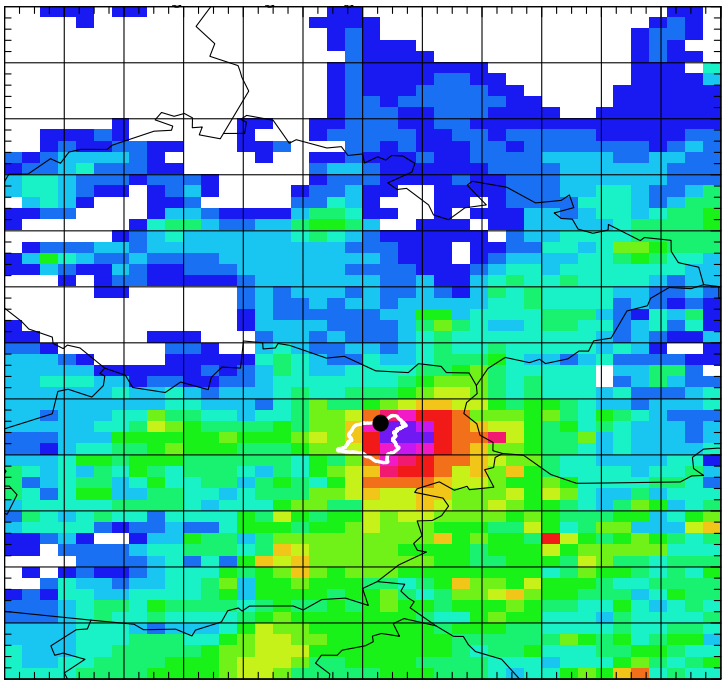

Final Report for the Project "Sources of Air Pollution Relevant for Austrian Biosphere Reserves: Quantification, Trends, Scenarios" Man and Biosphere Programme (MaB), Austrian Academy of Sciences (ÖAW)

Institut für Meteorologie (BOKU-Met)
Department Wasser – Atmosphäre – Umwelt
Universität für Bodenkultur Wien

June 2010

ISSN 1994-4179
ISSN 1994-4187 (on-line)

BOKU-Met Report 20

Petra Seibert, Sabine Radanovics, Bernd C. Krüger

Sources of Air Pollution Relevant for the Austrian Biosphere Reserve Wienerwald

Final Report
for the Project "Sources of Air Pollution Relevant for Austrian Biosphere Reserves: Quantification, Trends, Scenarios"

Man and Biosphere Programme (MaB),
Austrian Academy of Sciences (ÖAW)

BOKU-Met Report 20

Diese Publikation sollte folgendermaßen zitiert werden:

Petra Seibert, Sabine Radanovics, Bernd C. Krüger (2010): Sources of Air Pollution Relevant for the Austrian Biosphere Reserve Wienerwald. Final Report for the Project "Sources of Air Pollution Relevant for Austrian Biosphere Reserves: Quantification, Trends, Scenarios", Man and Biosphere Programme (MaB), Austrian Academy of Sciences (ÖAW).
BOKU-Met Report **20**, 80 pp. ISSN 1994-4179, ISSN 1994-4187 (on-line). Available at
`http://www.boku.ac.at/met/report/BOKU-Met_Report_20_online.pdf`.

Title image: see Figure 38 on page 45.

Medieninhaber und Herausgeber:

Universität für Bodenkultur Wien
Department für Wasser-Atmosphäre-Umwelt
Institut für Meteorologie
Peter-Jordan-Str. 82
1190 Wien, Österreich

URL http://met.boku.ac.at/

Contents

List of Tables

List of Figures

1 Introduction

1.1 Motivation

Although the general situation with respect to air pollution has much improved in the past 20 years, in certain regions high concentrations which are a burden for the ecosystems and negative for human health still occur. There are episodes with advection of sulphur dioxide from other countries, and the NO/NO_2 emissions are still high in Austria and other countries due to the traffic increase. This leads also to increased ozone levels under suitable meteorological conditions. Therefore it is desirable to better quantify the origin of such pollution, especially for designated biosphere reserves.

While Eulerian chemistry-transport models are the state-of-the art tool for air pollution modelling, they have certain limitations, the most important one being the computer time requirements for seasonal or longer simulations, especially if a high resolution is desired. In this type of model the resolution of the driving meteorological fields needs to match the resolution of the chemistry-transport model. Thus for high resolution, regional meteorological modelling is also required which increases the computational costs. Also, these models have conceptual difficulties to attribute the simulated pollution to specific sources, even though some models include an approximate source attribution method (Krüger, 2004).

Lagrangian models do not have these limitations, they are computationally much cheaper, and in a receptor-oriented mode they allow the determination of the sources. Back trajectory analysis has been a classical tool for many years, more recently superseded by Lagrangian particle models (Stohl, 1998; Stohl et al., 2002). Therefore, in this study, mainly modelling with the Lagrangian particle model FLEXPART was be applied in a region of interest comprising one of Austria's biosphere parks registered with UNESCO. In addition, comparisons with the trajectory model FLEXTRA were carried out. As ozone is too reactive for modelling with a Lagrangian transport model without chemistry, NO_x and SO_2 were the main pollution compounds investigated.

1.2 Selection of target area and interaction with stakeholders

A number of biosphere reserves exists in Austria[1], and transport of air pollution to these regions is of interest for all of them. However, those in Western Austria are all in high-mountain terrain. Transport modelling based on meteorological fields available from a global meteorological model is not very appropriate for them. In eastern Austria, the region of Neusiedler See has been investigated already by Eckhardt (2001).

As recommended by ÖAW, the present project focussed on the new biosphere reserve Wienerwald (Vienna Woods)[2]. This is a forested area forming the end of the Alpine bow. Its highest elevation is Schöpfl (893 m asl), the last peak near Vienna, Kahlenberg, is 484 m asl, whereas the plains to the east are at about 200 m asl. The city of Vienna is just to the east of the northern part of Wienerwald.

ÖAW encouraged cooperation with another project focussing on this area, *Monitoring of environmental pollutants (NO_x and SO_2 deposition of heavy metals and PAH's) by bryophytes in the 'Biosphere Reserve Wienerwald'* (Zechmeister et al., 2007).

[1] `http://www.biosphaerenparks.at/`

[2] See also `http://www.biosphaerenpark-wienerwald.org/`

Based on communication with H. Zechmeister, it was decided that our model calculations will be carried out mainly for four receptor points in the NW, NE, SW and SE of the target area. A finer resolution is not warranted by the underlying meteorological fields. Furthermore, it was agreed that as far as possible sampling points for the bryophytes should be selected near the air quality monitoring stations, so that results obtained for these stations can be taken as representative also for at least a part of the bryophyte sampling sites. The long integration time of the bioindication samples implies also that the work in our project had to rely strongly on the continuous air quality monitoring sites, as otherwise validation of the models used would not be possible. A further aspect is that the moss is mainly taking up the pollutants through wet deposition. Therefore, taking into account the wet deposition data from Wien-Auhof would be interesting, but it turned out to be beyond the possibilities of this project.

According to the communication with H. Zechmeister, there are no immediate other studies that would be interested in direct cooperation with our project.

1.3 Structure of the report

At first, the data (observations and input to models) are presented. Then the models and evaluation methods are introduced. Finally, results are shown and discussed, followed by conclusions and outlook. As the work deals with a massive amount of data, it includes many figures, some of which have been put into an Appendix to make the report more easily readable.

2 Air pollution data

2.1 Air quality monitoring data

2.1.1 Selection of monitoring sites

After a survey of available stations, a set of stations has been selected which was investigated more in detail (see Figure 1). These stations represent the regions which we expect to be discernable with respect to the different influence regions, namely the northern and southern part of the eastern and western slope of the Wienerwald, respectively. In addition to this, the station Streithofen in the northwest was included because the AUPHEP projects on aerosols and health has already collected and analysed data from this site (Gomiscek et al., 2004). Another addition is the station Lainzer Tiergarten – Auhof which is relevant because it is the only station with wet deposition (WADOS) data (Leder et al., 2003). Thus, the list of stations is (numbers refer to Figure 1):

33 Streithofen (NW, AUPHEP site)
35 Tulbinger Kogel (NW)
25 Forsthof – Schöpfl (SW)
22 Bad Vöslau – Gainfarn (SE)
5 Wien Hermannskogel – Jägerwiese (NE)

A part of the calculations have been carried out also for

20 Auhof – Lainzer Tiergarten (NE, wet deposition site)
30 Purkersdorf (NE)

but are not presented furtheron.

2.1.2 Overview of measurements at selected sites

Figures 2, 3 and 4 give an overview of observed mixing ratios / concentrations of SO_2, PM, and NO_2 and NO in 2003. SO_2 mixing ratios are generally low as Austrian emissions are low nowadays, but there are still some peaks, predominantly in the cold season. Highest values are found at Hermannskogel. PM10 diurnal means are lower in summer than in winter, but short-term peaks do occur in summer and they are even higher than in winter. NO_2 and NO data show a typical annual course with winter maxima, and are higher on the eastern side of Wienerwald than on its western side, possibly indicating the stronger air pollution in the basin of Vienna.

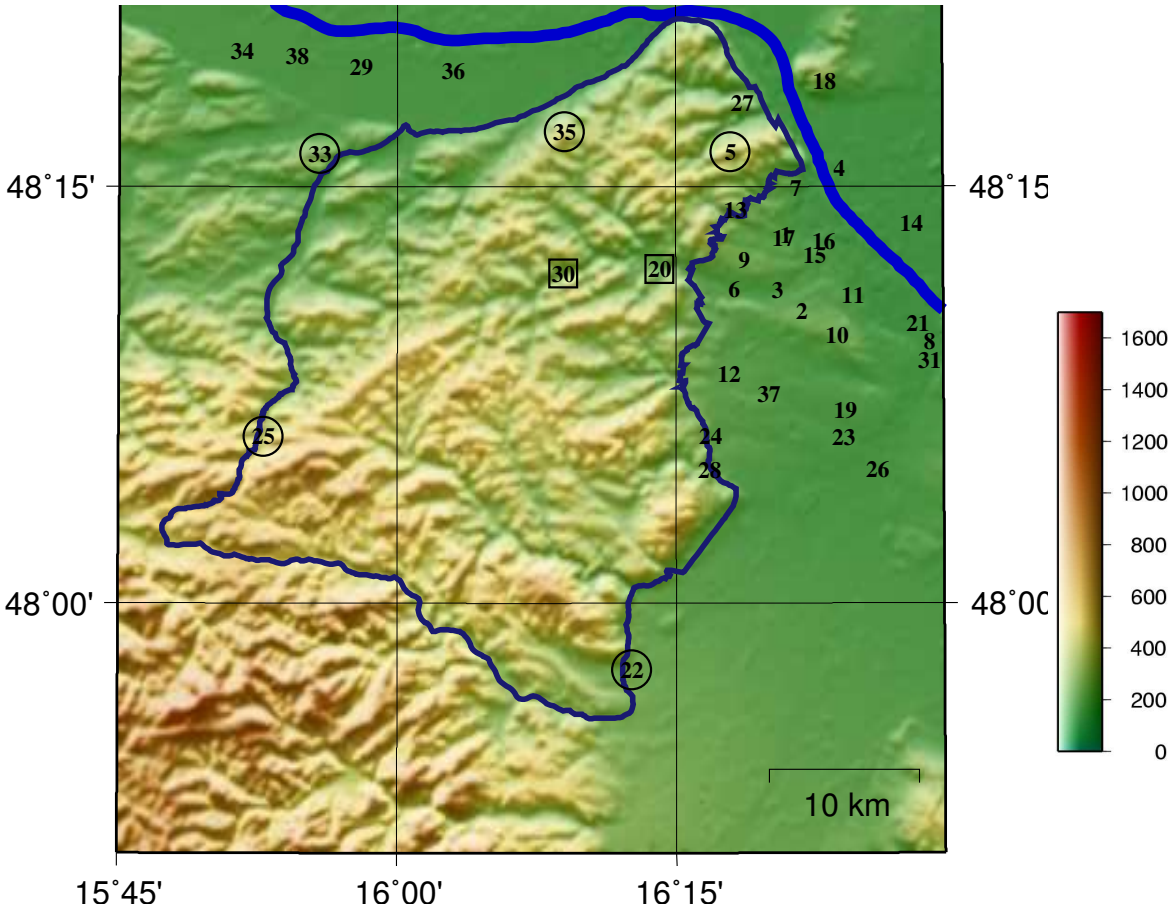

1	Wien/AKH Dach	20	Lainzer Tiergarten—Auhof
2	Wien/Belgradplatz	21	Ostautobahn-A4—Kanzelgarten
3	Wien/Gaudenzdorf	22	Bad-Voeslau—Gainfarn
4	Wien/Gerichtsgasse	23	Biedermannsdorf
5	Hermannskogel/Jaegerwiese	24	Brunn am Gebirge
6	Wien/Hietzinger Kai	25	Forsthof/Schoepfl
7	Wien/Hohe Warte/ZAMG	26	Himberg
8	Wien/Kaiserebersdorf	27	Klosterneuburg
9	Wien/Kendlerstrasse	28	Moedling
10	Wien/Laaerberg	29	Neusiedl im Tullnerfeld
11	Wien/Rinnboeckstrasse	30	Purkersdorf
12	Wien/Liesing An-dem-Steinfeld	31	Schwechat
13	Wien/Schafbergbad	32	Stockerau
14	Wien/Stadlau	33	Streithofen
15	Stephansplatz/Kerzenkammer	34	Trasdorf
16	Wien/Taborstrasse	35	Tulbinger Kogel
17	Wien/Waehringerguertel	36	Tulln
18	Bisamberg	37	Voesendorf
19	Laaer Wald	38	Zwentendorf

Figure 1: Topography of the Wienerwald and surroundings and sites of monitoring stations. Sites selected as receptors for dispersion modelling are marked with a circle, sites that were partially used with a square. The dark blue line indicates the border of the Biosphere Park Wienerwald (unofficial).

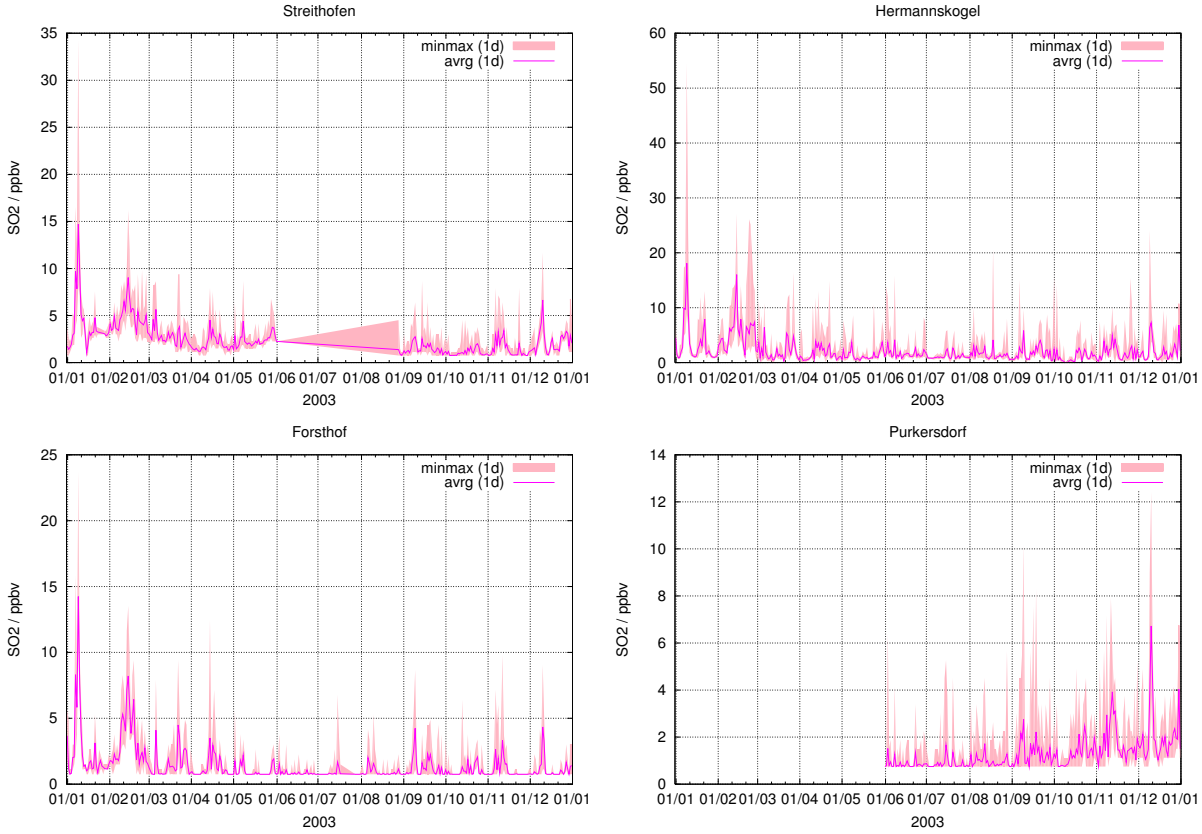

Figure 2: SO_2 measurements in 2003, at Streithofen, Hermannskogel, Forsthof, and Purkersdorf; diurnal means (line) and diurnal range of half-hourly means (colour) in ppbv. Attention, variable scaling of the graphs!

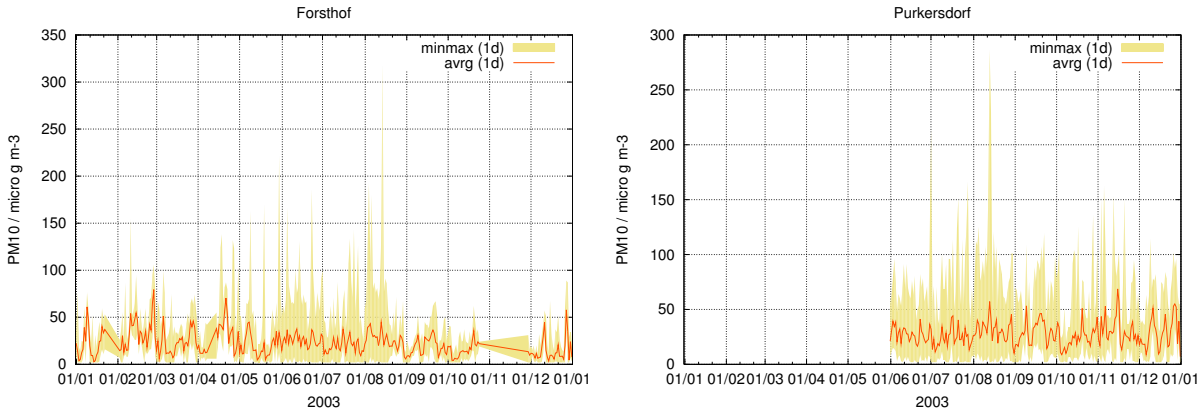

Figure 3: PM10 measurements in 2003, at Forsthof and Purkersdorf; diurnal means (line) and diurnal range of half-hourly means (colour) in $\mu g\, m^{-3}$. Attention, variable scaling of the graphs!

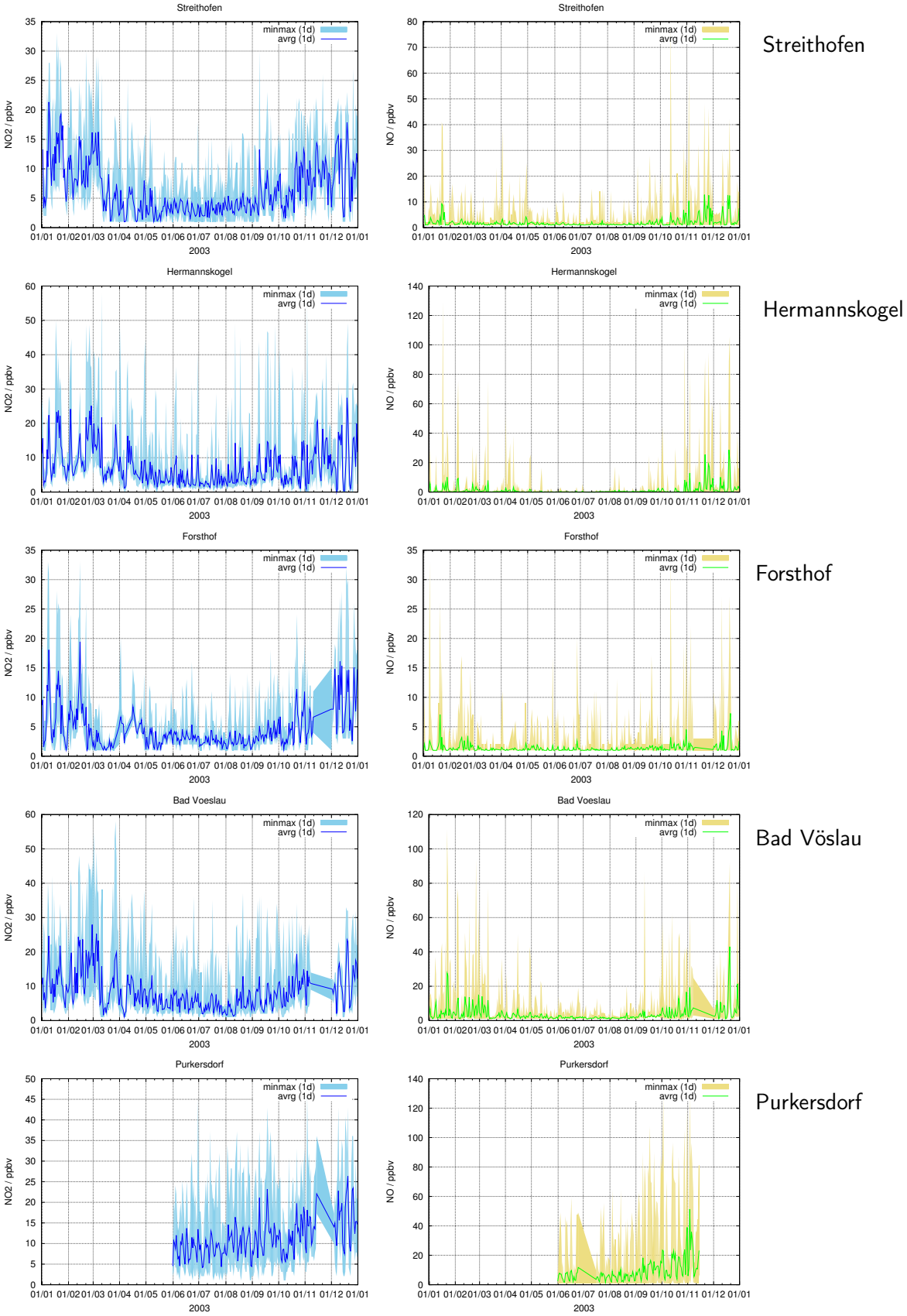

Figure 4: NO_2 (left column) and NO (right column) measurements in 2003, diurnal means [line] and diurnal range of half-hourly means (colour) in ppbv. Attention, variable scaling of the graphs!

2.2 Emission data

The anthropogenic emissions used in this study are based on the UNECE/EMEP data base [1] for European emissions (Vestreng et al., 2005) for the year 2003. The "expert emissions" are derived from the national totals reported by the individual countries and have been completed and corrected for the use in dispersion modelling. These data comprise the annual sums of the emissions of NO_x, CO, non-methane hydrocarbons, SO_2, NH_3, fine particles (<2.5 μm) and coarse particles (2.5 μm to 10 μm) on a 50 km $\times$ 50 km grid. Eleven sectors of anthropogenic activity are distinguished.

For the Pannonian countries Austria, Czech Republic, Hungary, and Slovakia the EMEP data for the year 2003 have been scaled down to a spatial resolution of 5 km $\times$ 5 km. An emission inventory for these countries from the year 1995 (Winiwarter and Züger, 1996) is used as database for the spatial distribution of the emissions within the 50 km $\times$ 50 km EMEP grid cells.

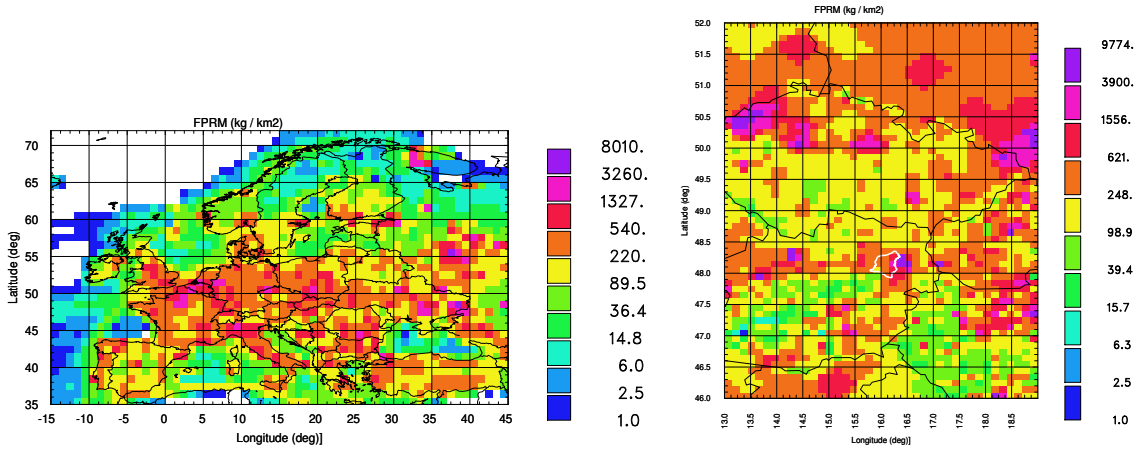

Figure 5: Emission data, annual totals of fine PM in kg km^{-2}, coarse (left) and fine (right) grid. Attention, in this and the following figures, the colour scale is always adapted to the maximum value found, and thus differs between the fine and the coarse grid! The boundary of the Biosphere Park Wienerwald is marked by a white line in the fine grid plots.

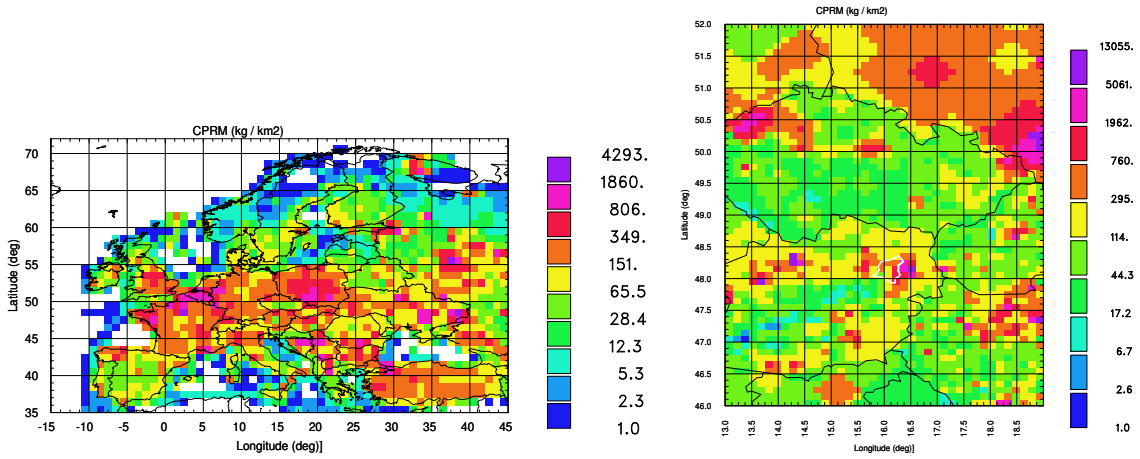

Figure 6: Emission data, annual totals of coarse PM in kg km^{-2}, coarse (left) and fine (right) grid.

The emission model distributed the emissions from the spatial distribution of the inventories to the output grid of FLEXPART. Figures 5 to 11 show the spatial distribution of the annual total of

[1] Available on-line at `http://webdab.emep.int/`

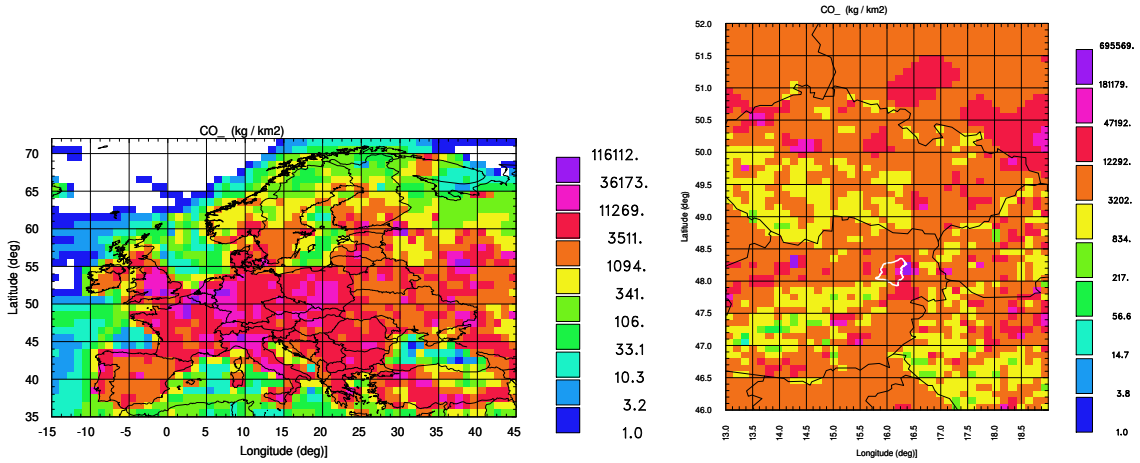

Figure 7: Emission data, annual totals of CO in kg km^{-2}, coarse (left) and fine (right) grid.

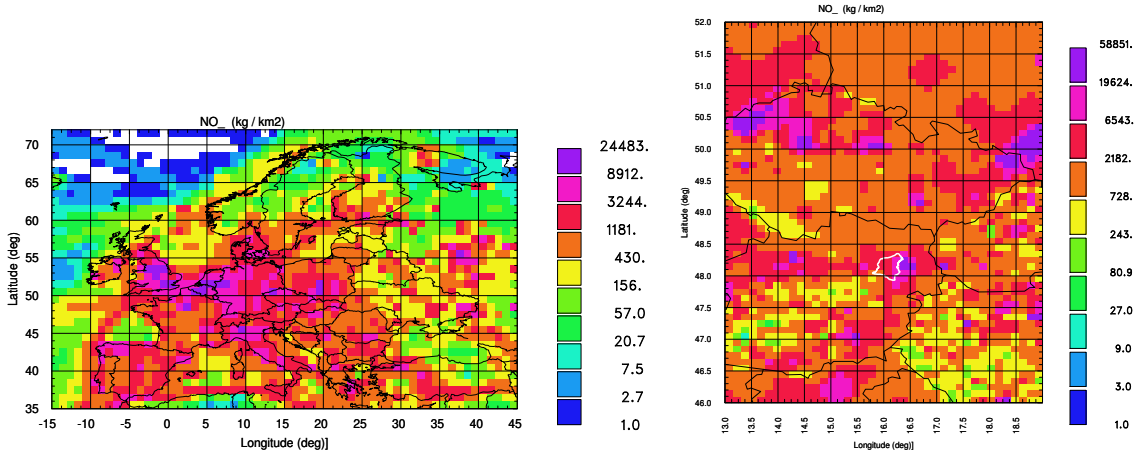

Figure 8: Emission data, annual totals of NO (as NO_2) in kg km^{-2}, coarse (left) and fine (right) grid.

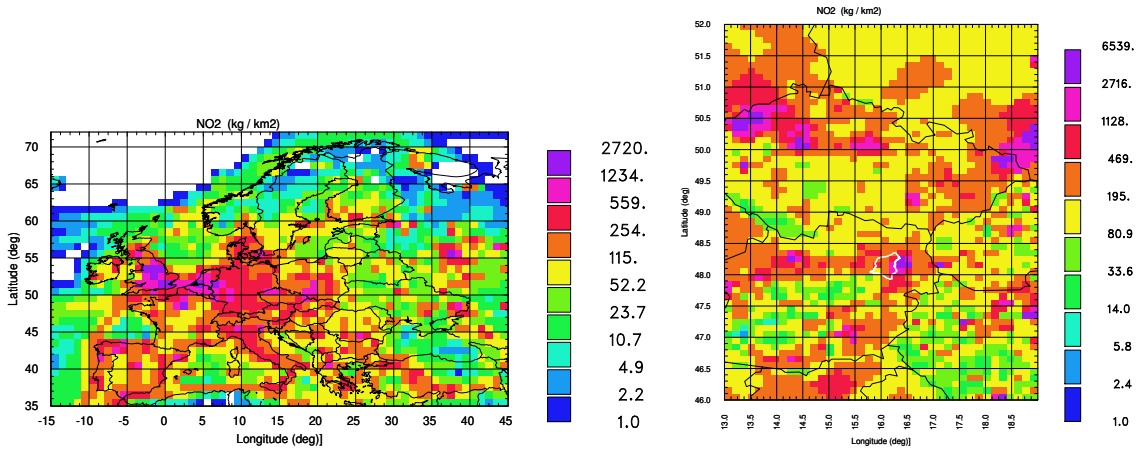

Figure 9: Emission data, annual totals of NO_2 in kg km^{-2}, coarse (left) and fine (right) grid.

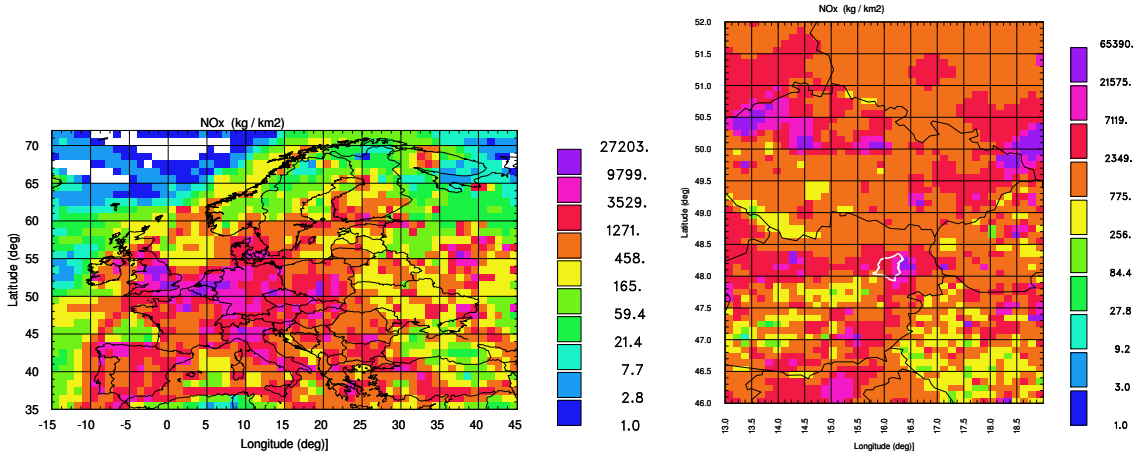

Figure 10: Emission data, annual totals of NO_x in kg km^{-2}, coarse (left) and fine (right) grid.

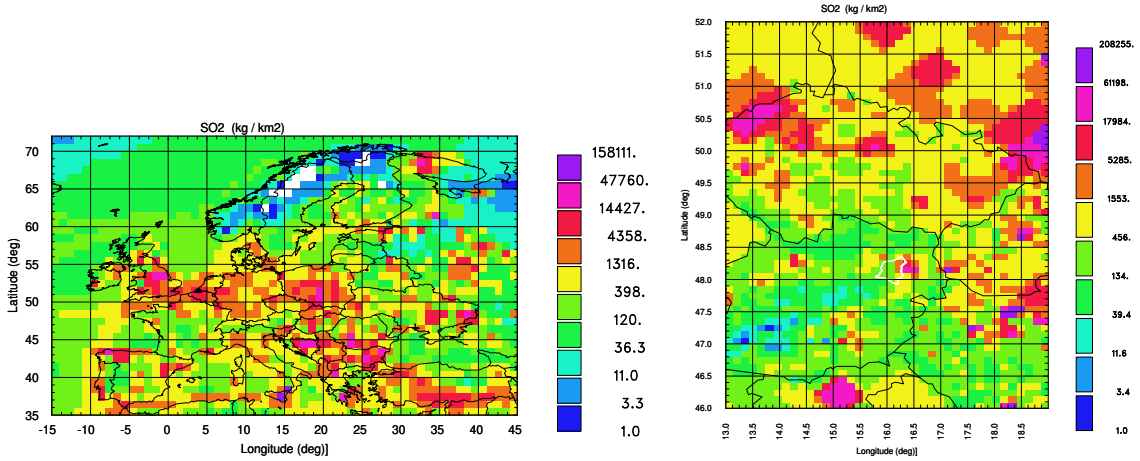

Figure 11: Emission data, annual totals of SO_2 in kg km^{-2}, coarse (left) and fine (right) grid.

emissions on the two grids. One can see that in countries such as Poland and Slovenia only the coarse EMEP resolution is available, even for the fine, nested grid, which may of course have negative effects on the accuracy of results.

For every sector the emission model applies different patterns for the month, the day of the week and the hour of the day for the temporal disaggregation. The disaggregation factors are taken from the inventory by Winiwarter and Züger (1996). They are available for the Pannonian countries. For all other countries the disaggregation data for Austria have been used.

The emissions from the inventories must be split for each emission sector into the required speciation of the chemical compounds. In the case of NO_x it is assumed in all sectors of anthropogenic emissions that 10% are NO_2 and 90% are NO (molar percentages). The emissions of non-methane hydrocarbons and of NH_3 were not used in this study.

Let us take a closer look on the SO_2 and NO_x emission data which form the base of the modelled concentrations that have been studied.

The emissions of NO_x (Fig. 10) are less localised than those of SO_2. Apart from the high Alps, the emission level in Austria is similar to that in the surrounding countries. Vienna, Graz and Linz are again main emission regions, but due to the traffic emissions along the highways, also outside the

city regions values are high. As the "A1 Westautobahn" and "A21 Außenringautobahn" (motorways Vienna – Linz – Salzburg and the shortcut from A1 to the "Südautobahn") crosses the Biosphere Park Wienerwald, we find relatively high emissions even inside this region. However, Emissions in southern Poland and northwestern Czech Republic exceed those from the Austrian agglomerations.

SO_2 emissions (Fig. 11) are generally low in Austria. The main emission region is Vienna, just next to Wienerwald. Then there are some emissions in Linz and the Graz region. Emission maxima are found in the northwest of the Czech Republic, in southern Poland, northern Hungary, and in Slovenia. In Slovakia we find higher emissions in the small region of Bratislava, not far from Vienna. Note the coarser resolution of the data for example in Slovenia where the emissions are in reality closely concentrated to the sites of larger coal-fired power plants. The coarse-grid map including the whole of Europe shows various other SO_2-emitting regions, including the Balkans, England and Germany.

3 Atmospheric transport modelling

We have applied receptor-oriented modelling methods, a simple trajectory model (FLEXTRA) and a Lagrangian particle dispersion model (FLEXPART). Both models cannot describe nonlinear chemical reactions, for example ozone formation. However, it is expected that useful results can be obtained for compounds with an atmospheric lifetimes of several days or more, such as NO_x and SO_2.

3.1 Meteorological input data

With both models, analyses and short-term (3 h) forecast data of the European Centre for Medium Range Weather Forecasts (ECMWF) were used. These data were extracted from ECMWF's MARS archive with 0.5° horizontal resolution, the full vertical resolution, and three hour temporal resolution. One year of these data is equivalent to 28 GBytes of data in GRIB format.

3.2 Receptor points

Six receptor points, serving as start points for the back trajectories and as release points for particles in FLEXPART, have been selected among the sites of the monitoring stations in the air pollution networks of Lower Austria and Vienna. They are listed in Table 1. They represent both the eastern and the western side of the Wienerwald hills, and the southerly as well as the northerly region. An important issue is the difference in height between the smoothed model surface and the real topography. All the stations on hill tops (Tulbinger and Hermanns-"Kogel", Forsthof) are too low in the model, while it is vice versa for stations in valleys. In principle, one could lift the hill-top release sites a bit to better match their real height, though one looses the property of being sited at ground level. For valley stations, such a remedy is not possible. In this study, lifting the hill-top stations has not been applied. At least for stations on the top of higher mountains, in recent years it has been found to be useful (Seibert and Skomorowski, 2008).

3.3 FLEXTRA trajectory model

Back trajectories were calculated with the FLEXTRA model, version 3.3[1] (Stohl et al., 1995) and a new version, FLEXTRA_MH, which calculates mixing heights at the trajectory positions, so that it can be decided whether the trajectory is inside or above the mixing layer. The calculations were done in 3-D mode, with both horizontal and vertical wind velocity from the meteorological input from the ECMWF model. The length of the back trajectories was 6 d, and trajectories were started in intervals of 1 h at 100 m above model ground. Site Bad Vöslau was calculated only with FLEXTRA_MH.

The output data set contains the horizontal trajectory position, the vertical trajectory position in the η-coordinates of the ECMWF model, pressure, height above sea level and height above ground, as well as the potential vorticity, the potential temperature and either the specific humidity or the mixing height, depending on the FLEXTRA version. The output has hourly resolution along each trajectory. These data set is in ASCII files and comprise about 700 MBytes for each version.

[1] FLEXTRA is freely available from `http://transport.nilu.no/flexpart`. In this website, additional background information on FLEXTRA and FLEXPART is available.

Trajectories are a rather simple tool for atmospheric transport studies and simulate the relevant processes in a manner that is extremely simplified compared to calculations with a Lagrangian particle dispersion model like FLEXPART (see next section). However, the additional efforts for the trajectory calculations are small, and their results, comprising only about 4% in size, can be used as quick-looks. Furthermore, many researchers still use trajectory data for the similar purposes as pursued in this project. This gives the possibility to do also some evaluations based on these simple trajectories and compare the results with the FLEXPART-based results.

Quantitative use of trajectories and comparison with a dispersion model (such as FLEXPART) required the conversion of the trajectory output to gridded residence times. The residence time of an air parcel in a grid cell is proportional to the length of the trajectory segment which falls into the grid cell and inverse proportional to its velocity. In addition, a vertical boundary of the grid cell needs to be defined. Using calculated mixing heights appears to be the most meaningful way of defining such a vertical boundary.

Table 1: Receptor points for FLEXTRA and FLEXPART calculations. Note that the height refers to the height of the model topography!

Site name	abbreviation	longitude (°E)	latitude (°N)	height (m asl) model	real	difference
Forsthof – Schöpfl	FORST	15.880	48.100	492	581	–89
Streithofen	STREI	15.930	48.270	400	220	+180
Tulbinger Kogel	TULBI	16.150	48.283	322	495	–173
Hermannskogel	HERMA	16.299	48.271	276	520	–244
Lainzer Tiergarten – Auhof	AUHOF	16.235	48.201	314	230	+84
Bad Vöslau – Gainfarn	BADVO	16.210	47.960	387	286	+101

3.4 FLEXPART Lagrangian particle model

3.4.1 Model description and set-up

Backward (receptor-oriented) dispersion modelling was carried out with the Lagrangian particle dispersion model FLEXPART (Stohl et al., 1998, 2005). FLEXPART has been validated with data from continental-scale tracer experiments (Stohl et al., 1998) and has been used in a large number of studies on long-range atmospheric transport (Stohl et al., 2003; Eckhardt et al., 2008). FLEXPART tracks computational particles displaced by the mean winds interpolated from the input meteorological fields plus random motions representing turbulence (Stohl and Thomson, 1999).

FLEXPART was run for the same six receptor sites as FLEXTRA (see Table 1). The temporal resolution at the receptor was 1 h, and 1000 particles were released during this interval. Particles were tracked backwards for 10 d; this implies that 192 000 particles had to be kept in memory. Each run covered one receptor month. The temporal resolution of the potential sources was 3 h. As turbulence will correctly mix the particles, they were released at a height near model ground (8 m, corresponding to a typical air inlet height, though the exact value is not very important). The output sampling time interval was set to 900 s, and simulations were done in the mode taking into account the Lagrangian time scale of turbulence. All simulations were carried out for a pure tracer (no decay and deposition), and for an NO_2 proxy (no decay, dry and wet deposition active, parameters are standard FLEXPART values (Stohl et al., 2005, Section A3.7 of the Supplement). Simulations were made for the years 2003 and 2004. However, a part of the 2004 simulations were affected by errors

in the meteorological fields caused by a buggy extraction programme we were relying on. Therefore, only 2003 was finally used in the evaluations. The output was collected on a coarse grid with $1^\circ \times 1^\circ$ (approx. 70 km $\times$ 111 km) resolution, covering the region 15°W to 46°E and 35°N to 73°N, and a nested grid with $0.15^\circ \times 0.1^\circ$ (approx. 11 km $\times$ 11 km) resolution, covering the regions 13°E to 19°E and 46°N to 52°N (i.e., 6 $\times$ 6 coarse grid cells). The output grid cell height was 150 m.

A special feature of FLEXPART is the possibility to run it in a backward, receptor oriented mode to calculate source-receptor relationship (Seibert and Frank, 2004). This feature was used here, setting the input parameters to source in mass units and receptor in mixing ratio units.

3.4.2 Postprocessing

The FLEXPART output was converted to a more simple format nick-named SRM format. FLEXPART 6.2 writes one output file for each source time interval, which does not correspond well to studies focussing on a receptor time series. In SRM, each receptor time interval is one file. In this file, all grid cells are listed together with their source-receptor sensitivity value, that have nonzero sensitivities. This list is repeated for each source time interval with nonzero values. In this process, the source units which in FLEXPART are assumed to be volume sources are converted to sources per grid cell, by division of the source-receptor relationships with the output grid cell volume. Source-receptor sensitivities created by the model (unit in the SRM format $\mathrm{s\,kg^{-1}}$) can be multiplied with source strengths derived from an emission inventory (unit $\mathrm{kg\,s^{-1}}$), yielding a dimensionless mass mixing ratio at the receptor (see, e.g., Seibert and Frank, 2004; Wotawa et al., 2003; Stohl et al., 2007).

One year of these FLEXPART output data is about 1.4 GBytes per station in the FLEXPART's binary format and 2.0 GBytes in the more convenient SRM format. The computation time for one year and one receptor is about 24 hours on one AMD Opteron 250 processor (2.4 GHz, 1 MB L2 cache).

3.4.3 Calculation of concentrations

Source-receptor sensitivities created by the model (unit in the SRM format $\mathrm{s\,kg^{-1}}$) can be multiplied with source strengths derived from an emission inventory (unit $\mathrm{kg\,s^{-1}}$), yielding a dimensionless mass mixing ratio at the receptor (see, e.g., Seibert and Frank, 2004; Wotawa et al., 2003; Stohl et al., 2007).

A rather complex Fortran programme was developed that reads the hourly emission data for each grid cell (cf. Section 2.2), adds them up to match the 3-hourly output of FLEXPART, multiplies them with the corresponding SRM values and then adds up all the grid cell contributions to yield the modelled value at the receptor. Optionally, the contribution of each grid cell can be written out to a file for later evaluation. While dry and wet deposition is accounted for in the FLEXPART simulation, losses through chemical reactions were parameterised in a simple way in the concentration calculation by assuming a chemical half-life of 48 h for SO_2 and 72 h for NO_x. NO_xconcentrations are calculated by counting the NO emissions as NO_2 emissions (mole-wise) as NO is quickly converted to NO_2 in the atmosphere.

This procedure is, in principle, carried out for the coarse and for the nested domain separately. In order to obtain the combined results, the $6^\circ \times 6^\circ$ region of the nested domain can be masked in the coarse-domain evaluation. Then, the concentrations from the two domains are added up, thus using the high resolution where available but still including the contributions from the coarse domain.

3.4.4 Definition of metrics for comparison of observed and modelled concentrations

A number of metrics have been used to quantify the skill of the model in simulating the concentration time series. Most but not all of them are standard parameters. For convenience, the definition of all of them is provided below. All values have been derived only for the subset of data pairs where both model and observation data are available.

The data pairs are designated (x_i^o, x_i^m), $i \in [1, N]$, where the superscript o denotes observed values, and the superscript m modelled values. In the case of a model intercomparison, models can be compared pair-wise, thus o denoting one model, m another one (for a set of M models, $(M^2 - M)/2$ pairs).

Parameters related to the mean values

Mean of observed concentrations:

$$\overline{x^m} = \frac{1}{N} \sum_{i=1}^{N} x_i^m \tag{3.1}$$

Mean of modelled concentrations:

$$\overline{x^o} = \frac{1}{N} \sum_{i=1}^{N} x_i^o. \tag{3.2}$$

Bias (systematic error):

$$B = \overline{x^m} - \overline{x^o} \tag{3.3}$$

Relative bias (definition of variances see below):

$$\mathrm{RB} = \frac{B}{\sqrt{\frac{1}{2}(\sigma_m^2 + \sigma_o^2)}}. \tag{3.4}$$

Bias skill score:

$$S_b = \frac{1}{1 + a\mathrm{RB}^2}. \tag{3.5}$$

The vale $a = 10$ was chosen as reasonable, leading to the relationship between RB and bias skill score as presented in Table 1.

Parameters related to variances

Standard deviation of observations:

$$\sigma_o = \sqrt{\frac{1}{N} \sum_{1}^{N} ((x_i^o - \overline{x^o})^2} \tag{3.6}$$

Table 2: Some numerical values for the bias skill score as defined in Eq. 19 with $a = 10$.

RB	0.0	0.1	0.2	0.3	0.4	0.5	0.6	0.7	0.8	0.9	1.0	2.0
S_b	1.00	0.91	0.71	0.53	0.38	0.29	0.22	0.17	0.14	0.11	0.09	0.02

Standard deviation of modelled values:

$$\sigma_m = \sqrt{\frac{1}{N}\sum_{1}^{N}((x_i^m - \overline{x^m})^2} \tag{3.7}$$

Mean absolute error:

$$\text{MAE} = \frac{1}{N}\sum |x_i^m - x_i^o| \tag{3.8}$$

Root mean square error:

$$\text{RMSE} = \sqrt{\frac{1}{N}\sum_{i=1}^{N}(x_i^m - x_i^o)^2} \tag{3.9}$$

Bias-corrected RMSE:

$$\text{BCRMSE} = \frac{1}{N}\sqrt{\sum_{i=1}^{N}[(x_i^m - \overline{x^m}) - (x_i^o - \overline{x^o})]^2} = \sqrt{\text{RMSE}^2 - B^2}. \tag{3.10}$$

Correlation coefficient:

$$R = \frac{\sum_1^N x_i^m\ x_i^o\ -\ N\overline{x^m}\ N\overline{x^o}}{N\sqrt{\sigma_o\sigma_m}} \tag{3.11}$$

Overall parameters

Taylor's skill score (Taylor, 2001) :

$$S_r = 2\,(1+R)\,\left(\frac{\sigma^m}{\sigma^o} + \frac{\sigma^o}{\sigma^m}\right)^{-2} \tag{3.12}$$

Total skill score (average of Taylor's skill score, measuring RMSE and R, and the bias skill score):

$$S = \frac{1}{2}\,(S_r + S_b) \tag{3.13}$$

Fraction of data pairs with a deviation within a factor of 2 :

$$\text{prob2} = \frac{N\,(x_i^m/x_i^o \geq 0.5 \wedge x_i^m/x_i^o \leq 2)}{N} \tag{3.14}$$

Fraction of data pairs with a deviation within a factor of 2 :

$$\text{prob5} = \frac{N\,(x_i^m/x_i^o \geq 0.2 \wedge x_i^m/x_i^o \leq 5)}{N} \tag{3.15}$$

The value of α is rather arbitrary and would depend on the application.

4 Results

4.1 Residence times calculated from FLEXTRA trajectories

Residence time plots have been created for

1. all stations, full year (Fig. 12)
2. station Auhof, every month (see Appendix B)
3. full year, differences for all station pairs (not shown)
4. at all stations, full year, differences between residence times resulting from mixing height values set to 100 m, 150 m, 500 m, and taking the mixing height computed by FLEXTRA (not shown).

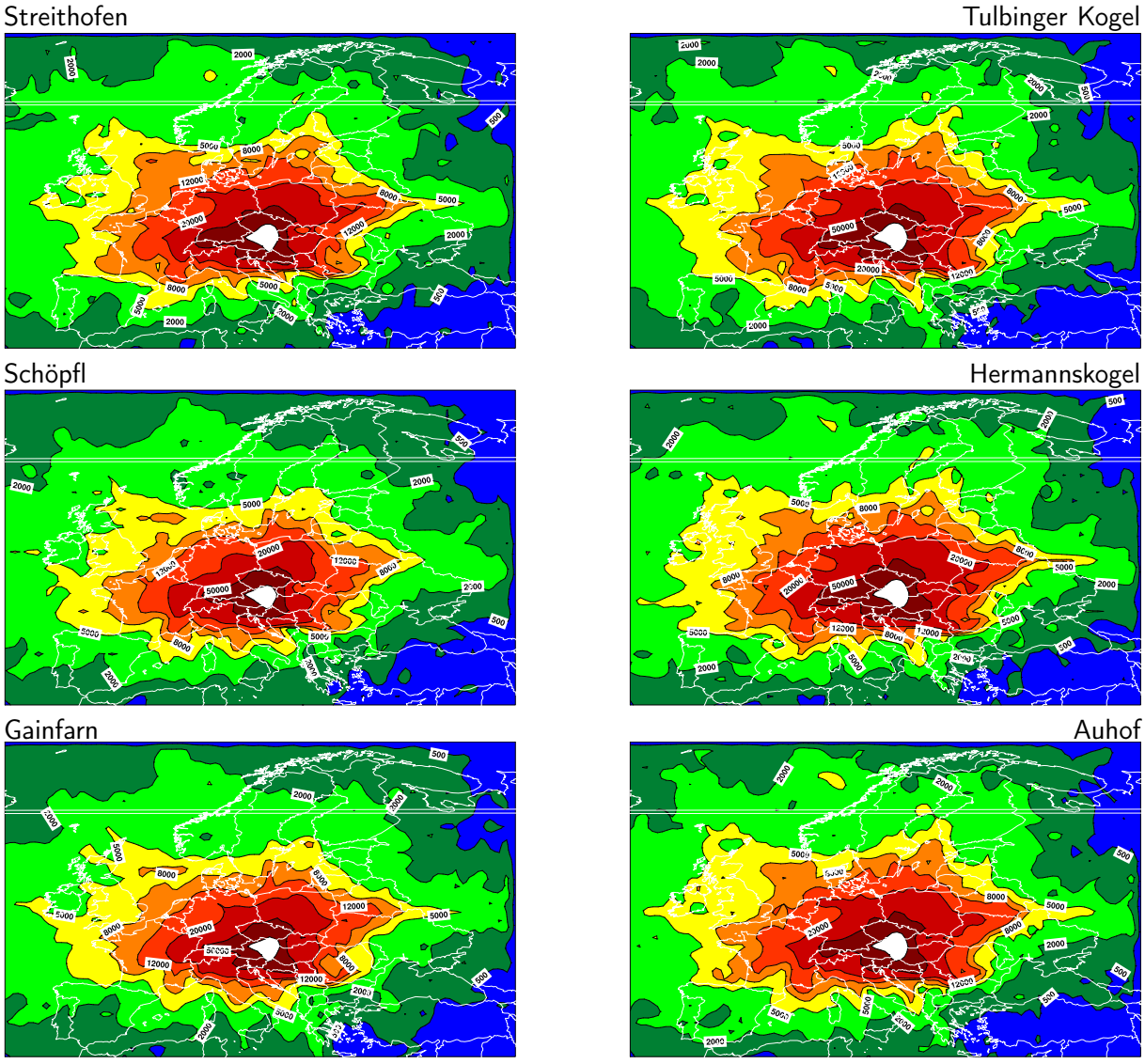

Figure 12: Residence times derived from trajectory calculations with FLEXTRA, year 2003.

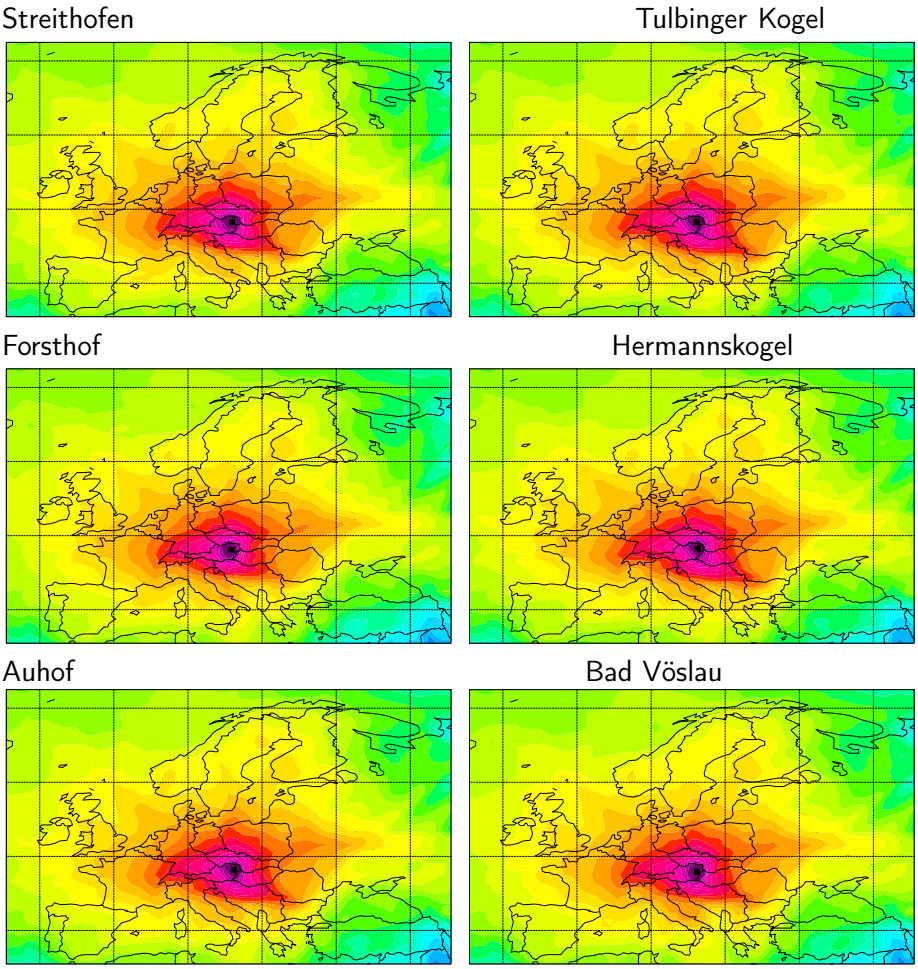

Figure 13: Source-receptor sensitivities calculated by FLEXPART averaged over the whole year 2003, coarse domain, in relative units with a logarithmic scaling.

If not mentioned otherwise, always FLEXTRA_MH was used. As Fig. 12 shows, the fields of the residence times become noisy towards the boundaries of the domain because the number of trajectories per grid is insufficient to yield stable statistics. Also one sees that on this scale, significant differences between the various receptor points are small and hardly visible.

The Appendix B shows that in individual months, certain synoptic patterns prevail. As only a single year has been considered, these patterns cannot be generalised. In the FLEXPART concentration evaluation, annual or seasonal means are used which are less affected by such peculiarities of a specific year, although of course they still cannot represent climatological mean conditions.

4.2 Source-receptor relationships calculated by FLEXPART

Source-receptor relationships describe the sensitivity of the concentration at a receptor site to emission sources, in our case on the coarse and nest output grid of FLEXPART. Without wet or dry deposition or decay, they represent residence times (Seibert and Frank, 2004). Correspondingly, the patterns of the trajectory residence times (Fig. 12) and source-receptor (s–r) sensitivities on the coarse grid (Fig. 13) are similar. However, as FLEXPART calculated the trajectories of thousands of particles for each measurement time interval and as it included turbulent diffusion, the mean s–r fields are not noisy like the residence times. Many of the patterns in Fig. 13 appear for all the stations; they

are a common feature of the whole Wienerwald region. We can notice the influence of the Alps on the transport patterns: transport from the southwest is weaker than from the other directions. The Iberian peninsula has little influence, as does Greece and Turkey. Due to the preferred transport along the northern edge of the Alps, southern Germany contributes more than northeastern Germany though their direct distance is similar. There seem to be preferred transport patterns, e.g. from the Balkan region along the Danube river, and through southern Poland from Ukraine. Also the North Sea is a preferred pathway, maybe as a channelling effect between the mountains of Scotland and Norway.

Difference between the sites are hard to see, especially on the coarse grid scale. One of the visible difference is the stronger influence of regions to the east at Hermannskogel (look at the Danube and southern Poland pathways and compare to Forsthof). The patterns in the nest region (Fig. 14) are more differentiated. Streithofen has more influence from the west, and relatively little from Hungary. Tulbinger Kogel has more influence from the north. Forsthof is affected to a relatively high degree from Hungary and especially the Sopron region. Hermannskogel also does not have so much influence from Hungary and Bratislava, but it does have influence from Styria. This is even more prominent for Bad Vöslau. Also, Hermannskogel has a relatively symmetric distribution of the zone of strongest influence (dark red), whereas Forsthof appears to have more channelled winds, either from west or southeast, with a secondary maximum from the northeast.

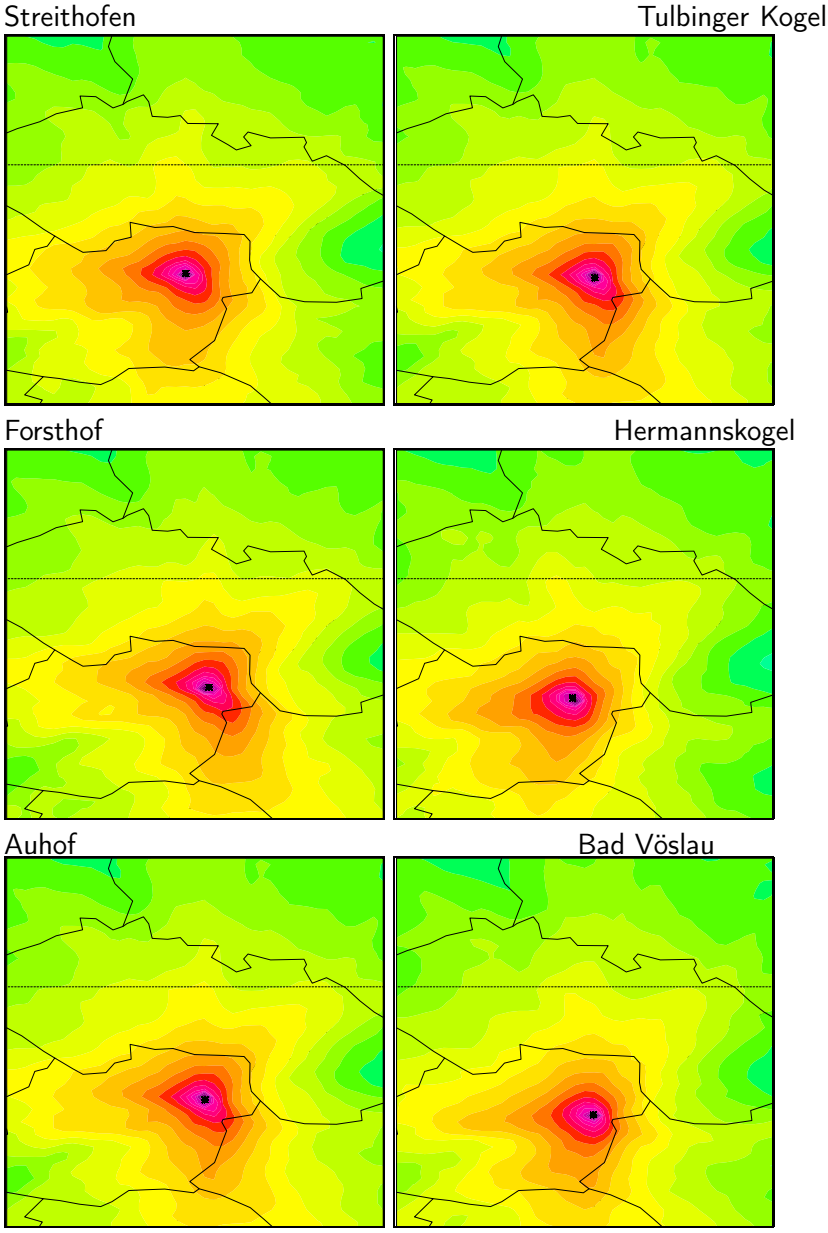

Figure 14: Source-receptor sensitivities calculated by FLEXPART averaged over the whole year 2003, nest domain, in relative units with a logarithmic scaling.

4.3 Concentrations

All modelled concentration time series discussed in this section were obtained from the FLEXPART output, as described in Section 3. If not otherwise mentioned, they represent the combination of coarse and nested domain contributions. Station Auhof is only for wet deposition and there are no concentration observations. Wet deposition finally was not included in the work, Thus, the site Auhof is not included in the following.

4.3.1 Time series

A graphical representation of the time series of all observed and modelled concentrations is provided in Appendix A. As one can see immediately, the modelled NO_x comes almost entirely from the nest domain, whereas for SO_2, there is a substantial and often dominating contribution from the outer domain. This can be understood easily from the different pattern of the respective emissions (see Figures 10 an 11: only NO_x is emitted in high quantities in Eastern Austria. Table 3 shows this quantitatively: for NO_x, between 85% and 92% of the simulated concentrations are due to emissions in the nest domain, with the higher values for the stations closer to Vienna, while for SO_2, the respective shares are between 61% and 71%.

Table 3: Relative contributions (in percent) of inner and outer domains to simulated concentrations. The outer domain is the coarse domain without the area occupied by the inner (nest) domain.

Site	nitrous oxides		sulphur dioxide	
	outer domain	inner domain	outer domain	inner domain
Streithofen	13.0	87.0		
Tulbinger Kogel	10.7	89.3		
Hermannskogel	7.7	92.3	28.9	71.1
Forsthof	14.3	85.7	39.4	60.6
Bad Vöslau	10.7	89.3		

4.3.2 Overall statistical performance measures

Table 4 gives an overview of the performance of the model simulations. As the figures in Appendix A show, it is not uncommon that the model shows a short peak a bit earlier or later than the observations. Observations also have a high-frequency component of variation. For looking at the model skill, it was therefore found appropriate to introduce a smoothing with a running 7 h mean filter before the calculation of the performance parameters.

There is a relatively strong overprediction of the mean concentrations at Hermannskogel, and underprediction at Streithofen and especially Bad Vöslau. The hypothesis that these over- and underpredictions are caused by the deviation between the height of the station according to the model topography and the real topography is corroborated by Fig. 15, showing a distinct correlation between this height difference and the relative bias. Stations on hill tops have too high concentration, those in valleys or in the plains next to the slope too low concentration.

The correlation coefficients vary between 0.27 and 0.56, and Taylor's skill scores between 0.46 and 0.68. These values indicate a moderate skill of the model, but in terms of air pollution modelling they

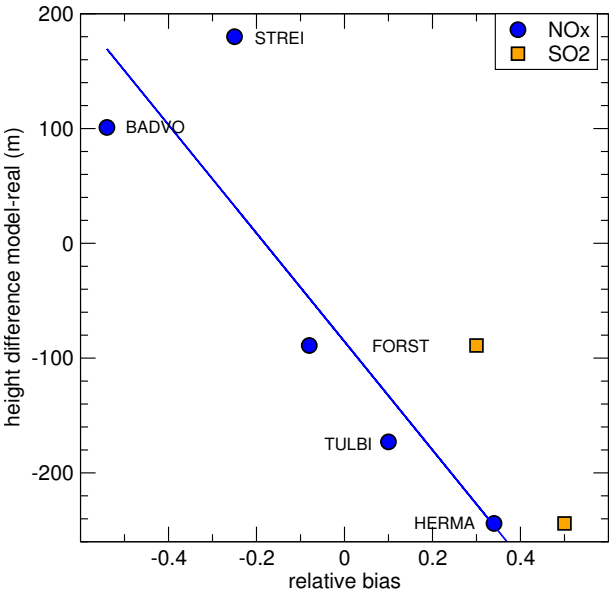

Figure 15: Correlation between relative bias of annual mean NO_x and SO_2 concentrations and the difference in the station height between model and reality.

Table 4: Overall metrics of observed versus modelled concentrations, hourly values with running 7-h averages, full year. Concentrations are in $\mu g\,m^{-3}$, RMSE is the root-mean-square error, BCRMSE is the bias-corrected RMSE, R is the correlation coefficient and N is the number of data pairs (note that a full year has 8760 hours).

Station	STR	TUL	HER	FOR	BVO	HER	FOR
Substance	nitrous oxides					sulphur dioxide	
mean obs	15.65	15.10	16.60	11.24	23.33	5.51	3.72
mean model	12.90	16.47	24.24	10.57	14.42	10.47	5.24
bias	-2.76	1.37	7.64	-0.67	-8.91	4.95	1.52
relative bias	-0.25	0.10	0.34	-0.08	-0.54	0.50	0.30
bias skill score	0.61	0.92	0.46	0.94	0.26	0.28	0.53
stdev obs	11.83	10.94	18.21	8.43	20.51	6.05	3.79
stdev model	9.98	17.20	25.60	7.98	11.55	12.49	6.11
mean absolute error	8.01	9.38	13.10	6.24	13.81	6.14	2.77
RMSE	12.39	16.08	22.94	9.97	22.47	11.90	5.38
BCRMSE	12.08	16.02	21.63	9.95	20.63	10.82	5.16
R	0.40	0.42	0.56	0.27	0.27	0.50	0.54
Taylor's skill score	0.68	0.58	0.69	0.63	0.46	0.46	0.62
total skill score	0.65	0.75	0.58	0.78	0.36	0.37	0.57
prob2	0.70	0.66	0.61	0.69	0.57	0.59	0.71
prob5	0.98	0.98	0.93	0.98	0.94	0.90	0.96
N	8311	7810	8690	7932	7952	8485	8466

Table 5: Selected metrics of observed versus modelled concentrations, hourly values with running 7-h averages, per season. Concentrations are in $\mu g\, m^{-3}$.

Station	STR	TUL	HER	FOR	BVO	HER	FOR
Substance	nitrous oxides					sulphur dioxide	
seasonal means							
spring obs	11.78	12.46	14.50	8.53	21.12	4.43	3.34
model	10.00	13.12	20.05	8.68	12.52	7.81	4.01
summer obs	8.69	9.77	8.16	7.32	12.94	3.78	2.31
model	11.21	12.89	18.41	9.80	12.97	3.81	2.15
autumn obs	18.54	20.44	18.82	10.96	23.35	4.10	2.99
model	14.97	19.65	28.22	11.39	14.99	12.17	5.62
winter obs	24.29	17.16	25.12	17.95	35.45	9.67	6.13
model	15.58	20.01	30.38	12.42	17.34	18.36	8.90
relative bias							
spring	-0.24	0.07	0.33	0.03	-0.63	0.59	0.21
summer	0.38	0.36	0.79	0.46	0.00	0.01	-0.13
autumn	-0.29	-0.05	0.37	0.06	-0.59	0.78	0.59
winter	-0.70	0.17	0.19	-0.53	-0.82	0.67	0.38
R							
spring	0.39	0.31	0.39	0.16	0.24	0.62	0.57
summer	0.30	0.10	0.41	0.17	0.05	0.56	0.22
autumn	0.35	0.46	0.59	0.16	0.12	0.42	0.29
winter	0.37	0.40	0.58	0.32	0.34	0.42	0.53
Taylor's skill score							
spring	0.66	0.54	0.55	0.43	0.52	0.56	0.64
summer	0.32	0.10	0.36	0.21	0.48	0.77	0.43
autumn	0.67	0.58	0.70	0.50	0.54	0.16	0.24
winter	0.64	0.58	0.73	0.58	0.37	0.55	0.69

are quite reasonable. This is also shown by the fraction of values within factors of 2 and 5 (factor of 2 indicates decent agreement, factor of 5 still some skill). Between 90% and 98% of the data fall into the factor 5 category, and between 57% and 71% in the factor 2 category. With respect to correlation, Hermannskogel has the best one, Forsthof and Bad Vöslau the worst; Streithofen and Tulbinger Kogel are inbetween. Interestingly, for SO_2, Forsthof has even better results than Hermannskogel. We may presume that the transport from close sources such as the A1 motorway is not represented well in our coarse model and thus responsible for the low performance for NO_x, while the SO_2 concentrations are more determined by long-range transports. Here Hermannskogel suffers from the incorrect representation of the terrain and is too much influenced by emissions from Vienna.

In comparison, Krüger (2004) obtained correlation coefficients varying between 0.45 and 0.85 for ozone simulations of stations n Eastern Austria in summer with a chemistry-transport model including chemistry and a resolution of 3 km.

In Table 5, the main score parameters have been differentiated for the four seasons, defined as usual in meteorology (spring as March – May, summer as June – August, and autumn as September – November, winter as December – February). In summer, all the underpredictions disappear for NO_x. Hermannskogel has the highest positive bias. The correlations and Taylor scores are very low in this season. This is not the case for SO_2. A possible explanation would be that generally weaker winds encountered in this season are less well reproduced by the meteorological fields available. The high

positive bias at Hermannskogel could be attributed to strong turbulence, leading to more turbulent spreading of pollution from the Vienna region to the mountain site in the model, especially through horizontal diffusion which in this model version is following the model levels and not being truly horizontal. For SO_2, situations with more wind are more relevant and those are modelled better. As the SO_2 emissions from the Vienna region are relatively low compared to those of NO_x, the turbulent diffusion has less detrimental effects.

In general, correlations and Taylor scores are better in autumn and winter, both characterised by a more stable atmospheric stratification. This agrees with the hypothesis on the influence of advection and wind speed developed for summer, just with the opposite sign. The underprediction at the "valley" sites Streithofen and Bad Vöslau is most extreme in winter. For example, the seasonal mean of NO_x modelled at Bad Vöslau is 17 $\mu g\,m^{-3}$, while 35 $\mu g\,m^{-3}$ were observed. This is due to the stable stratification which shields the station wrongly from emissions in parts of the Vienna basin that are lying lower in the model topography.

4.3.3 Origin of air pollution at the Wienerwald monitoring sites

The origin of the NO_x and SO_2 arriving at the selected monitoring sites is visualised by plotting the contribution of each emission grid cell to the annual or seasonal mean concentration (Figures 16 – 20 for the annual means, and Figures 21 – 30 for the seasonal means). The colour scale represents the contributions per grid cell, regardless of its size. The scaling is the same for the coarse domain and the nest domain, only the upper boundary of the last class is adjusted to the higher maxima of the nest domain. It is also important to be aware that the contributions from those grid cells of the coarse domain which lie inside the nest domain are hypothetical in the sense that the modelled receptor concentrations don't use them, as the fine grid emissions and source-receptor values are used for the contribution from the nest domain.

Let us first consider the contributions to the annual mean. For Bad Vöslau, at the southeastern corner of the Wienerwald Biosphere Park and bordering to the basin of Vienna and it southern neighbourhood ("Industrieviertel"), the NO_xcontributions in the nest domain (Fig. 16), the main sources are the surroundings of the site and Vienna. We see also some contributions from the area just west to the Biosphere park, the cities of Linz and Graz, but these are lower by one order of magnitude. Sources in neighbouring countries, Such as Bratislava, Brno, etc. are visible but low. In the distribution map for the coarse domain, outside the nest regions, the most important contributors are the heavy-industry region of southern Poland and southern Germany.

At Forsthof (Fig. 17), a site inside the Wienerwald hills near the western border of the Biosphere Park, the main source regions for NO_x are the region just west of the site (city of St. Pölten and surroundings, motorways) as well as Vienna. Linz is considerably more prominent as a source here than at Bad Vöslau which lies on the other side of the Wienerwald. A relevant amount of NO_x is also contributed from within the Biosphere Park boundaries. On the larger scale, again southern Poland and southern Germany appear as the most relevant regions. This stations also measures SO_2. As explained before, due to the low emissions of sulphur dioxide in Austria compared to some other countries, the contributions are shifted from the near field to larger distances. Still, the Vienna region is the most important source, but the regions of St. Pölten, Graz and Linz are much less visible than for NO_x. Considering that the heavy industry at Linz some years ago was a major emitter of SO_2, this indicates good results in pollution control. Slovenia shows up as a major region in both the nest and the coarse domain, probably due to its coal-fired power plants. Note that the contributions are

smeared out in the contribution map for the nest domain due to the low resolution of the available emission inventory in this country (cf. Fig. 11). All in all, southern Poland is by far the most important source of SO_2 for Forsthof. In addition to Slovenia, contributions from Bosnia, Serbia, Romania and from southern Germany are also relevant.

Streithofen (Fig. 19) is sited at the northwestern border of the Biosphere Park next to the Tullnerfeld (Fig. 1), a plain adjacent to the Danube river where Austria's largest coal-fired power plant, Dürnrohr, with 700 MW output, is located. This is reflected in a high contribution of NO_x from the northwestern neighbourhood of the station, more or less the Tullnerfeld region. We see also the motorway to the west and the city of Linz as emitters. However, Vienna ranks second after the Tullnerfeld, and also the Biosphere Park area itself with its motorways is a relevant source. Other contributions are from Industrieviertel, Graz and Brno. On the European scale, again southern Poland and southern Germany are the major additional contributing regions.

Hermannskogel (Fig. 18) is a site on a hill immediately bordering the city of Vienna, at the northeastern boundary of the Wienerwald. In the model, it is not high enough above the Vienna area and thus reveices (too) high contributions from this region with its high emission density. Compared to this, the other regions such as Tullnerfeld, Industrieviertel, Linz and Brno are contributing less. Interestingly, at this station, Bratislava is more important than Graz. Eon the European scale, the usual regions show up as relevant emitters. SO_2 is also measured at Hermannskogel. In the nested domain, only Vienna is showing up as an important source region within Austria. Outside, some cities in neighbouring countries to the east appear as relevant contributors, especially Bratislava and Budapest. Considering the coarse grid, Poland is more important and southern Germany less important as a source region than for NO_x. In addition, sources in Bosnia, Serbia and southern Romania appear as important contributors,

Tulbinger Kogel is sited between Hermannskogel and Streithofen, and the main influencing areas accordingly include Tullnerfeld as well as Vienna. Otherwise, it behaves similar to the other stations.

Now let us look at seasonal differences in the contribution patterns. These patterns are influenced by seasonal differences in the circulation patterns as well as in the emissions. At Bad Vöslau, coarse domain (Fig. 21), NO_x contributions from southern Poland have a minimum in summer and a maximum in winter. Sources in the Balkan are relevant only in winter. The Moscow region is visible as a minor source region, although only in summer. A few contributions from the Benelux region and the Ruhr area in northwestern Germany are visible in autumn. Italy and Greece are not among the important source regions, and their emissions are mainly felt in autumn and winter, obviously an effect of the frequent Mediterranean lows in this part of the year. In the nest domain (Fig. 22), the more frequent southerly flow patterns in autumn and winter are visibly through the increased contribution from the agglomeration of Graz. In summer, emissions from the immediate surroundings (Lower Austria and Vienna) are dominant.

The nearby emissions are relevant to the NO_x concentration at Forsthof all year round, whereas Linz is contributing more in spring and autumn, probably with predominant zonal circulation patterns, while Graz in the south contributes in autumn and a bit less in winter (Fig. 24). Interestingly, in autumn the industrial region of the Mur-Mürz valley is discernible as a region of elevated contribution, as is the strip along the northern edge of the Alps. The more distant emissions (Fig. 23) show a seasonal behaviour similar to Bad Vöslau.

At Hermannskogel, the coarse grid emissions (Fig. 25) in southern Poland are most relevant in winter and spring, while the emissions in southeastern Europe contribute mainly in autumn and winter. They

contribute more than at Bad Vöslau. In summer more distant sources are in general less important. With respect to the nest domain (Fig. 26), the Vienna area is the dominant source in all seasons, but there are some variations for the other agglomerations in the domain. Linz is contributing a bit more in winter, Praha and Brno mainly in summer, Bratislava and Budapest in autumn and winter. Graz is contributing much more in winter than in spring and summer according to the model.

At Streithofen (Fig. 27), the main emitters for the coarse domain, namely southern Germany, southern Poland and Bosnia/Serbia, contribute all most in winter. The Ruhr area is more relevant in autumn. In summer, like at the other stations, the distant sources contribute less. The contribution of Linz is relatively pronounced in the nest domain (Fig. 28), especially in summer and winter. In winter, a whole strip along the northern edge of the Alps appears as a discernible source region. Graz is relevant mainly in autumn and winter, like elsewhere.

Finally, at Tulbinger Kogel (Fig. 29), we can again observe that summer has less influence from distant regions, in autumn the influence from sources in the northwest has its maximum while in winter next to the sources in southern Germany also those in Poland and on the Balkan contribute. In the nest domain (Fig. 30), we find that Graz has little influence, especially in spring and summer, Bratislava is relevant in autumn, Brno most in summer, and Linz most in winter.

NOx

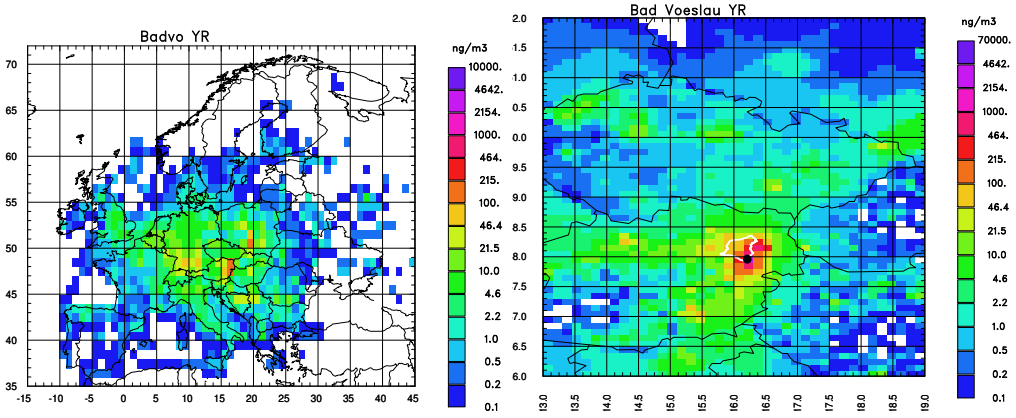

Figure 16: Geographical distribution of contributions to the NO_x concentration at Bad Vöslau for the whole year 2003 in ngm^{-3} per grid cell. Left column: coarse grid, right column: fine grid.

NOx

SO2

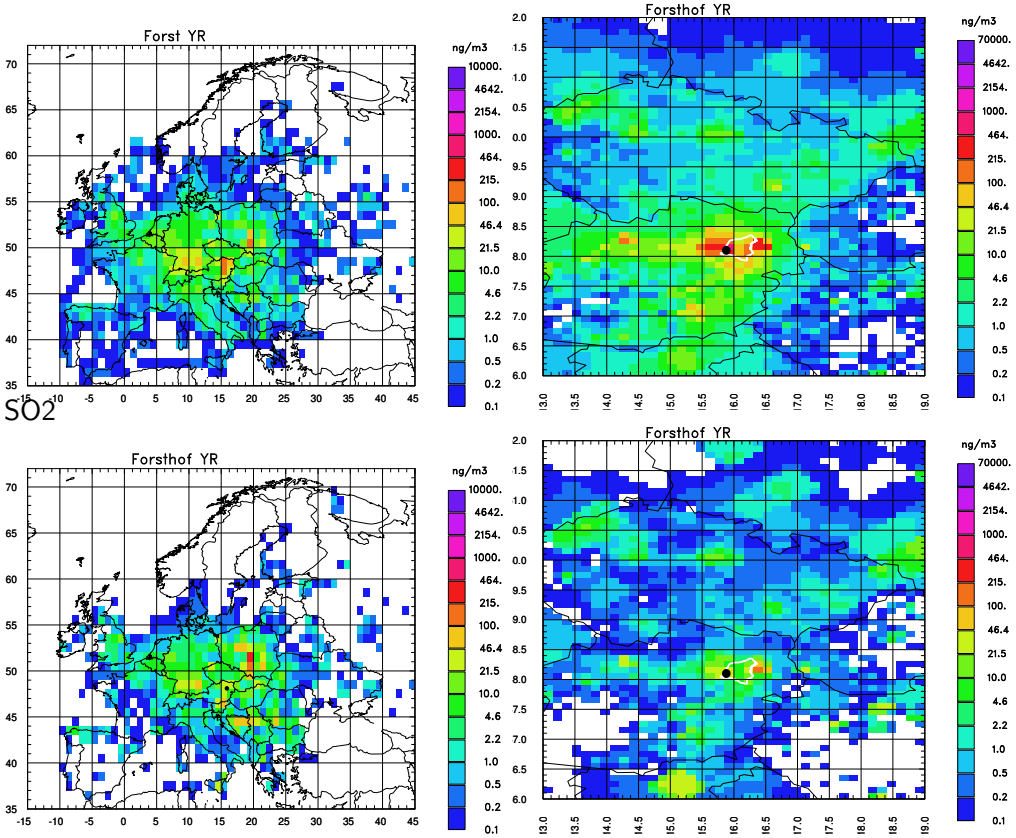

Figure 17: Geographical distribution of contributions to the NO_x (top) and SO_2 (bottom) concentration at Forsthof for the whole year 2003 in ngm^{-3} per grid cell. Left: coarse, right: fine grid.

NOx

SO2

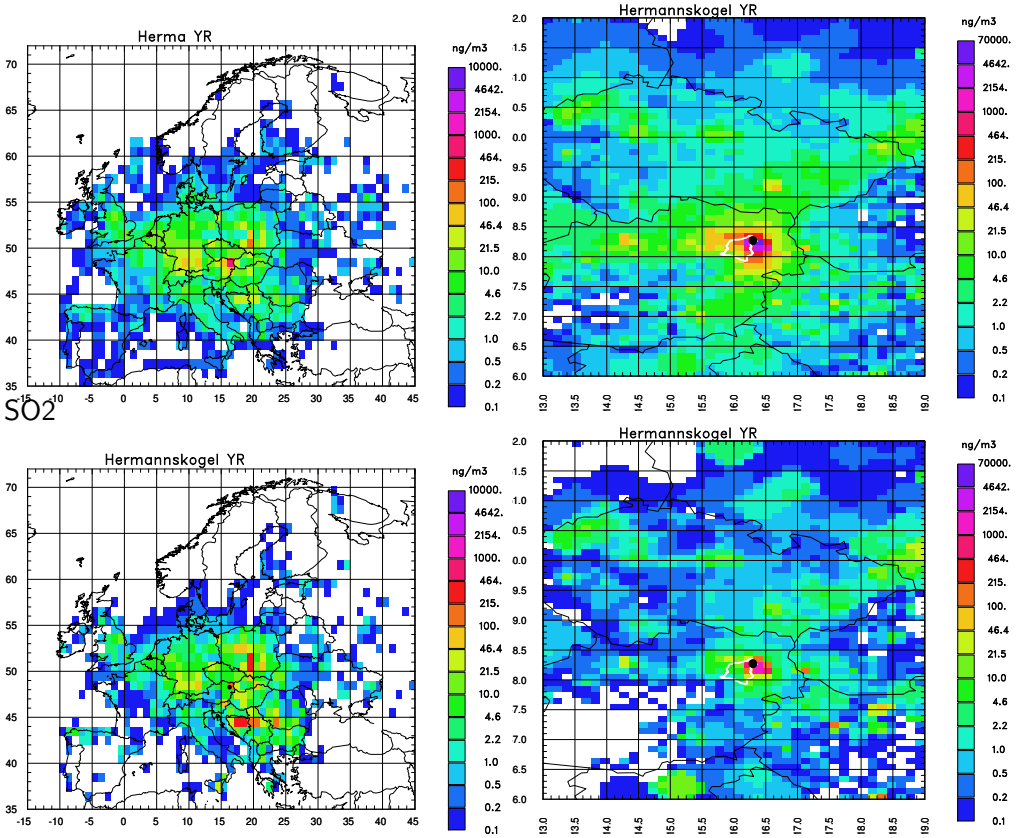

Figure 18: As Fig. 17, for Hermannskogel

NOx

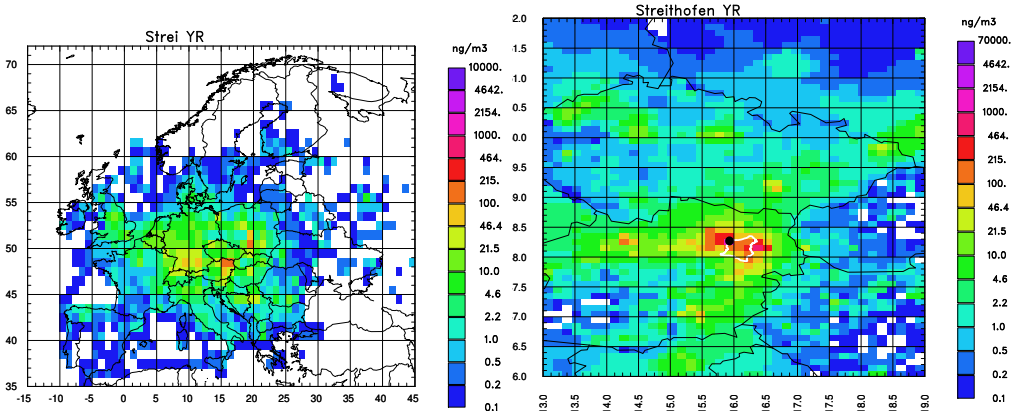

Figure 19: Geographical distribution of contributions to the NO_x concentration at Streithofen for the whole year 2003 in ngm^{-3} per grid cell. Left column: coarse grid, right column: fine grid.

NOx

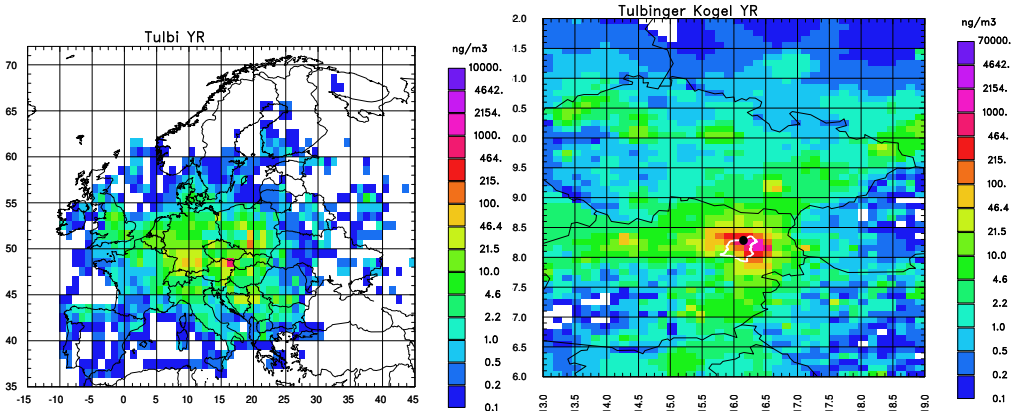

Figure 20: Geographical distribution of contributions to the NO_x concentration at Tulbinger Kogel for the whole year 2003 in ngm^{-3} per grid cell. Left column: coarse grid, right column: fine grid.

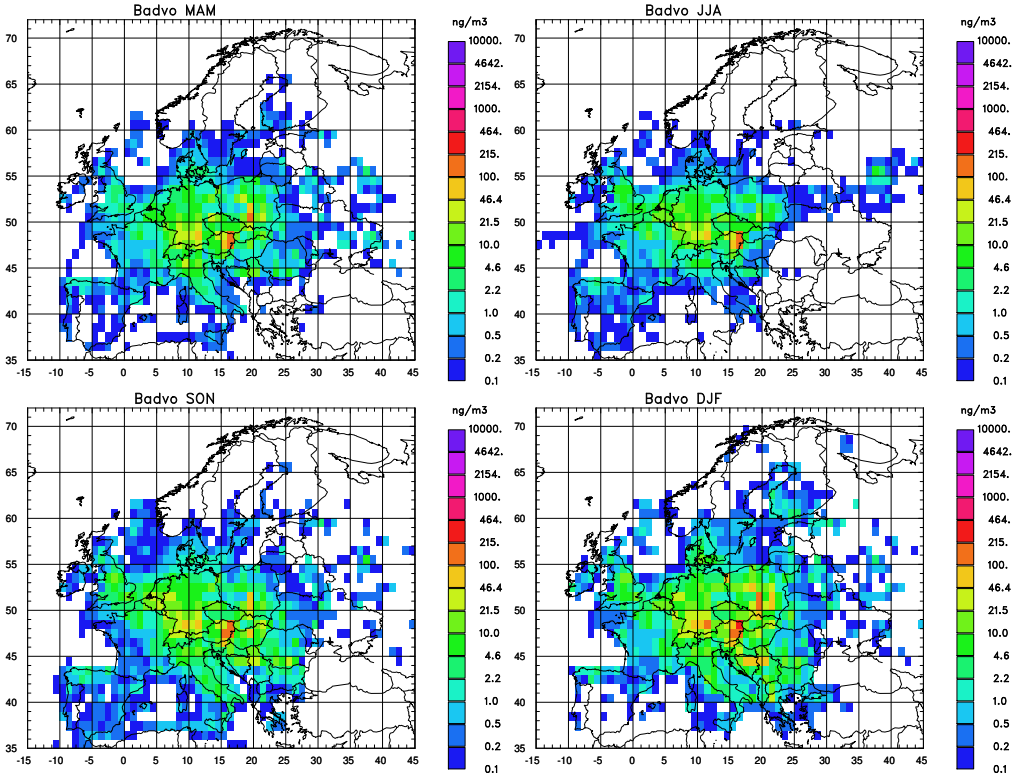

Figure 21: Geographical distribution of contributions to the NO_x concentration at Bad Vöslau for the four seasons in ngm^{-3} per grid cell.

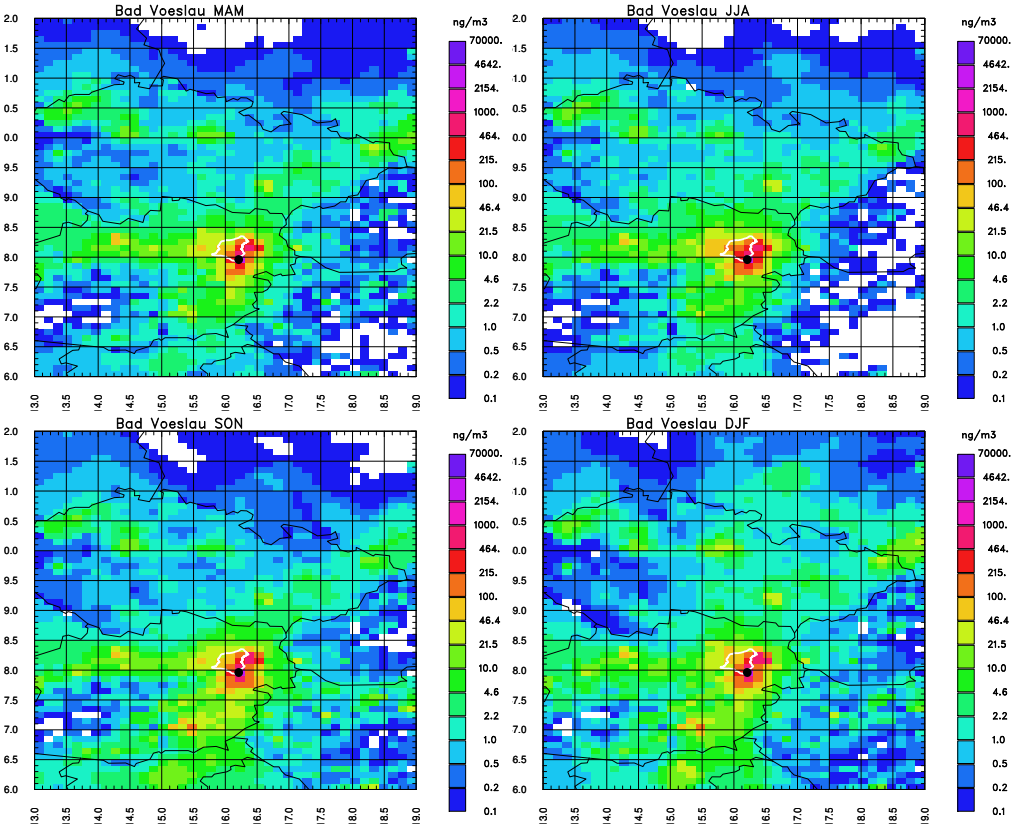

Figure 22: Geographical distribution of contributions to the NO_x concentration at Bad Vöslau for the four seasons in ngm^{-3} per grid cell for the nest domain.

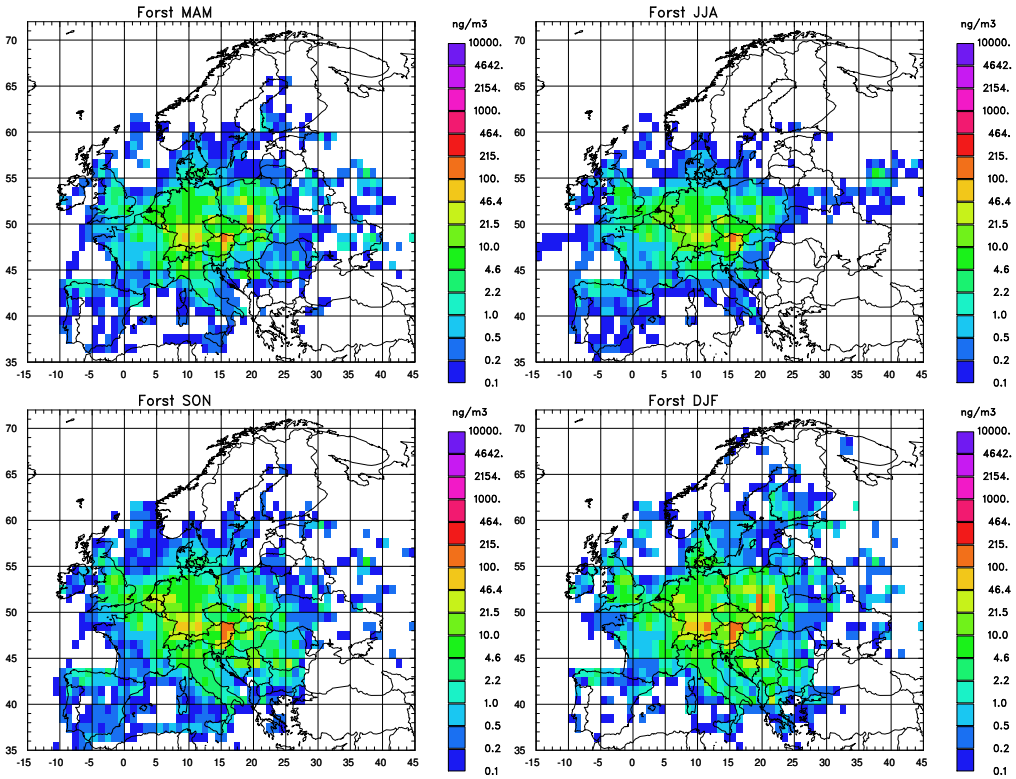

Figure 23: Geographical distribution of contributions to the NO_x concentration at Forsthof for the four seasons in ngm^{-3} per grid cell.

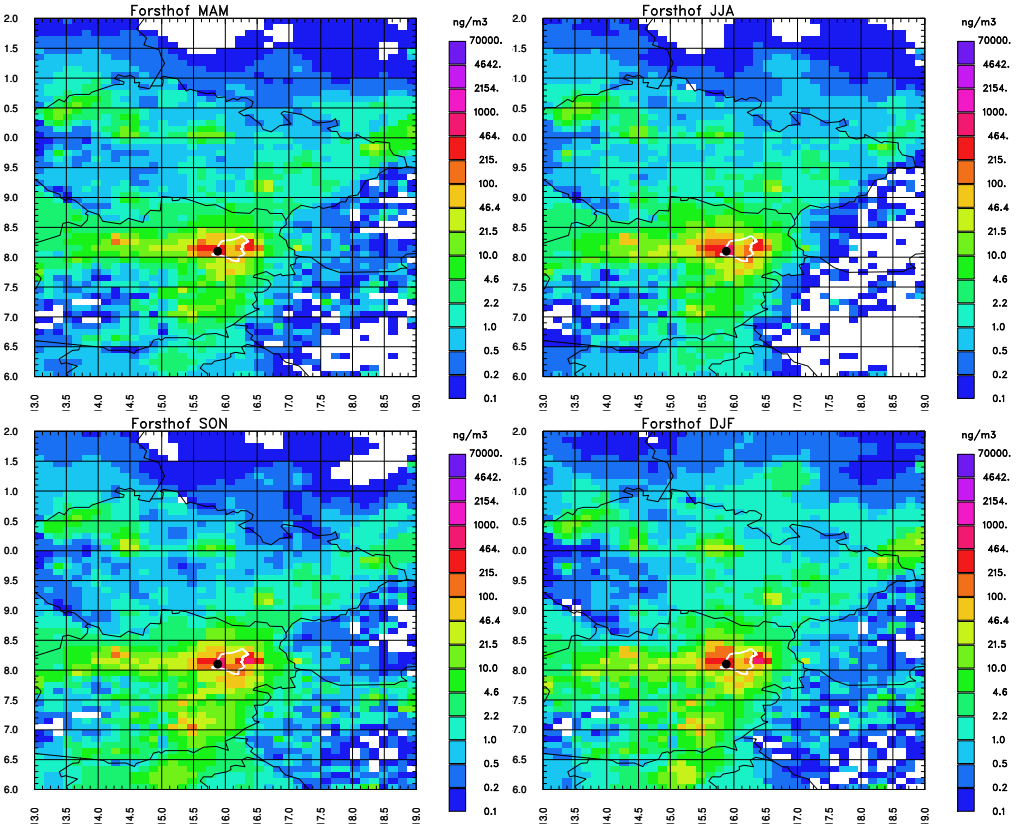

Figure 24: Geographical distribution of contributions to the NO_x concentration at Forsthof for the four seasons in ngm^{-3} per grid cell for the nest domain.

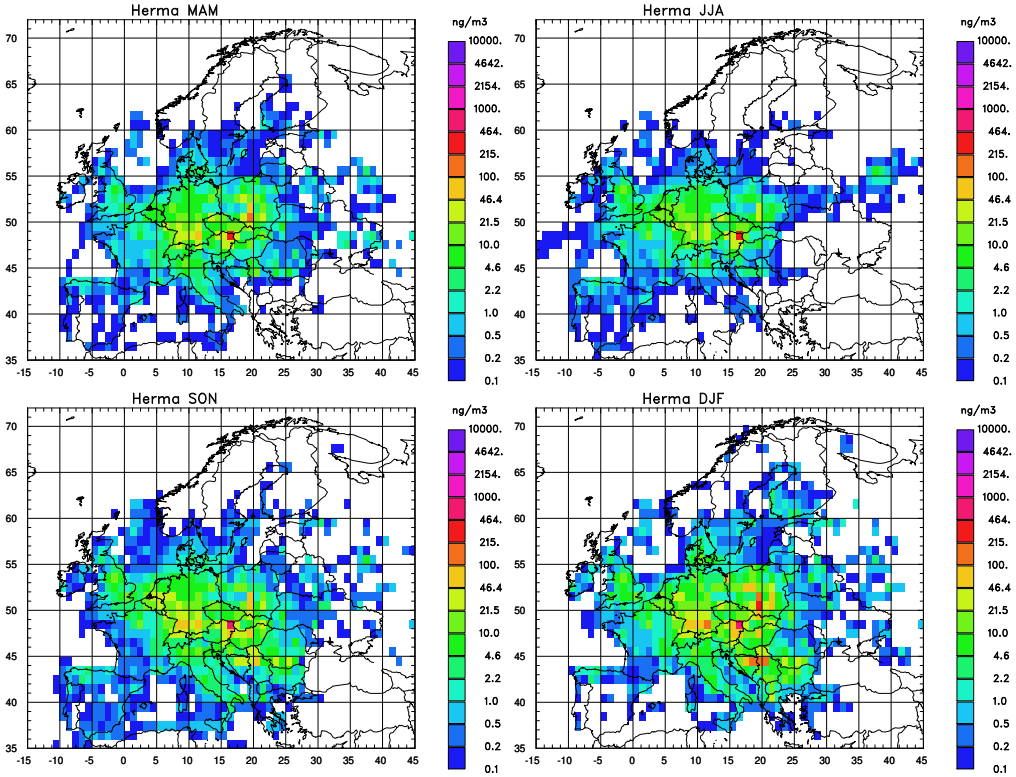

Figure 25: Geographical distribution of contributions to the NO_x concentration at Hermannskogel for the four seasons in ngm^{-3} per grid cell.

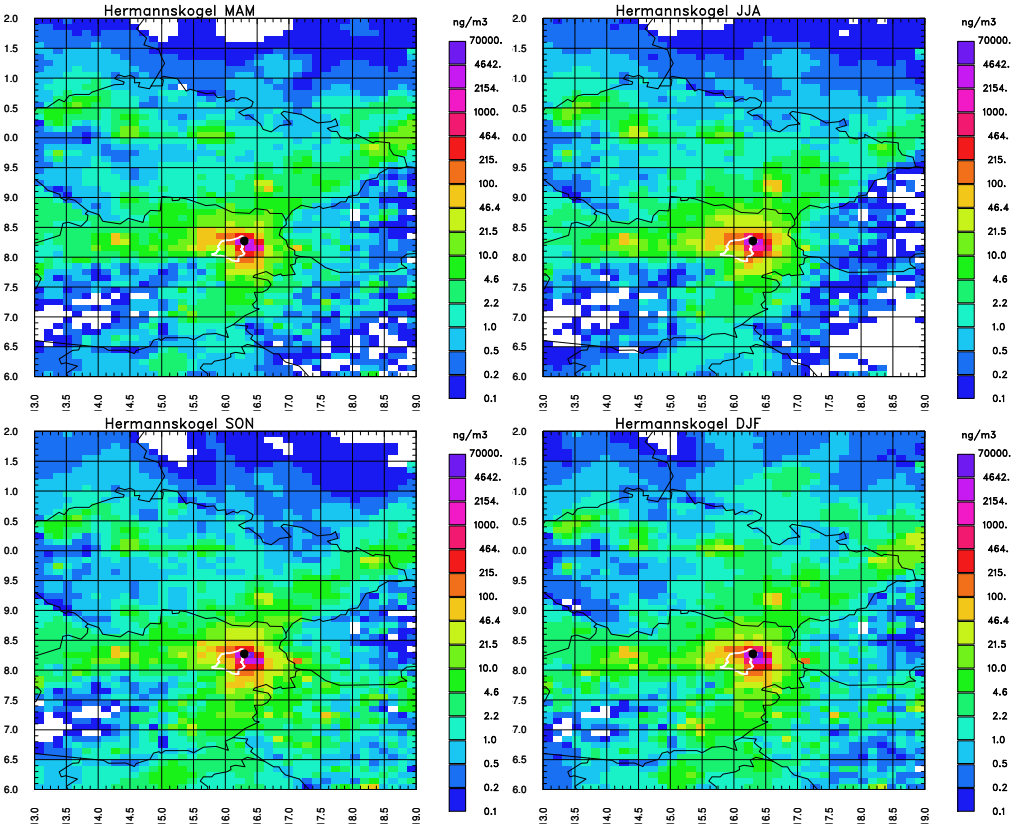

Figure 26: Geographical distribution of contributions to the NO_x concentration at Hermannskogel for the four seasons in ngm^{-3} per grid cell for the nest domain.

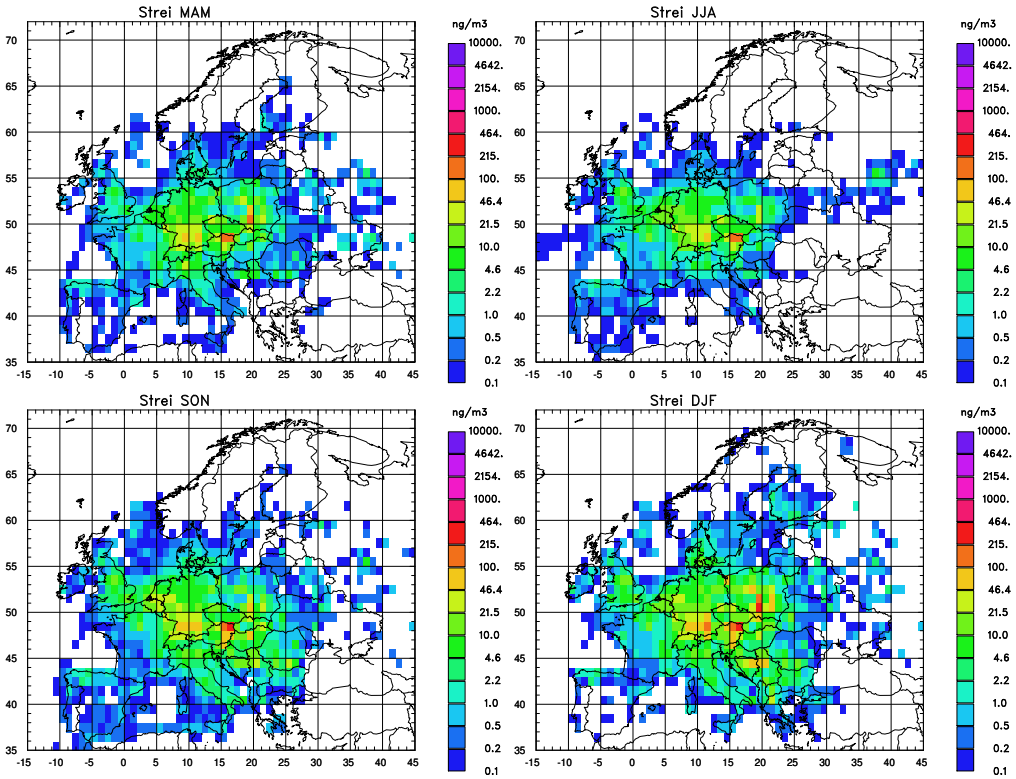

Figure 27: Geographical distribution of contributions to the NO_x concentration at Streithofen for the four seasons in ngm^{-3} per grid cell.

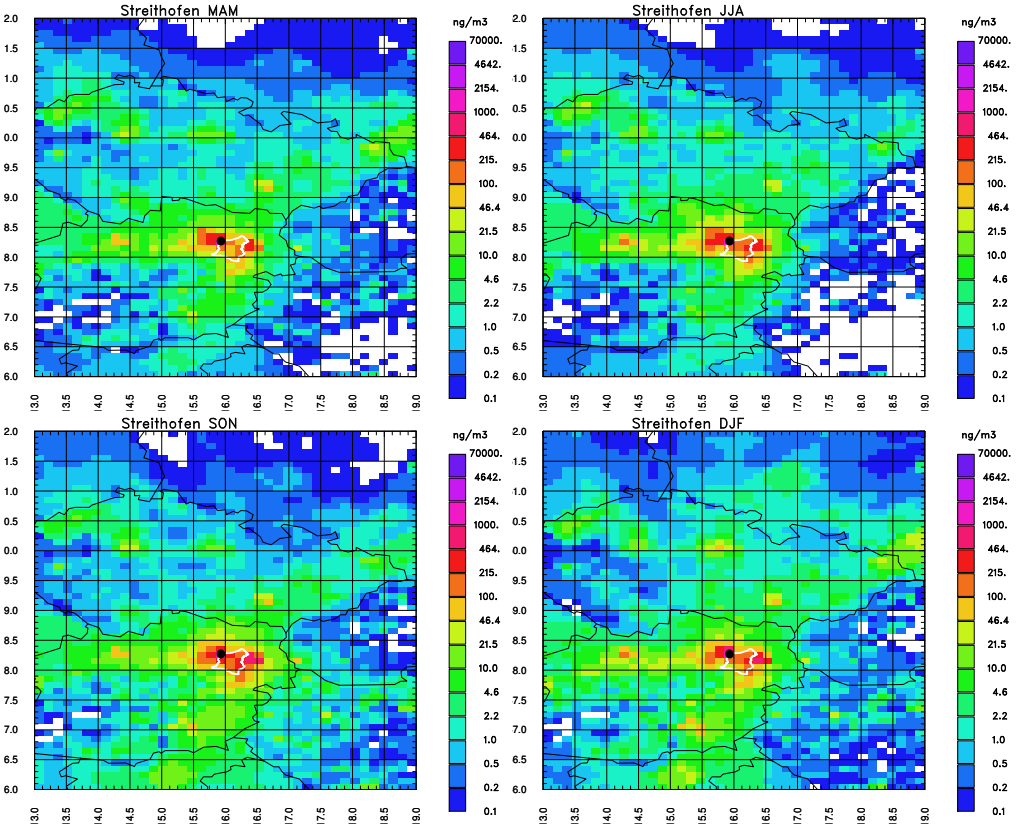

Figure 28: Geographical distribution of contributions to the NO_x concentration at Streithofen for the four seasons in ngm^{-3} per grid cell for the nest domain.

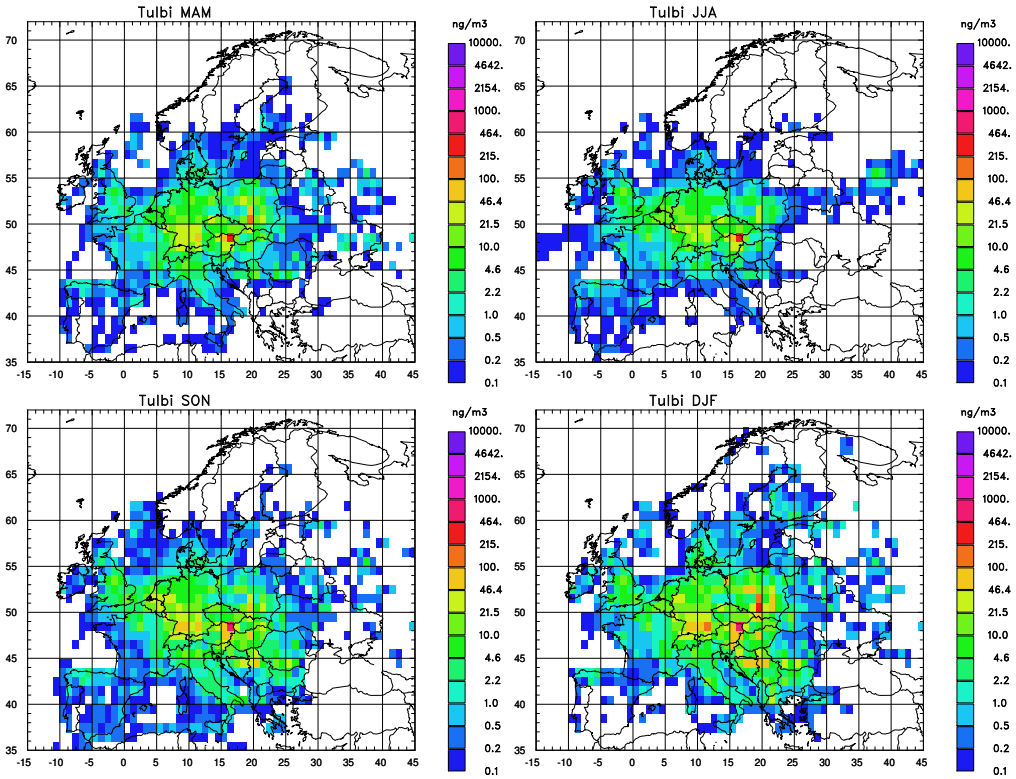

Figure 29: Geographical distribution of contributions to the NO_x concentration at Tulbinger Kogel for the four seasons in ngm^{-3} per grid cell.

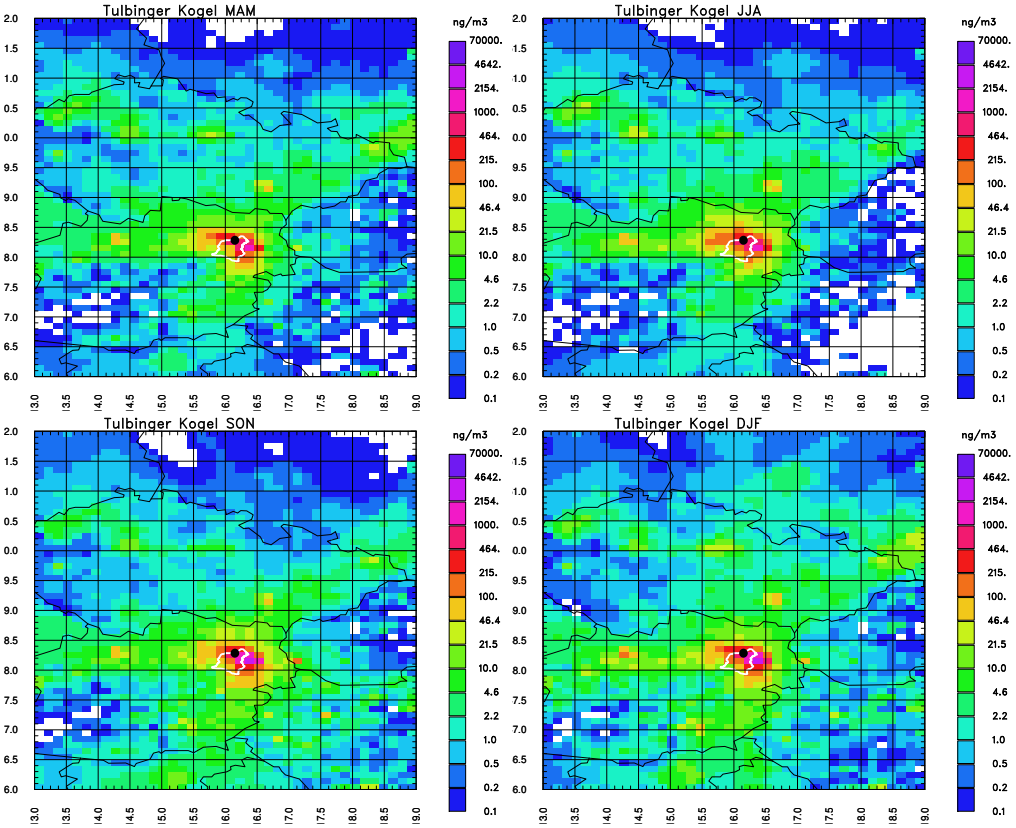

Figure 30: Geographical distribution of contributions to the NO_x concentration at Tulbinger Kogel for the four seasons in ngm^{-3} per grid cell for the nest domain.

The maps discussed above show the absolute contributions. In order to be able to see how much the strongest emission regions contribute, also plots of the cumulative geographical contribution in percent have been produced. For this purpose, the contributions from each grid are expressed as a percentage of the sum over the whole domain (nest or coarse), then these values are sorted starting with the strongest contributing cell, and added up to form a cumulative distribution.

As NO_x concentrations are mostly originating within the nest domain, only this domain has been evaluated (Fig. 31). We can see, for example, that at Hermannskogel the single grid cell to the southeast of the site alone is good for 30% of the modelled annual mean concentration, and all of Vienna together for 40%. 90% are obtained with the contributions from the more populated areas of eastern Austria until about Wels (a bit west of Linz), a few agglomerations in the Czech Republic and major sources in Slovenia, plus Bratislava and a few grid cells in Hungary. Most of the map remains white, indicating that these regions only contribute in the last 10%. Tulbinger Kogel and Bad Vöslau are also dominated by the Vienna emissions, whereas Forsthof and Streithofen all need contributions from Vienna as well as the Tullnerfeld and parts of the Wienerwald itself to reach 40%. We can also find out that Linz and Graz have the biggest relative importance at Forsthof, where they are included in the region needed to reach 40%.

The situation is quite different for SO_2. At Forsthof (Fig. 32), the red and orange grid cells (required to reach 40%) of the coarse domain are scattered between central Poland and southern Romania. The 60% region includes industrial centres of England as well as Etna. In the nest domain, the influence of Slovenia dominates, followed by Linz, Tullnerfeld, Vienna, Bratislava, and the area north of Budapest. We can clearly distinguish the industrialised regions of Austria and Czech republic as well. At Hermannskogel (Fig. 33), due to the dominant influence of Vienna, there is less geographical scatter. Also for SO_2, Vienna is good for 40% of the total contributions from the nest domain. On the coarse domain, Poland and the Balkan are most important.

4.3.4 Origin of air pollution for clean and polluted episodes

From all the 8760 hours in the year 2003, the 2% (175) with the highest and lowest simulated concentrations were extracted and the geographical pattern of the contributions plotted. This allows to see the characteristics of polluted and the clean episodes. First, NO_x episodes are discussed, followed by SO_2 episodes.

At Bad Vöslau (Fig. 34), pulluted episodes are characterised by strong contributions from the region of Vienna. They are combined at least in some cases with advection from the northeast (adding pollution from southern Poland) or from southeast (from Bosnia and Serbia). On the other hand, for the clean episodes it is striking that they have practically no contribution from the region east of the station at least in the nest domain; the air comes from northerly, westerly or southerly directions without picking up much pollution (the reason must be high wind velocities and/or transport at higher levels with subsidence close to the station).

At Forsthof (Fig. 35), the results are very similar, except that in the polluted case we see contributions from Tullnerfeld and higher contributions from the region of the three-country point Czech Republic – Slovakia – Poland.

At Hermannskogel (Fig. 36), the strongest pollution is associated as with strong contributions from Vienna and its surroundings as well as the region of Graz, with possible addition of emissions either from the southeast or from southern Germany. In the clean case, the air is mainly coming from northwest.

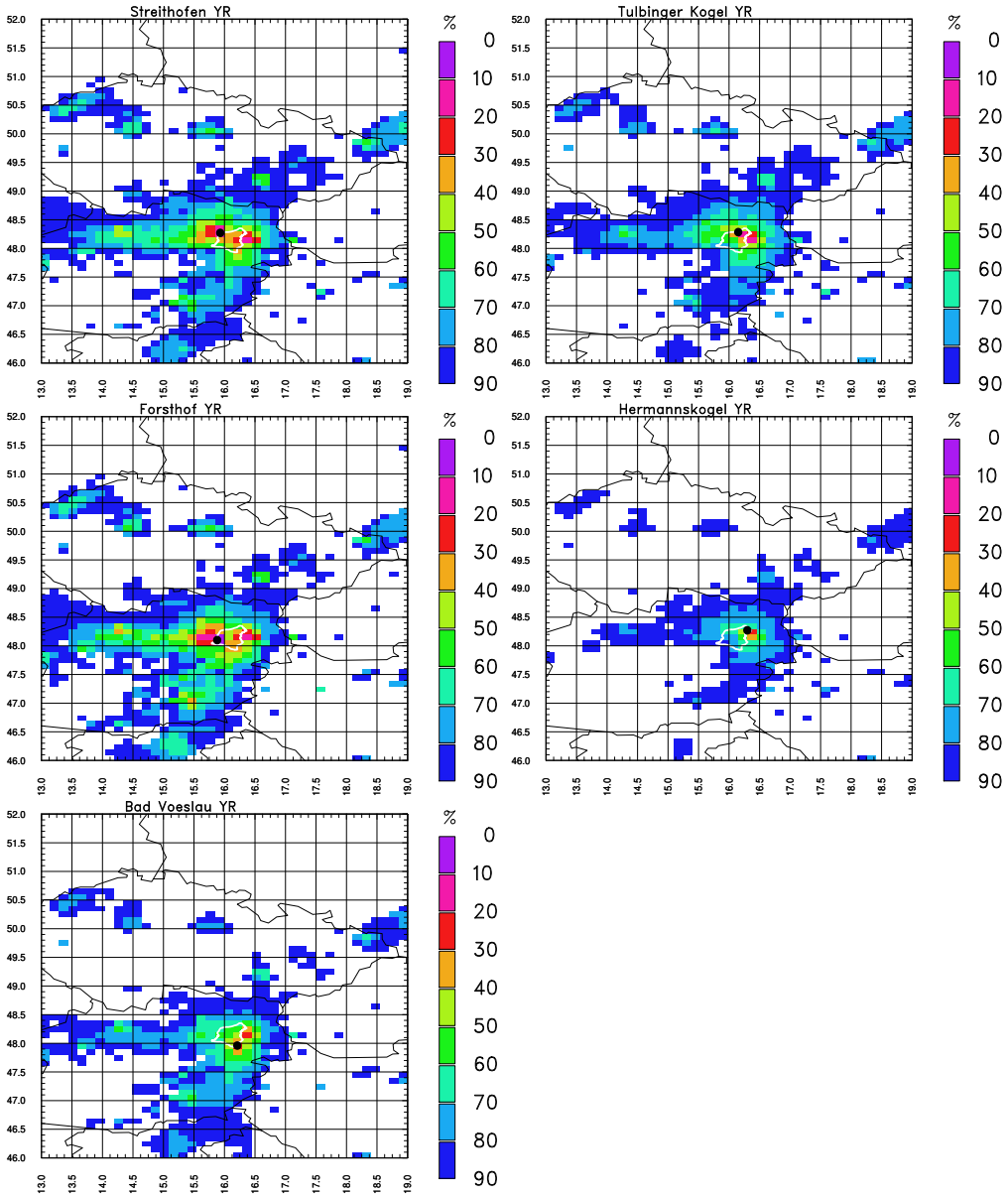

Figure 31: Cumulative geographical contributions to the mean annual NO_x concentrations from the nest domain at Streithofen, Tulbinger Kogel, Forsthof, Hermannskogel, and Bad Vöslau.

At Streithofen (Fig. 37), pollution episodes are obviously associated primarily with southeasterly flows and characterised by strong emissions from Vienna and surroundings, Graz and Budapest as well as additional contributions from southern Poland or the southeast, in this case including even northern Greece. Interestingly, the Po Basin in Italy also shows up as one of the more important contributors. Clean episodes are associated mainly with westerly or northwesterly flows where only Tullnerfeld and Linz are important emitters, to some extent southern Germany. In the clean cases, the air has not passed over the Vienna region.

At Tulbinger Kogel (Fig. 38), the polluted episodes have strong emissions from the region of Vienna and even the Wienerwald (A1 motorway), with additions from Hungary or Graz, Bosnia, Serbia, southern Romania and/or southern Poland. In the clean cases, the air comes from the northwest sector, picking up pollution from Tullnerfeld and southern Germany.

High SO_2 episodes at Hermannskogel (Fig. 40) are linked to high contributions from Vienna which is

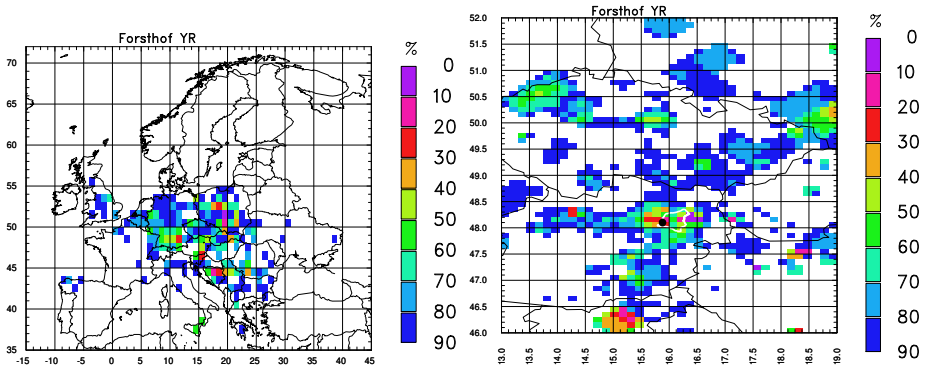

Figure 32: Cumulative geographical contributions to the mean annual SO_2 concentrations in the coarse (left) and nest (right) domain at Forsthof. Details see text

also the most relevant source region. Thus, a southeasterly wind is required, which leads to further contributions from Hungary in the nest domain and from almost all the Balkan countries in the coarse domain. Southern Poland is also visible but not dominant. The low SO_2 episodes are characterised by air arriving from the western sector. The nest domain map indicates two "clean pathways" through Czech Republic.

At Forsthof, the high SO_2 episodes still have an important contribution from Vienna, but this is not as dominant and in the nest domain, southern Poland, Vienna/Hungary, and Slovenia have similar chances to produce extreme SO_2 concentrations. Also on the coarse grid, both Poland and the Balkan appear as source regions. The clean episodes are rather more bound to the southwest wind sector, probably due to possible influence from Dürnrohr with northwesterly winds which would prevent really clean conditions there.

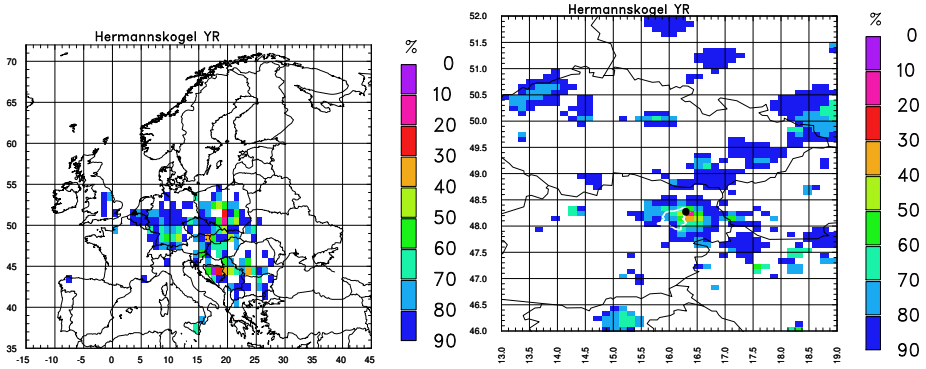

Figure 33: Cumulative geographical contributions to the mean annual SO_2 concentrations in the coarse (left) and nest (right) domain at Hermannskogel. Details see text

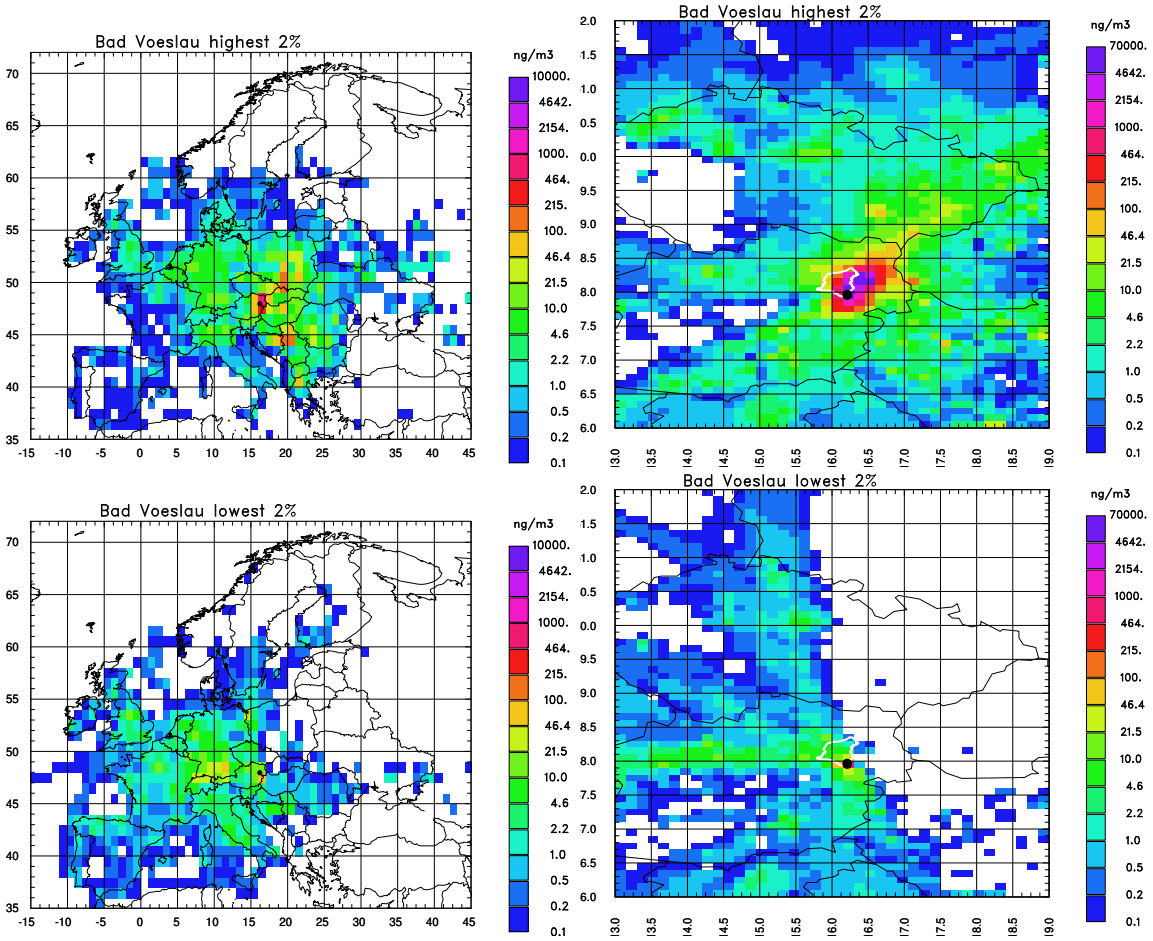

Figure 34: Geographical distribution of contributions to the NO_x concentration at Bad Vöslau for the upper (top) and lower (bottom) 2% of values. Left column: coarse grid, right column: fine grid.

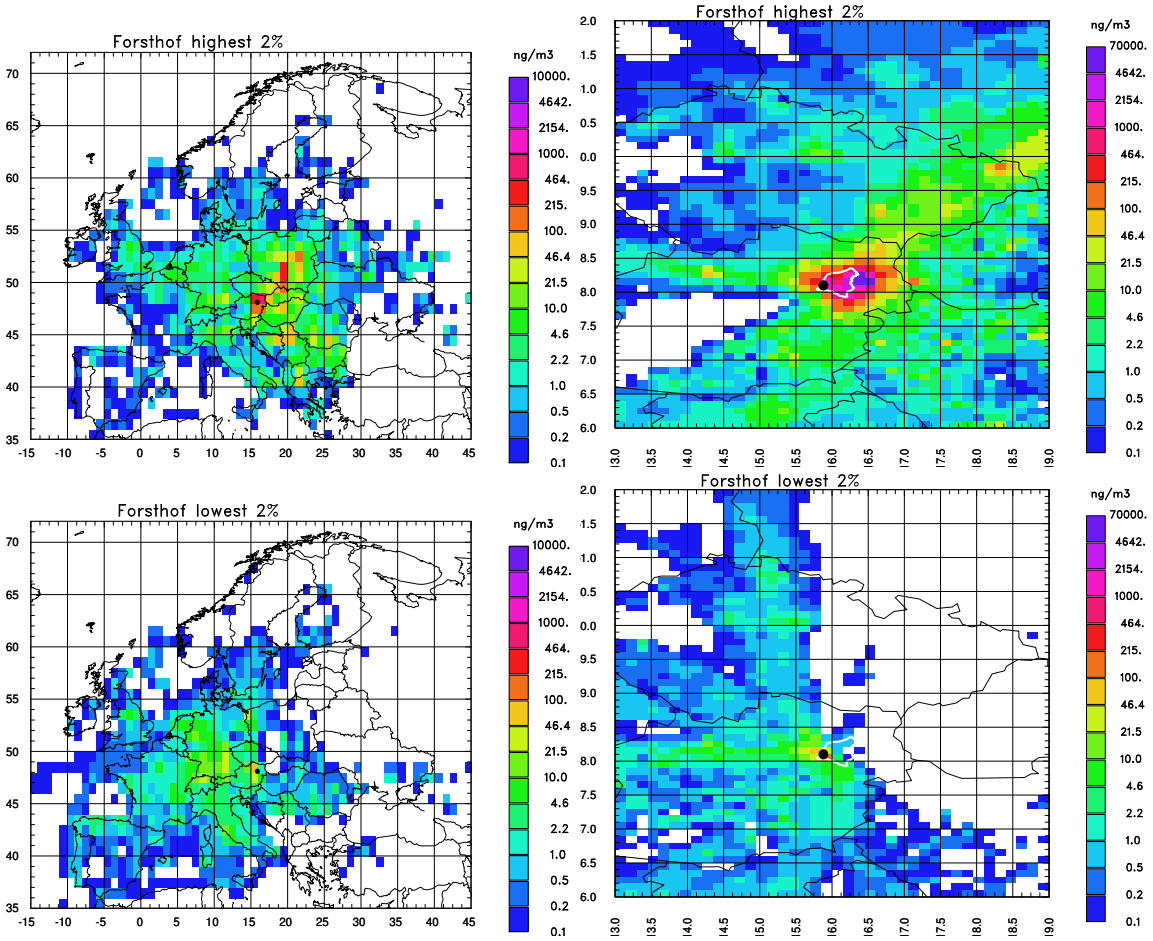

Figure 35: Geographical distribution of contributions to the NO_x concentration at Forsthof for the upper (top) and lower (bottom) 2% of values. Left column: coarse grid, right column: fine grid.

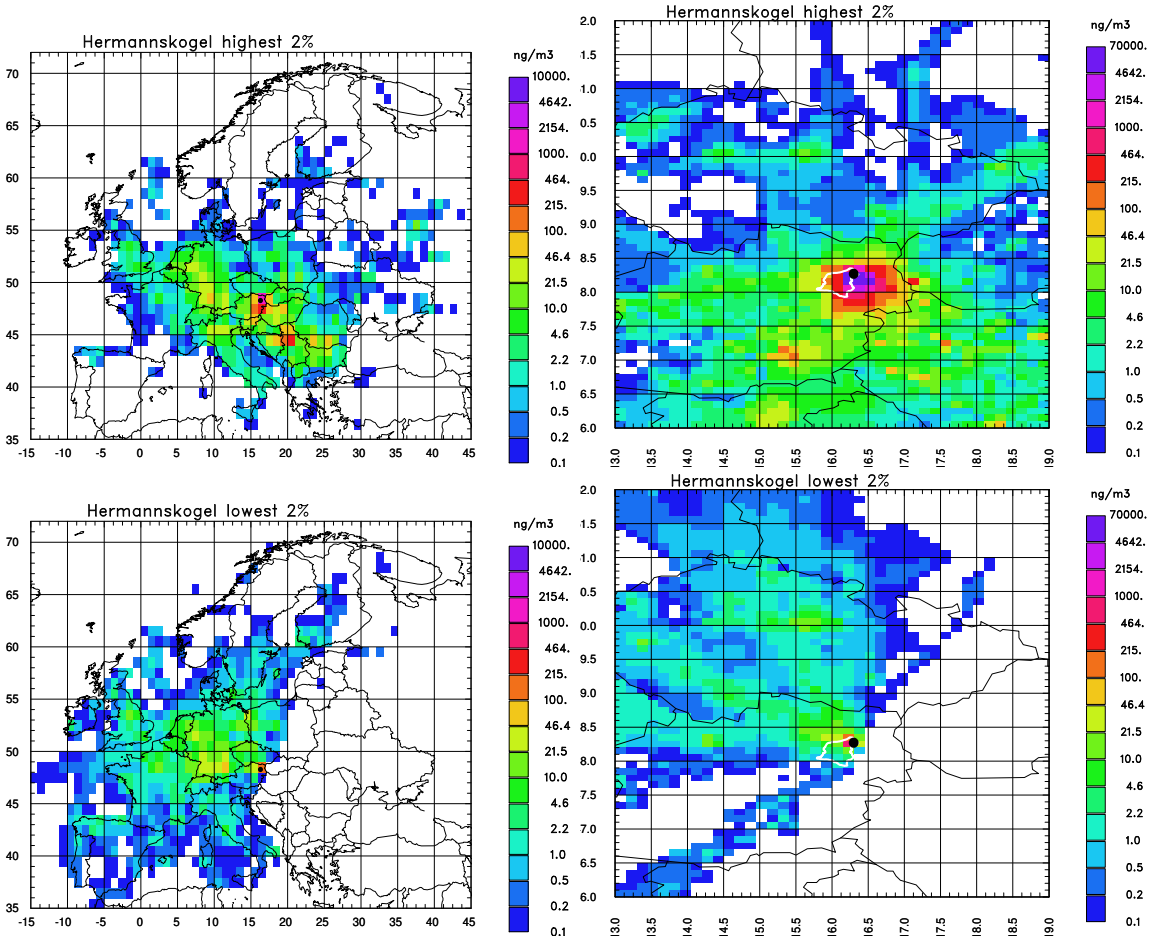

Figure 36: Geographical distribution of contributions to the NO_x concentration at Hermannskogel for the upper (top) and lower (bottom) 2% of values. Left column: coarse grid, right column: fine grid.

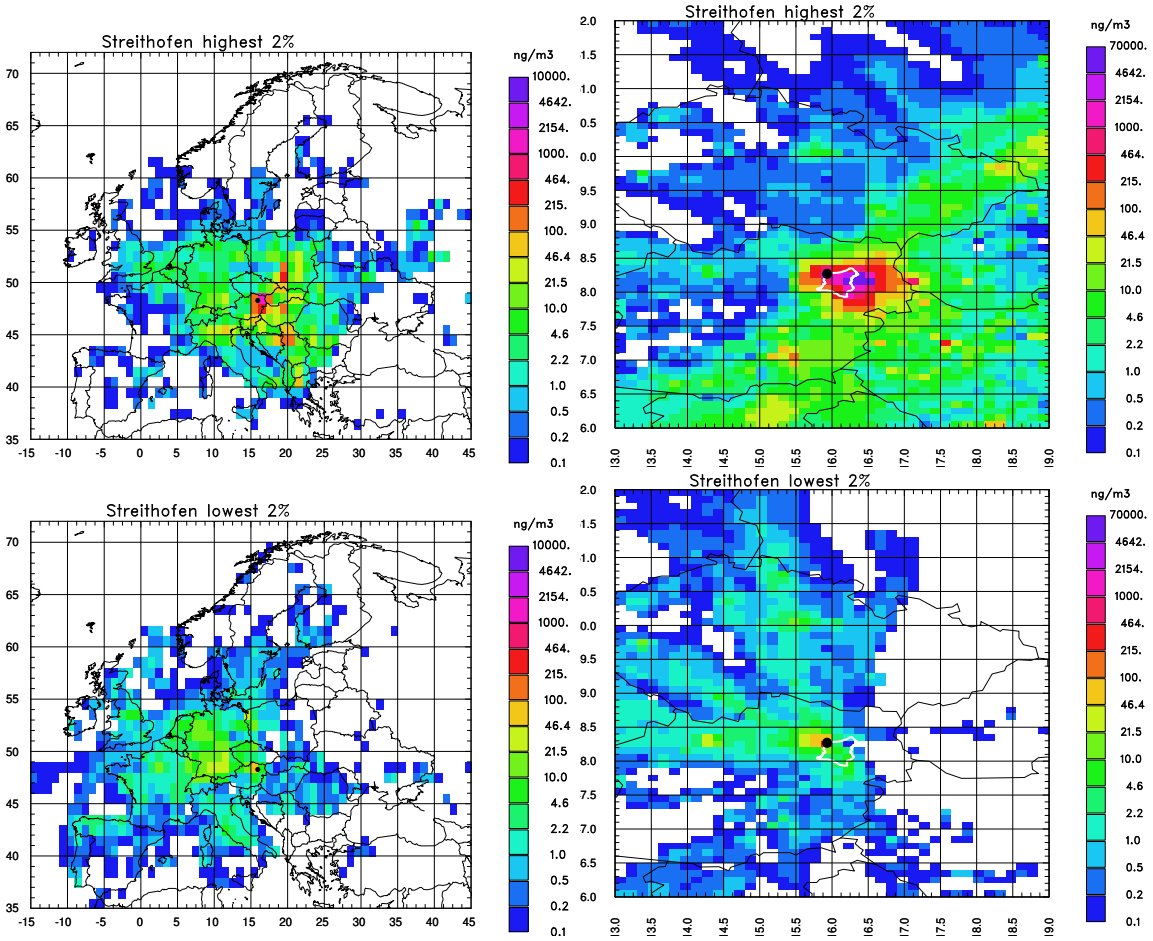

Figure 37: Geographical distribution of contributions to the NO_x concentration at Streithofen for the upper (top) and lower (bottom) 2% of values. Left column: coarse grid, right column: fine grid.

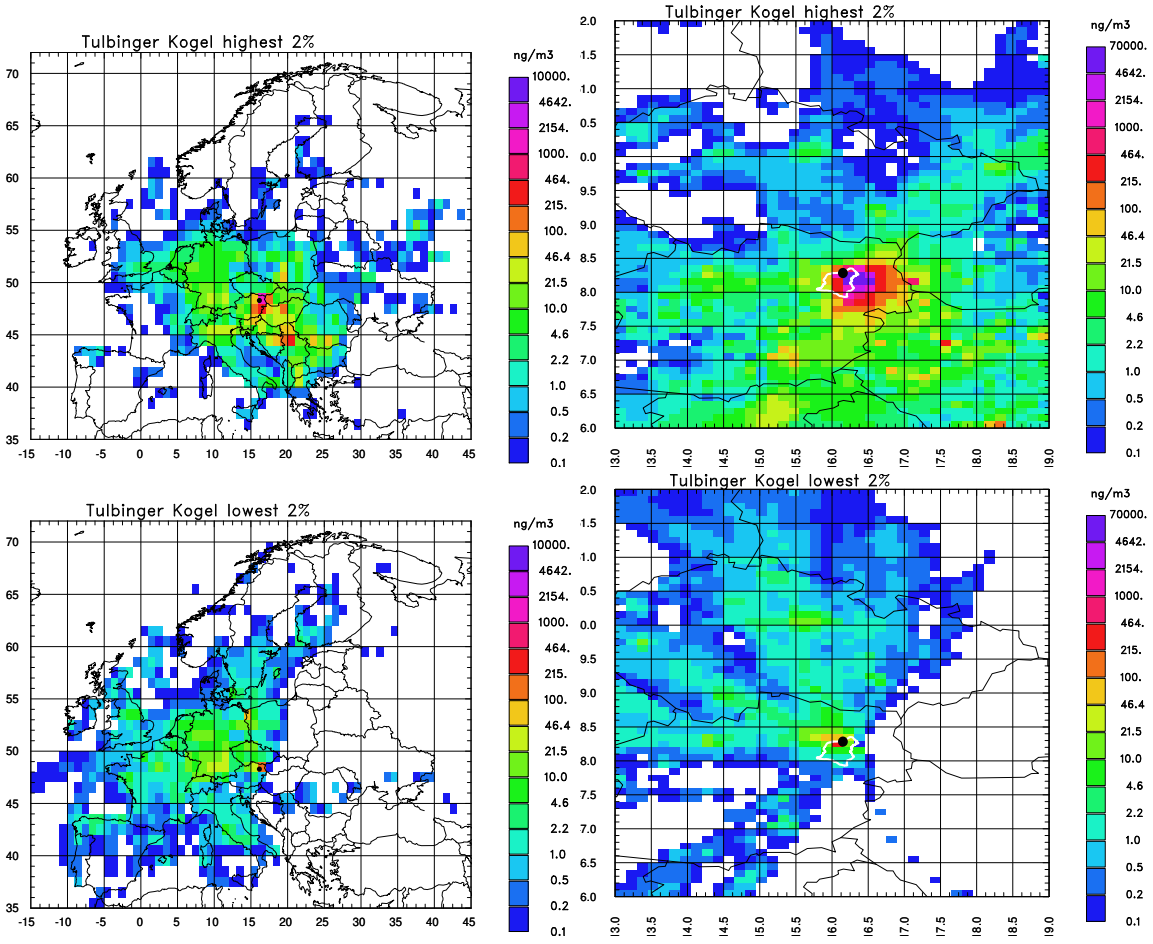

Figure 38: Geographical distribution of contributions to the NO_x concentration at Tulbinger Kogel for the upper (top) and lower (bottom) 2% of values. Left column: coarse grid, right column: fine grid.

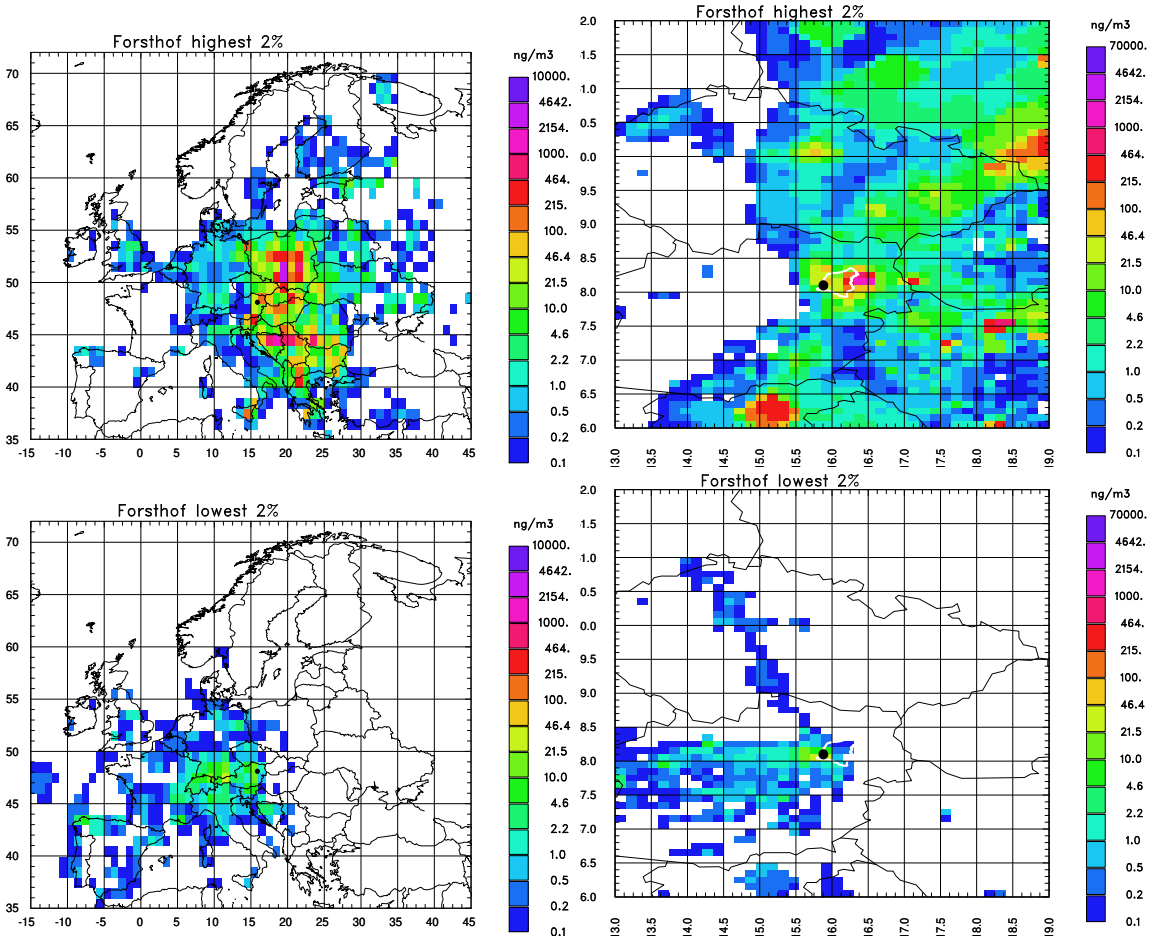

Figure 39: Geographical distribution of contributions to the SO_2 concentration at Forsthof for the upper (top) and lower (bottom) 2% of values. Left column: coarse grid, right column: fine grid.

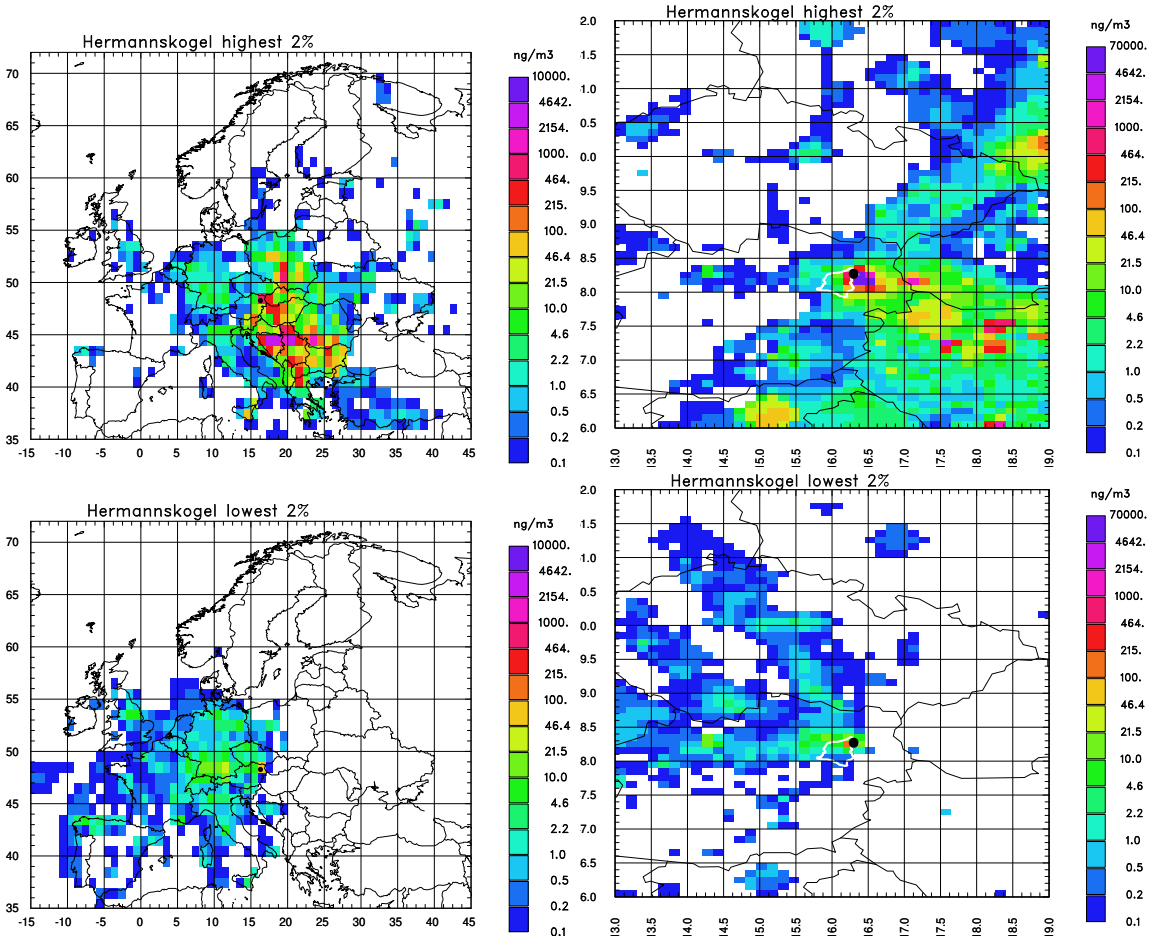

Figure 40: Geographical distribution of contributions to the SO_2 concentration at Hermannskogel for the upper (top) and lower (bottom) 2% of values. Left column: coarse grid, right column: fine grid.

5 Conclusions and outlook

5.1 Conclusions

This study aimed at a detailed quantification of the origin of the air pollution arriving at the monitoring sites in or near to the Wienerwald Biosphere reserve. Therefore, a Lagrangian particle dispersion model that simulates transport and dispersion very well was applied. In the receptor-oriented set-up used, it provides detailed information about the contribution from each of the emission grid cells. This comes, however, at the cost of not having detailed chemistry in the model. Emission data for Austria and some neighbouring countries had high resolution while emissions outside this area and the meteorological input data from the operational ECMWF global model were relatively coarse.

A comparison between observed and modelled concentrations of nitrous oxides (NO_x) and sulphur dioxide (SO_2) shows that this approach is roughly reproducing the observed features. There are strong indications that the observed skill is limited mainly due to the coarse meteorological input data. Chemical transformation probably plays only a minor role, especially as a large fraction of the NO_x is coming from sources at short distances.

It is valuable to see that even for a topography with amplitudes of a few hundred of metres, not high mountains, a coarse model is insufficient to reproduce well the pollution transport and diffusion.

Therefore, quantitative interpretation of the source regions for the observed pollution has to be taken with caution. One should also note that a period of one year as applied here does not yield generally valid climatological values, although the main characteristics and their seasonal variation should have been captured.

The following features were found:

- The NO_x burden to the Wienerwald stations is caused to a very large extent by sources within the region, especially from the Vienna basin and from distributed road traffic sources.
- The SO_2 burden is caused mainly by distant sources, especially in Poland, Slovenia and Balkan countries. The Vienna basin is an important source as well.
- The location of the stations with respect to the Wienerwald hills has a significant influence on the relevance of sources, even in the simulation with the coarse meteorological input data. Sites in the western part have more influence from sources in the north and west, while the sites on the eastern side are more influenced from the east and south.
- In summer, close sources are more relevant than in other seasons. Areas in the west and northwest contribute most in spring and autumn, those in the south and southeast in autumn and winter, while southern Poland contributes more in winter and spring.

Seibert and Skomorowski (2008) have conducted a somewhat similar study for the site Schauinsland in the Black Forest. This station is about 1000 m above the Rhine Valley, and the elevation of the Black Forest mountains above their surroundings is considerably higher than that of the Wienerwald hills. In this study, a nested meteorological model was used to simulate selected episodes with very high resolution, down to 0.67 km. However, available emission inventories were not highly resolved. Although in some weather situations with strong vertical gradients or with thermally driven valley and slope winds, the high-resolution model was clearly superior to a coarse-resolution simulation, the

overall results were also not very satisfactory. Thus it is an important conclusion that for modelling of air pollution in complex terrain we need high resolution in the meteorological fields as well as in the emission inventory.

5.2 Outlook

Since 26 January 2010, the operational ECMWF model has a resolution of about 16 km, compared to the 50 km used in the present study. The Austrian meteorological service, ZAMG, is running its operational limited-area model presently at a resolution of 5 km, initialised by ECMWF data. Such data sets will help to better describe the meteorological conditions in a topographically structured region such as the Wienerwald and the Vienna basin. However, as indicated by results with a Eulerian chemistry-transport model (B. Krüger, BOKU-Met, personal communication), the impact of topography on the model bias found in this study can still be identified in 5 km resolution simulations, although being weaker. For the future, it is therefore mandatory to use the growing computer powers for improving the resolutions. A project in the framework of the Austrian Climate Research Programme, HIRMOD,[1] is under way to look into these possibilities, including simulations for the Vienna basin – Wienerwald area.

[1] High-Resolution Atmospheric Modelling in Complex Terrain for Future Climate Simulations, URL `http://www.boku.ac.at/met/envmet/hirmod.html`

Acknowledgements

This project was kindly financed by the "Man and Biosphere" programme of the Austrian Academy of Sciences (ÖAW).

Access to ECMWF data was granted through the Special project "Modelling of tracer transport".

We thank the Magistrat der Stadt Wien, MA 22, and the Amt der niederösterreichischen Landesregierung, Abt. Umweltschutz, for the making available the air quality monitoring data.

Bibliography

Eckhardt, S. (2001), Luftqualität und Herkunftsanalyse von Luftschadstoffen im Nationalpark Neusiedler See – Seewinkel. Diplomarbeit, Univ. f. Bodenkultur Wien. Available from: https://zidapps.boku.ac.at/abstracts/oe_list.php?paID=3&paSID=2869&paSF=-1&paCF=0&paLIST=0&language_id=DE.

Eckhardt, S., A. J. Prata, P. Seibert, K. Stebel, and A. Stohl (2008), Estimation of the vertical profile of sulfur dioxide injection into the atmosphere by a volcanic eruption using satellite column measurements and inverse transport modeling. *Atmos. Chem. Phys.* **8**, 3881–3897. Available from: http://www.atmos-chem-phys.net/8/3881/2008/acp-8-3881-2008.html.

Gomiscek, B., A. Frank, S. Puxbaum, H.and Stoppera, O. Preining, and H. Hauck (2004), Case study analysis of PM burden at an urban and a rural site during the AUPHEP project. *Atmos. Environ.* **38**(24), 3935–3948.

Krüger, B. C. (2004), Aktionsplan für Sofortmaßnahmen gemäß § 15 Ozon-Gesetz – Meteorologisch chemische Modellrechnungen. Endbericht, Institut für Meteorologie, Universität für Bodenkultur Wien. Available from: http://www.wien.gv.at/umweltschutz/pool/pdf/ozon-sofort.pdf.

Leder, K., H. Puxbaum, P. Kreiner, and V. Tarmann (2003), Nasse Deposition im Land Wien Oktober 02 - September 03. Report on behalf of Magistrat der Stadt Wien, MA 22, Vienna, Austria, 81 pp. Available from: http://www.wien.gv.at/ma22/pool/pdf/boden2003.pdf.

Seibert, P. and A. Frank (2004), Source-receptor matrix calculation with a Lagrangian particle dispersion model in backward mode. *Atmos. Chem. Phys.* **4**, 51–63. Available from: http://www.atmos-chem-phys.net/4/51/2004/.

Seibert, P. and P. Skomorowski (2008), Untersuchung der orographischen Besonderheiten der Probennahmestellen Schauinsland und Freiburg und deren Auswirkungen auf die Genauigkeit von adjungierten atmosphärischen Ausbreitungsrechnungen. Bundesamt für Strahlenschutz, Salzgitter / Freiburg. Schriftenreihe Reaktorsicherheit und Strahlenschutz, BMU - 2008 - 713, 194 pp. Available from: http://www.bmu.de/strahlenschutz/schriftenreihe_reaktorsicherheit_strahlenschutz/doc/41875.php.

Stohl, A. (1998), Computation, accuracy and applications of trajectories – a review and bibliography. *Atmos. Environ.* **32**(6), 947–966.

Stohl, A., T. Berg, J. F. Burkhart, A. M. Fjæraa, C. Forster, A. Herber, Ø. Hov, C. Lunder, W. W. McMillan, S. Oltmans, M. Shiobara, D. Simpson, S. Solberg, K. Stebel, J. Ström, K. Tørseth, R. Treffeisen, K. Virkkunen, and K. E. Yttri (2007), Arctic smoke – record high air pollution levels in the European Arctic due to agricultural fires in Eastern Europe in spring 2006. *Atmos. Chem. Phys.* **7**(2), 511–534. Available from: http://www.atmos-chem-phys.net/7/511/2007/.

Stohl, A., S. Eckhardt, C. Forster, P. James, N. Spichtinger, and P. Seibert (2002), A replacement for simple back trajectory calculations in the interpretation of atmospheric trace substance measurements. *Atmos. Environ.* **36**(29), 4635–4648.

Stohl, A., C. Forster, S. Eckhardt, N. Spichtinger, H. Huntrieser, J. Heland, H. Schlager, S. Wilhlelm, F. Arnold, and O. Cooper (2003), A backward modeling study of intercontinental pollution transport using aircraft measurements. *J. Geophys. Res.* **108**, 4370, doi:10.1029/2002JD002862.

Stohl, A., C. Forster, A. Frank, P. Seibert, and G. Wotawa (2005), Technical note: The Lagrangian particle dispersion model FLEXPART version 6.2. *Atmos. Chem. Phys.* **5**, 2461–2474. Available from: `http://www.atmos-chem-phys.net/5/2461/2005/`.

Stohl, A., M. Hittenberger, and G. Wotawa (1998), Validation of the Lagrangian particle dispersion model Flexpart against large-scale tracer experiment data. *Atmos. Environ.* **32**(24), 4245–4264.

Stohl, A. and D. J. Thomson (1999), A density correction for Lagrangian particle dispersion models. *Bound.-Layer Meteorol.* **90**, 155–167.

Stohl, A., G. Wotawa, P. Seibert, and H. Kromp-Kolb (1995), Interpolation errors in wind fields as a function of spatial and temporal resolution and their impact on different types of kinematic trajectories. *J. Appl. Meteorol.* **34**, 2149–2165.

Taylor, K. E. (2001), Summarizing multiple aspects of model performance in a single diagram. *J. Geophys. Res.* **106**(D7), 7183–7192.

Vestreng, V., K. Breivik, M. Adams, A. Wagener, J. Goodwin, O. Rozovskkaya, and J. M. Pacyna (2005), Inventory review 2005, emission data reported to LRTAP convention and NEC directive, initial review of HMs and POPs. Technical report EMEP MSC-W 1/2005. Available from: `http://www.emep.int/publ/reports/2005/emep_technical_1_2005.pdf`.

Winiwarter, W. and J. Züger (1996), Pannonisches Ozonprojekt, Teilprojekt Emissionen. Endbericht. OEFZS-A-3817, Austrian Research Centers, Seibersdorf.

Wotawa, G., L.-E. DeGeer, P. Denier, M. Kalinowski, H. Toivonen, R. D'Amours, F. Desiato, J.-P. Issartel, M. Langer, P. Seibert, A. Frank, C. Sloan, and H. Yamazawa (2003), Atmospheric transport modelling in support of CTBT verification – overview and basic concepts. *Atmos. Environ.* **37**(18), 2529–2537. Available from: `http://www.sciencedirect.com/science/article/B6VH3-48DXMP5-1/2/3b053bfb9d6aa208f7c2d82cf3588c93`.

Zechmeister, H. G., A. Hanus-Illnar, V. Krommer, I. Roder, and S. Scharf (2007), Monitoring von Luftschadstoffen (NOx und SO2, Schwermetall-, Stickstoff-, Schwefel- und PAH-Depositionen) mittels Moosen im "Biosphärenpark Wienerwald". Final Report. Available from: `http://epub.oeaw.ac.at/?arp=0x00144d22`.

Appendices

A Time series of modelled and observed concentrations

On the following pages, the modelled and observed time series of NO_x and – where available – SO_2 for the year 2003 are shown. Observations are plotted as green lines. Note that there are some data gaps. The modelled values are plotted as coloured areas, where the blue area represents the contribution from the nest domain and the red area, on top of the blue one, the contribution from the coarse domain (without the area of the nest domain, of coarsse). Thus the top of the red area represents the total modelled concentration. The temporal resolution is one hour.

2003 Month 01 Part 1

Bad Vöslau NOx

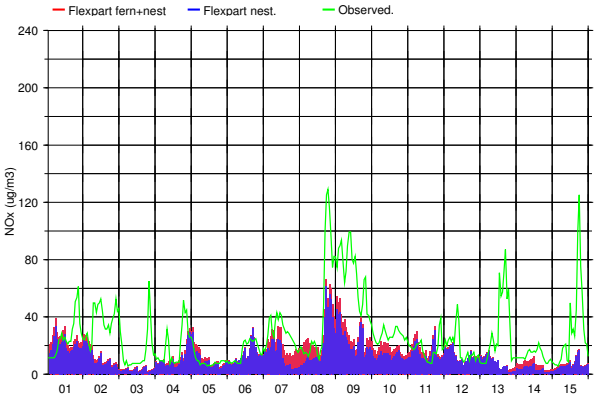

Streithofen NOx

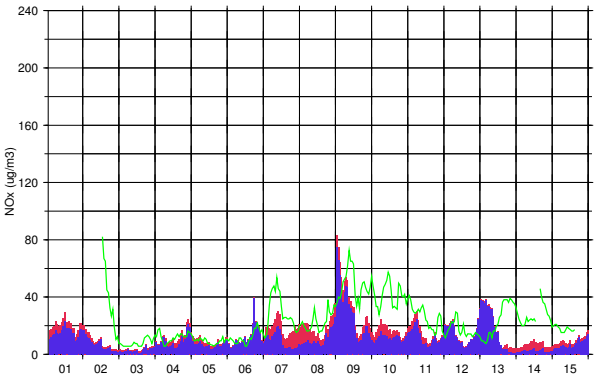

Tulbingerkogel NOx

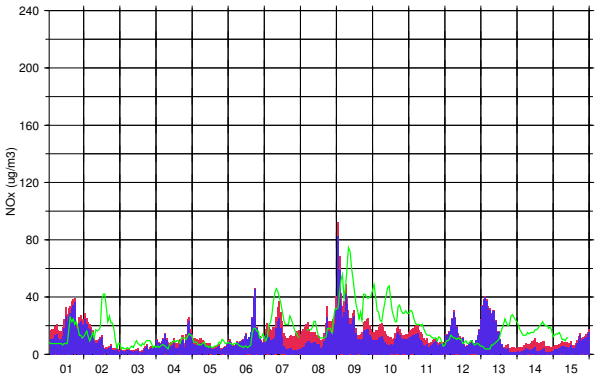

Forsthof NOx

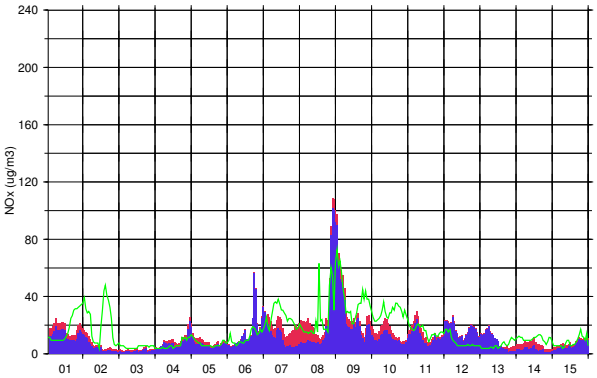

Hermannskogel NOx

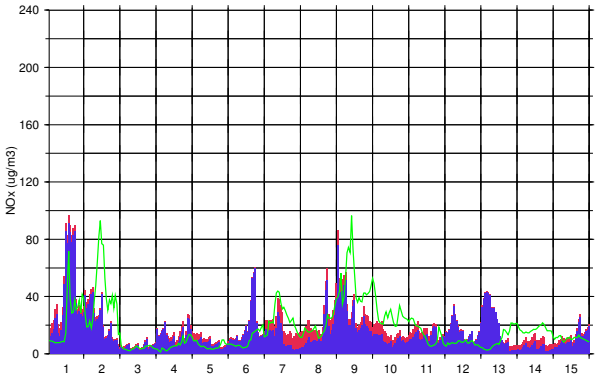

Forsthof SO2

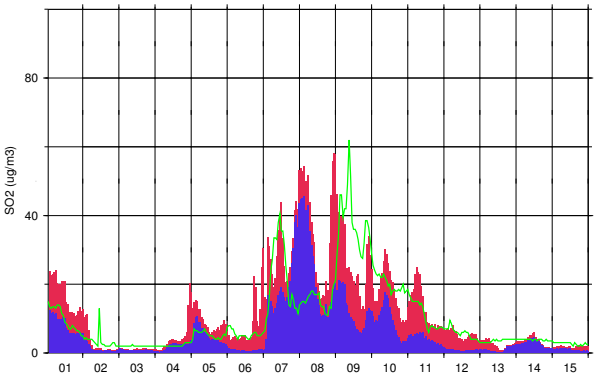

Hermannskogel SO2

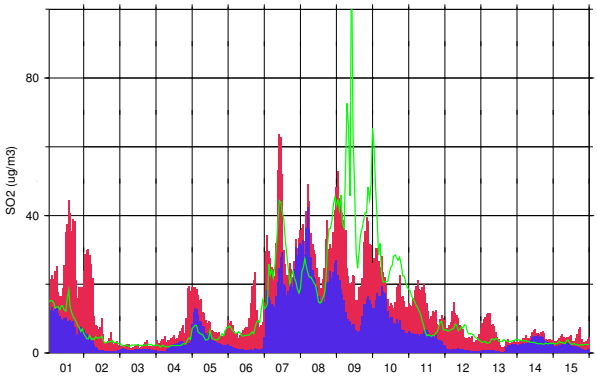

2003 Month 01 Part 2

Bad Vöslau NOx

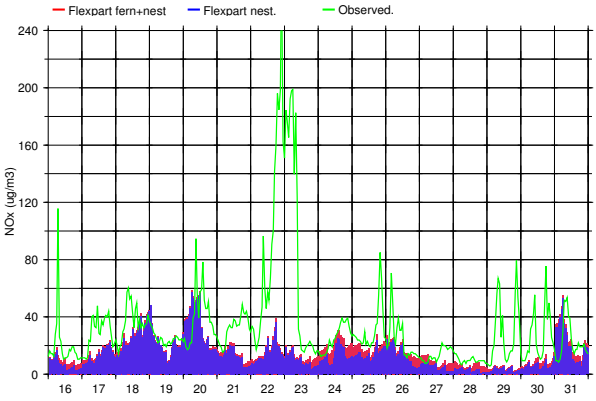

Streithofen NOx

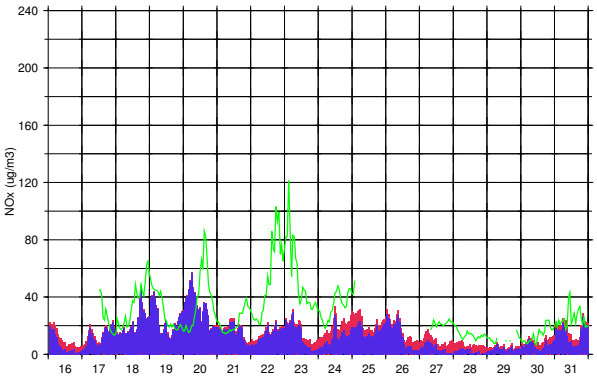

Tulbingerkogel NOx

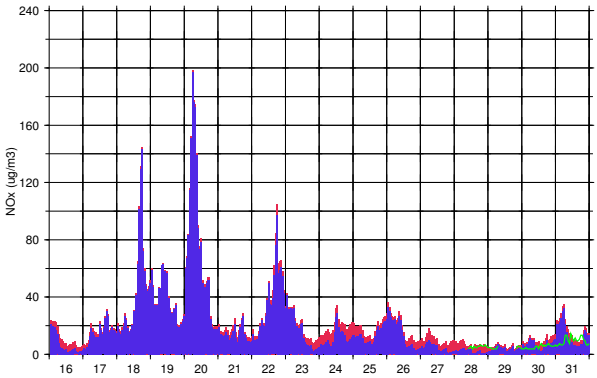

Forsthof NOx

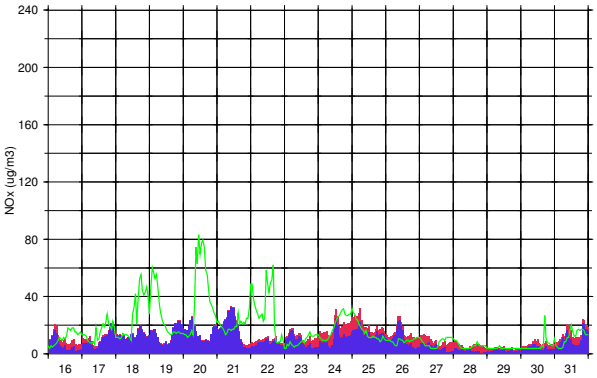

Hermannskogel NOx

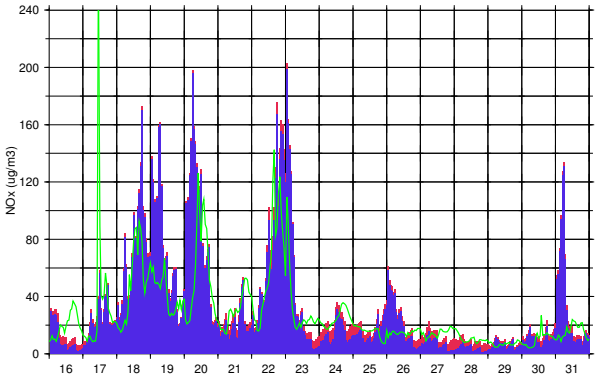

Forsthof SO2

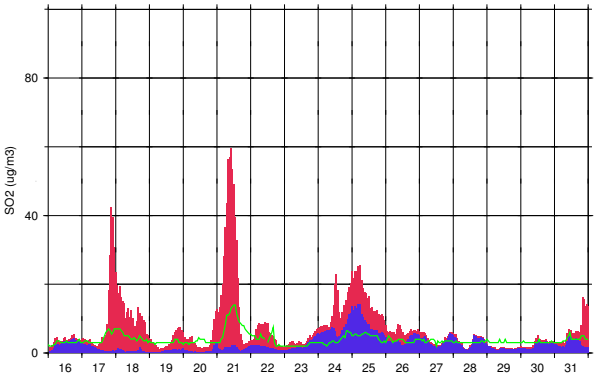

Hermannskogel SO2

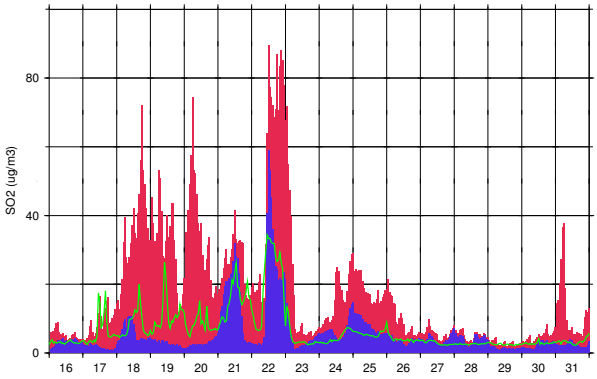

2003 Month 02 Part 1

Bad Vöslau NOx

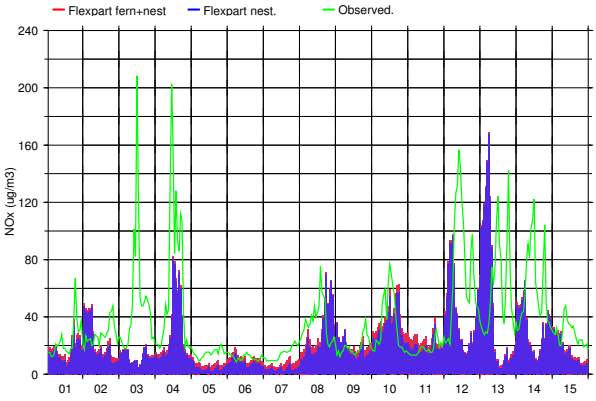

Streithofen NOx

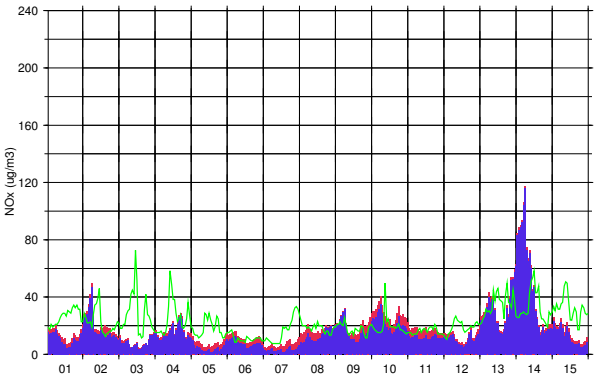

Tulbingerkogel NOx

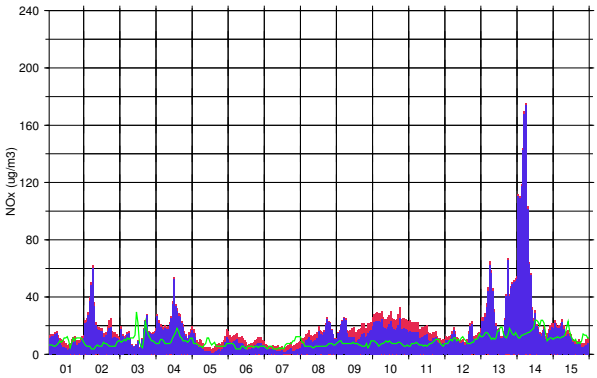

Forsthof NOx

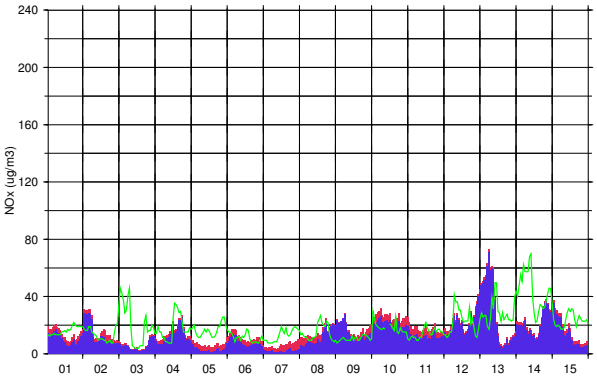

Hermannskogel NOx

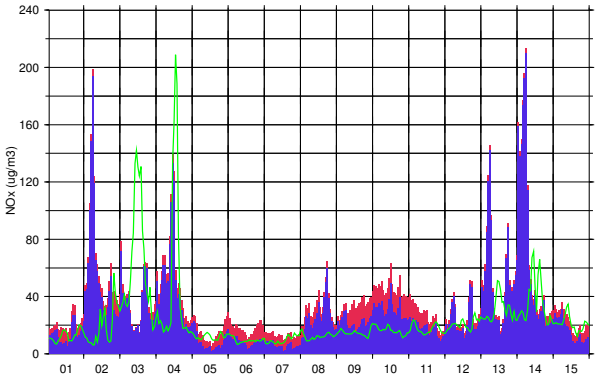

Forsthof SO2

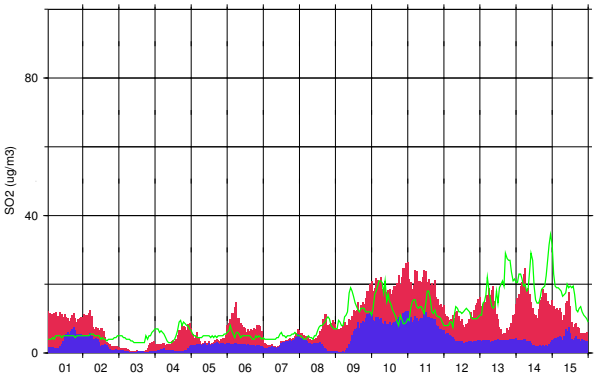

Hermannskogel SO2

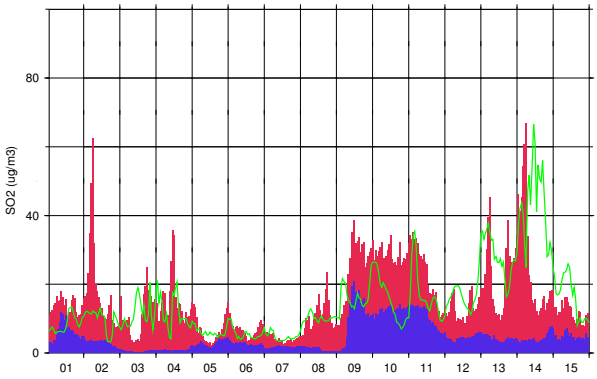

2003 Month 02 Part 2

Bad Vöslau NOx

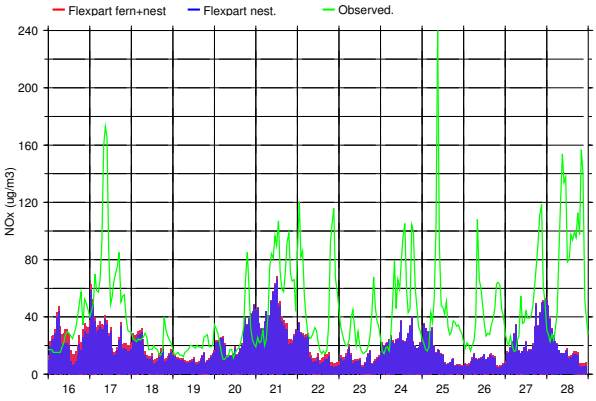

Streithofen NOx

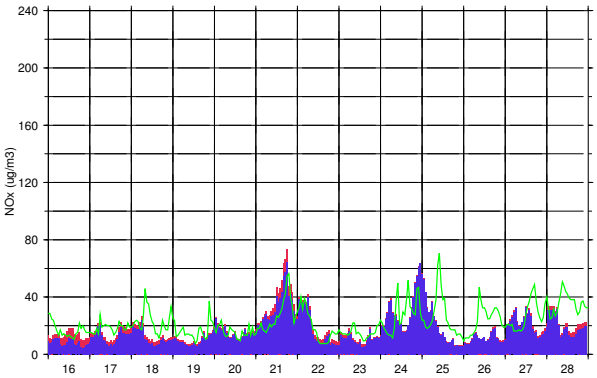

Tulbingerkogel NOx

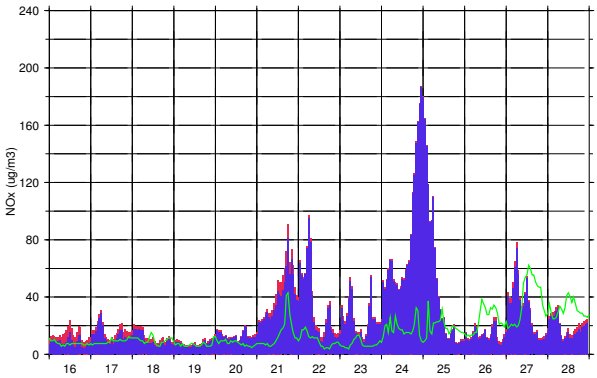

Forsthof NOx

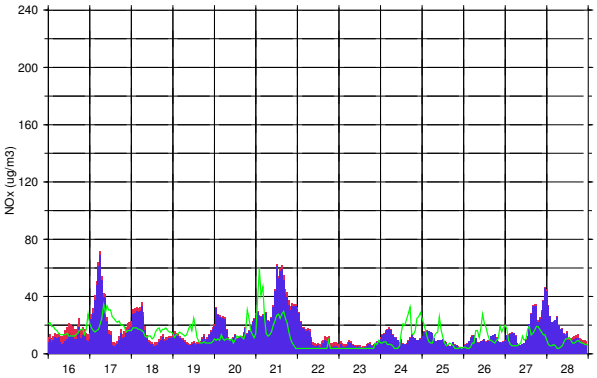

Hermannskogel NOx

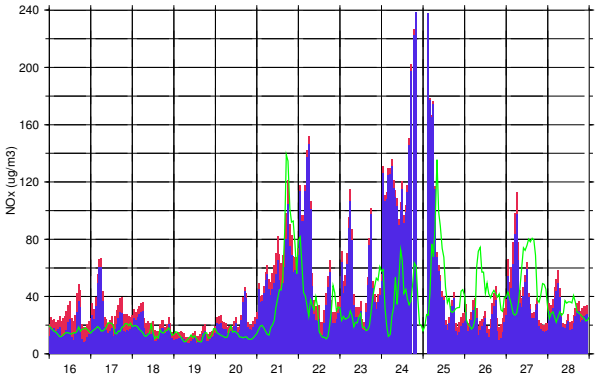

Forsthof SO2

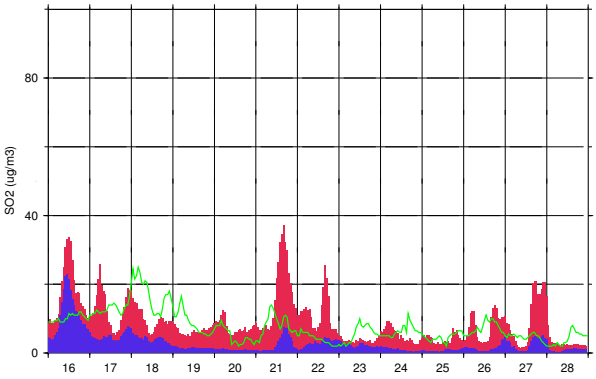

Hermannskogel SO2

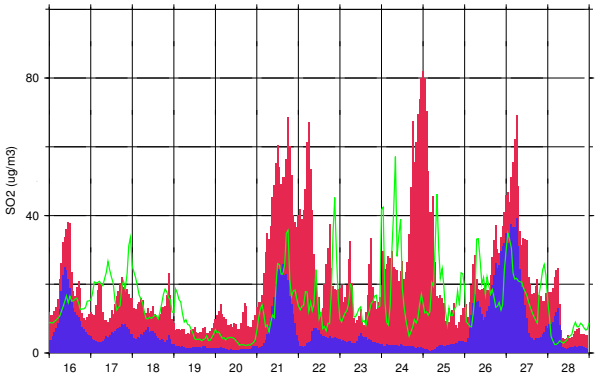

2003 Month 03 Part 1

Bad Vöslau NOx

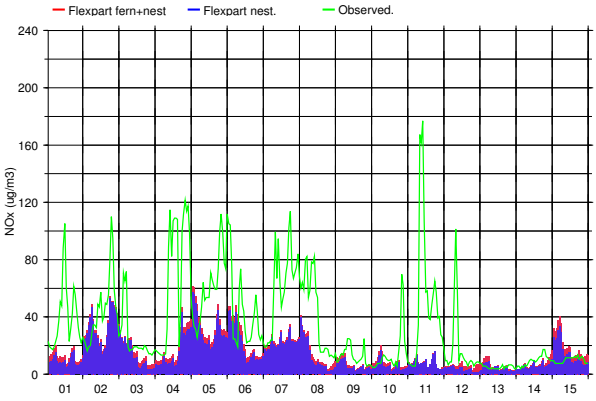

Streithofen NOx

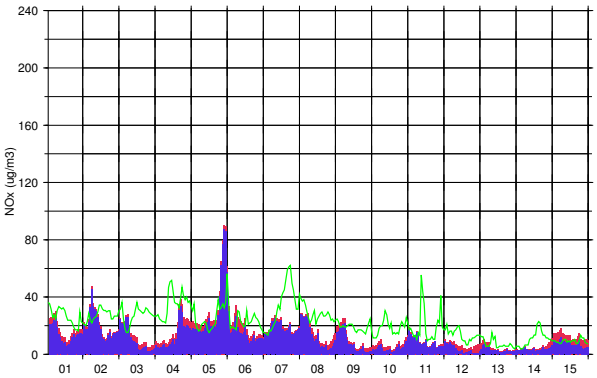

Tulbingerkogel NOx

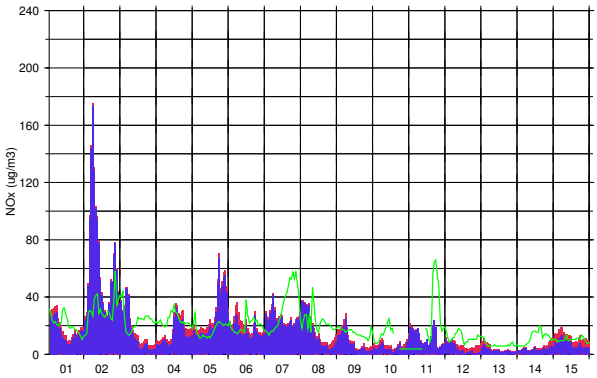

Forsthof NOx

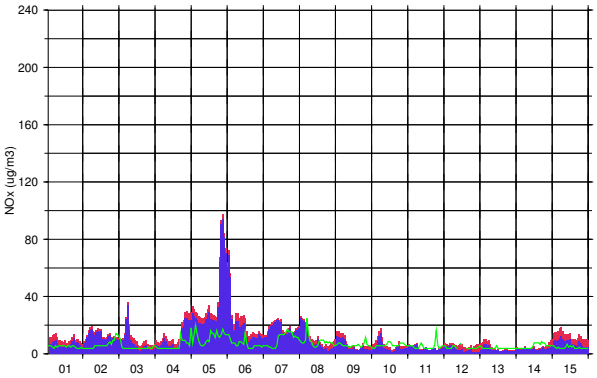

Hermannskogel NOx

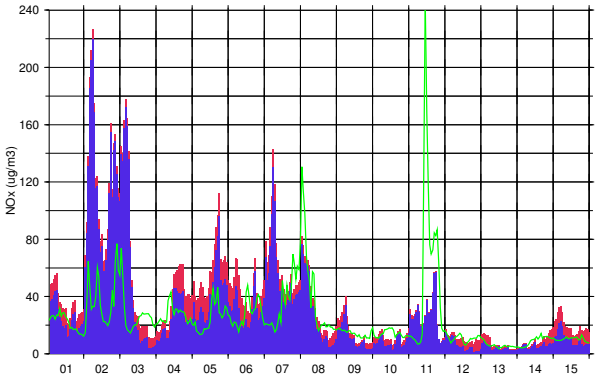

Forsthof SO2

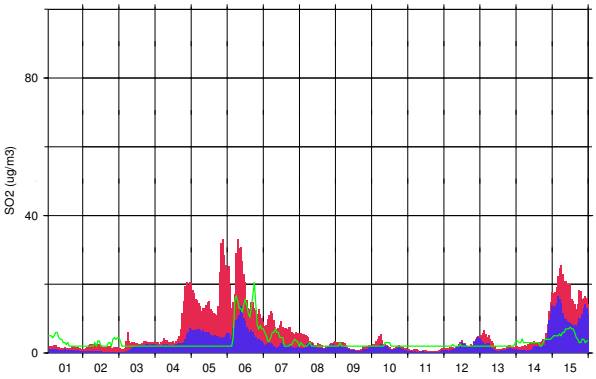

Hermannskogel SO2

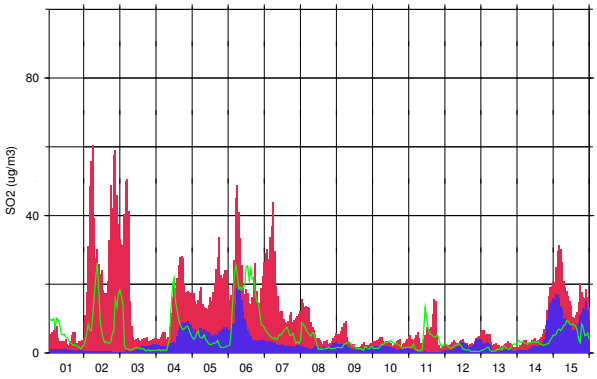

2003 Month 03 Part 2

Bad Vöslau NOx

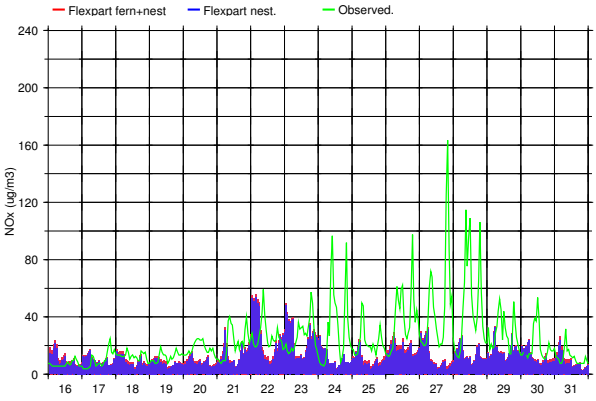

Streithofen NOx

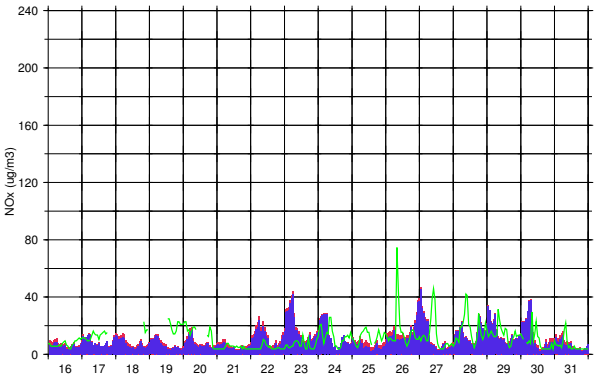

Tulbingerkogel NOx

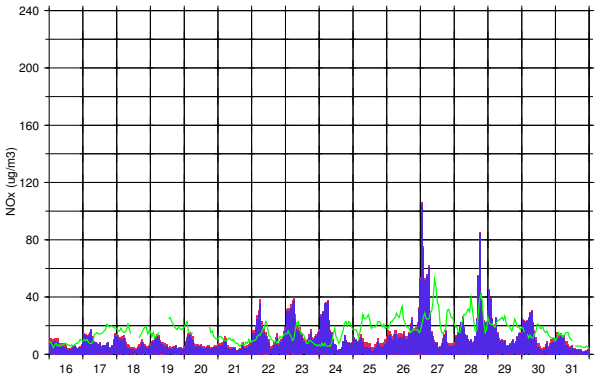

Forsthof NOx

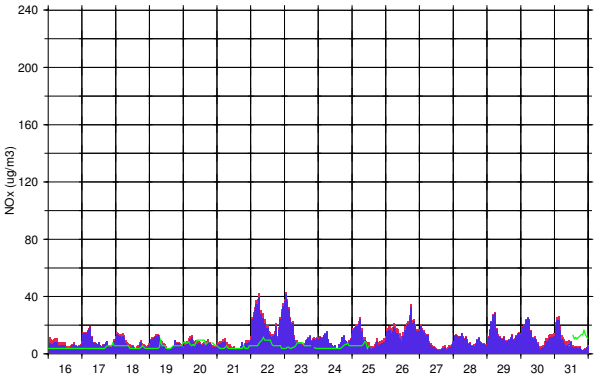

Hermannskogel NOx

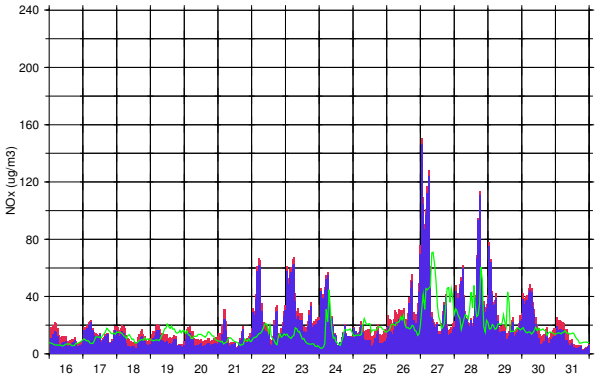

Forsthof SO2

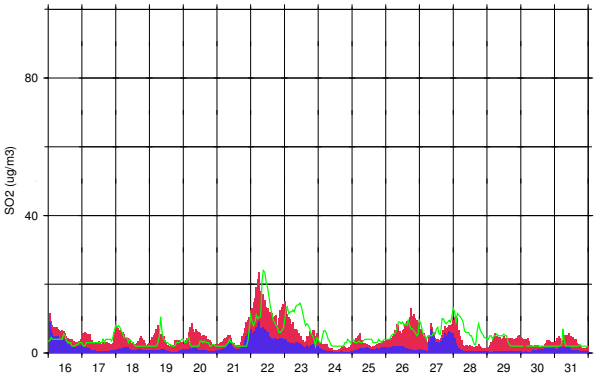

Hermannskogel SO2

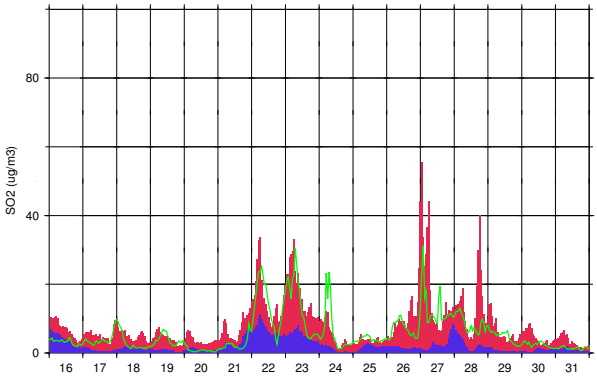

2003 Month 04 Part 1

Bad Vöslau NOx

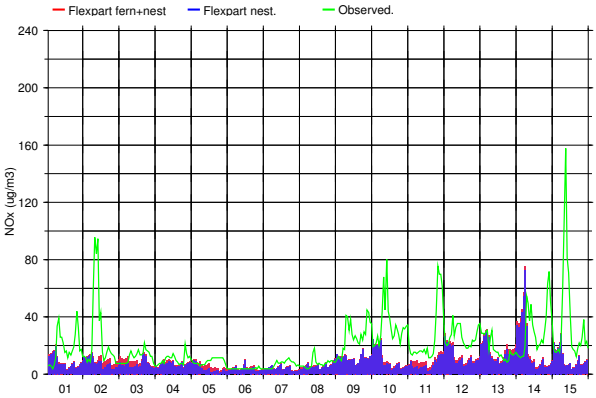

Streithofen NOx

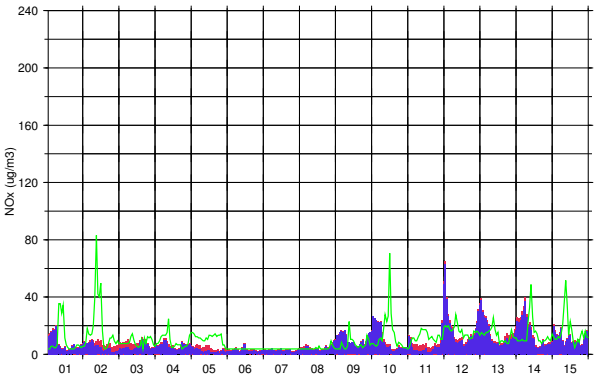

Tulbingerkogel NOx

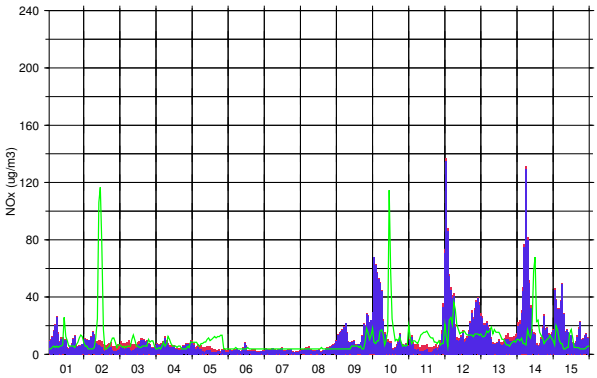

Forsthof NOx

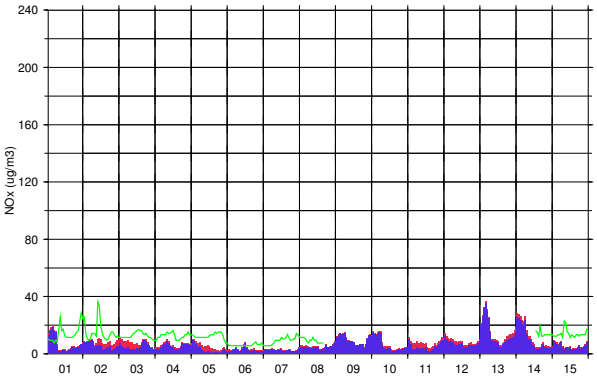

Hermannskogel NOx

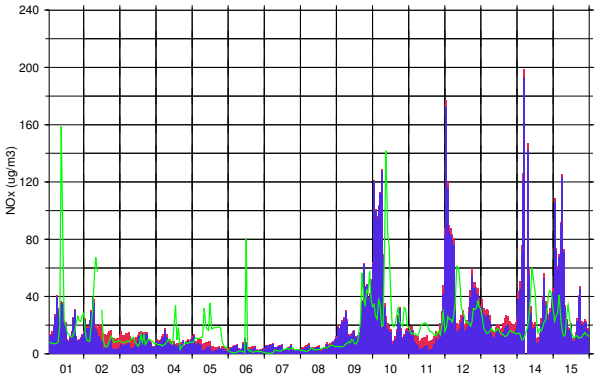

Forsthof SO2

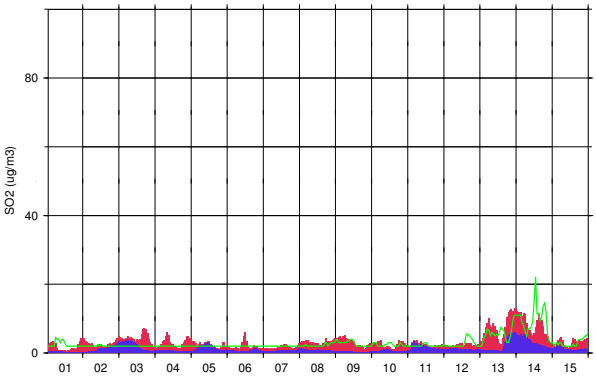

Hermannskogel SO2

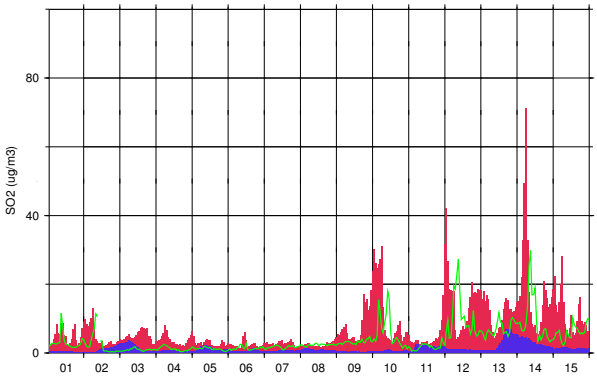

2003 Month 04 Part 2

Bad Vöslau NOx

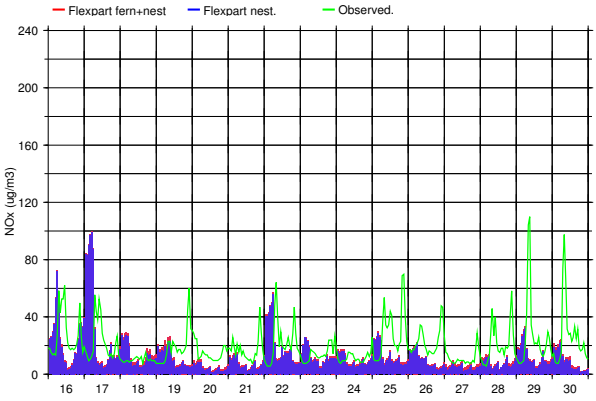

Streithofen NOx

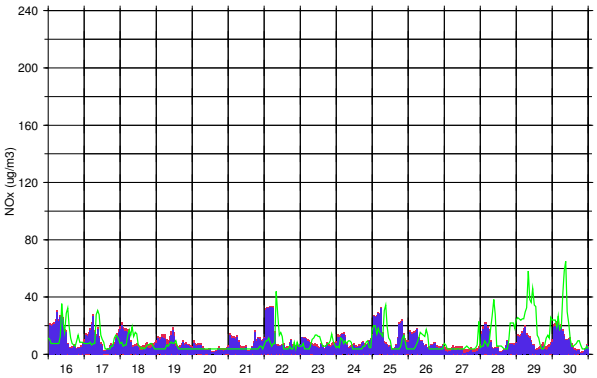

Tulbingerkogel NOx

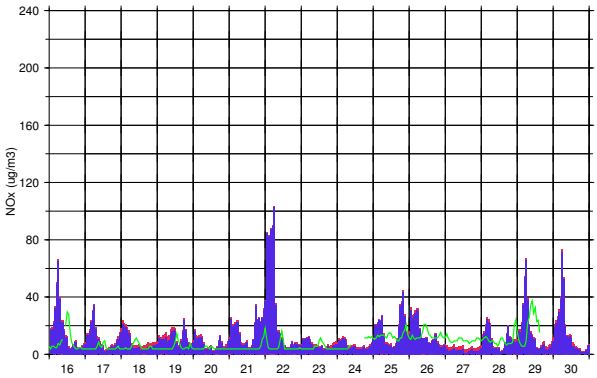

Forsthof NOx

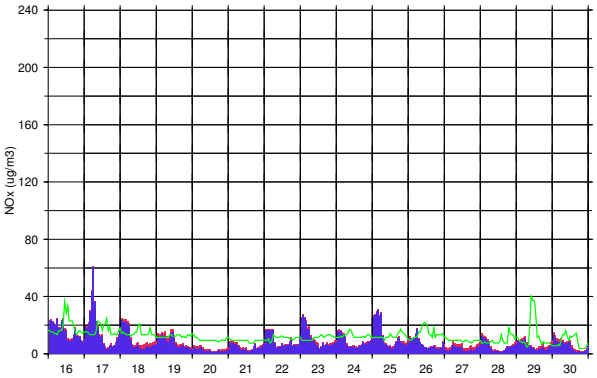

Hermannskogel NOx

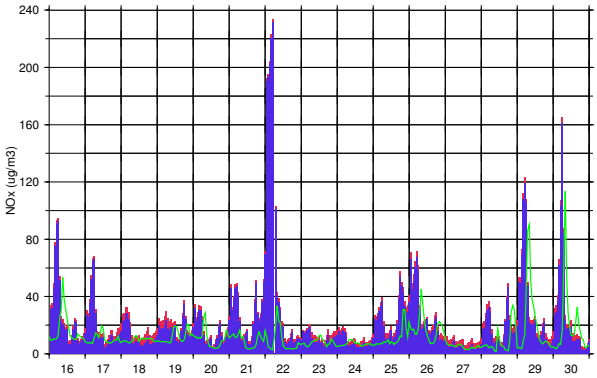

Forsthof SO2

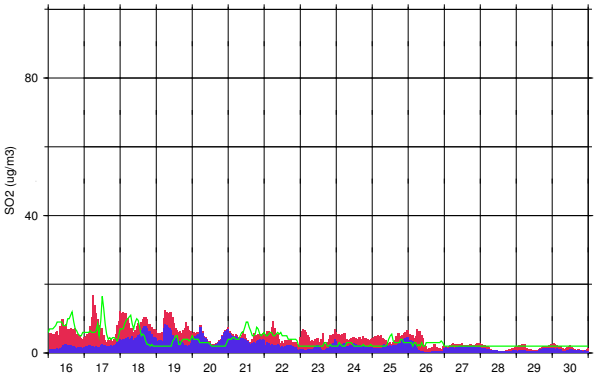

Hermannskogel SO2

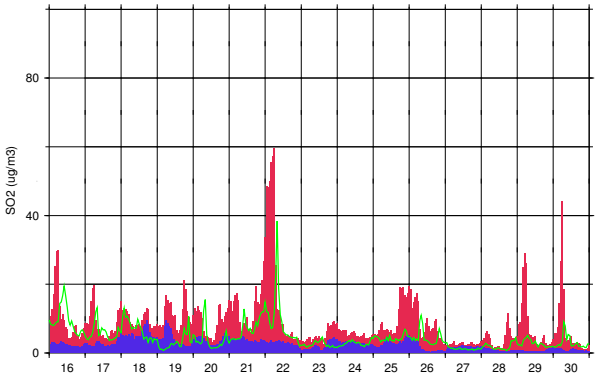

2003 Month 05 Part 1

Bad Vöslau NOx

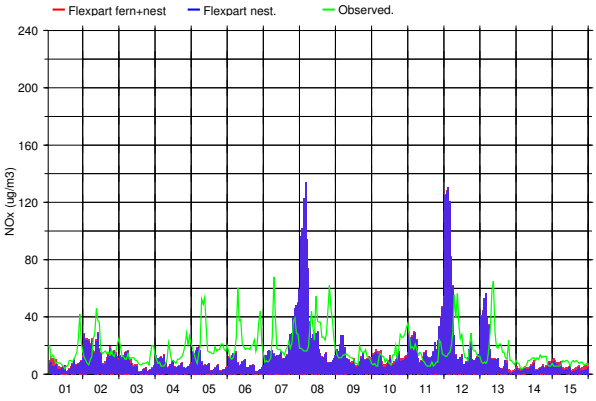

Streithofen NOx

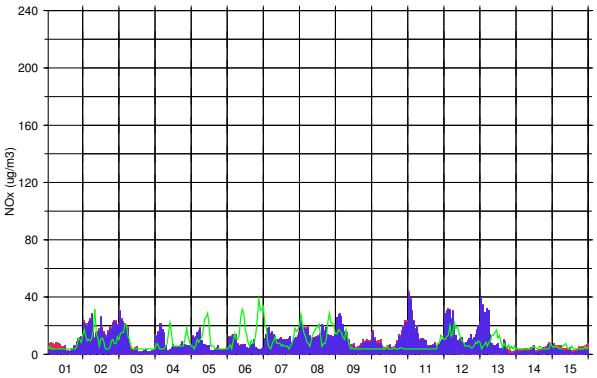

Tulbingerkogel NOx

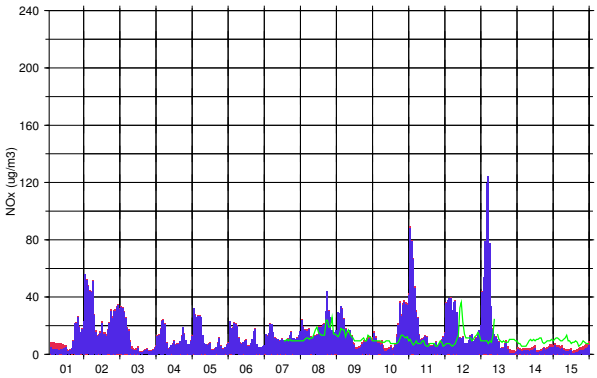

Forsthof NOx

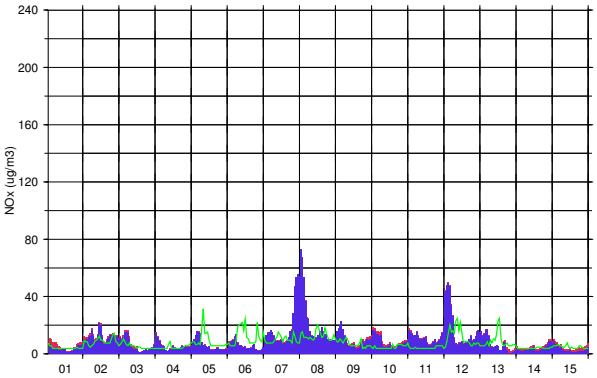

Hermannskogel NOx

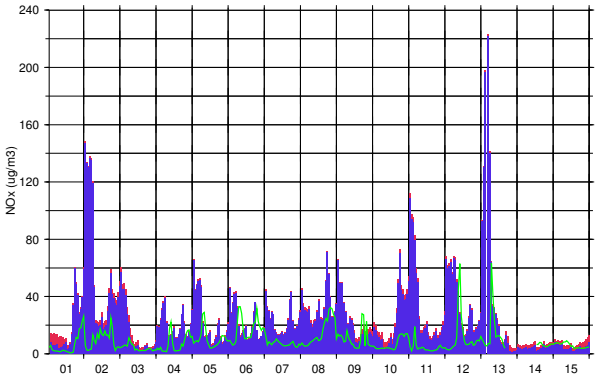

Forsthof SO2

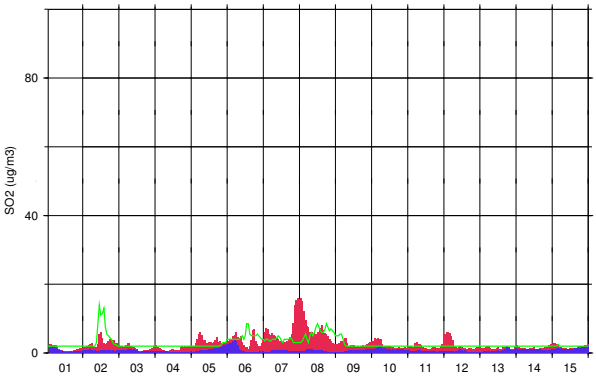

Hermannskogel SO2

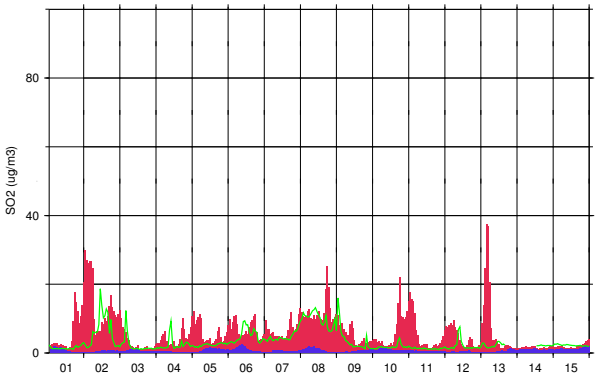

2003 Month 05 Part 2

Bad Vöslau NOx

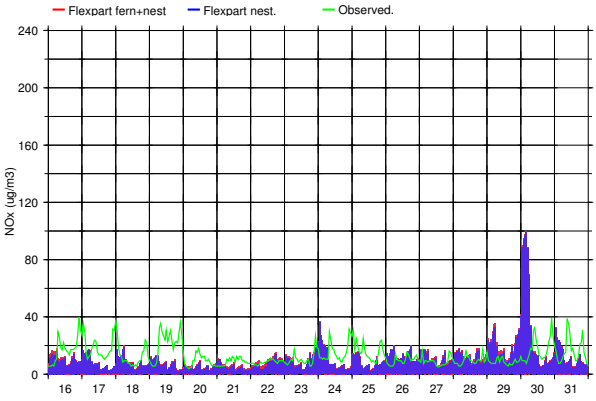

Streithofen NOx

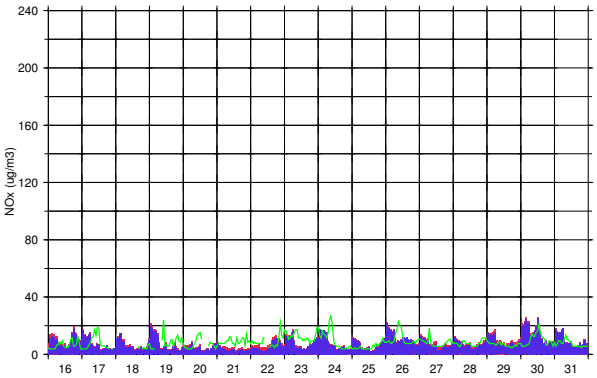

Tulbingerkogel NOx

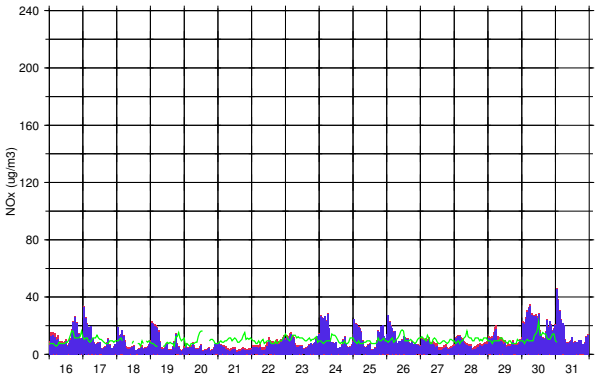

Forsthof NOx

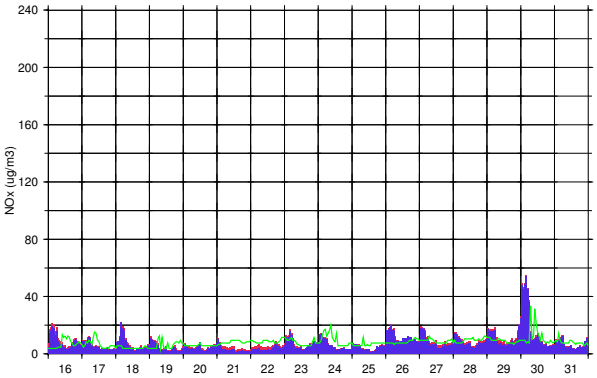

Hermannskogel NOx

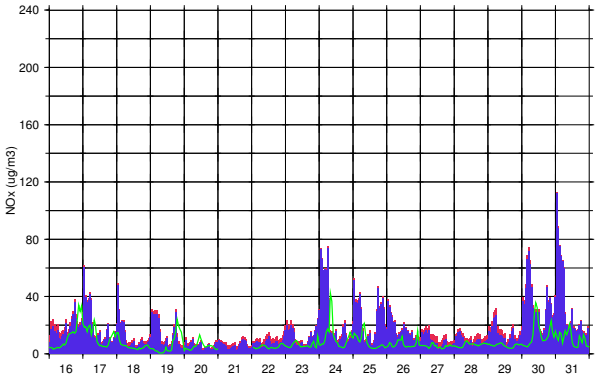

Forsthof SO2

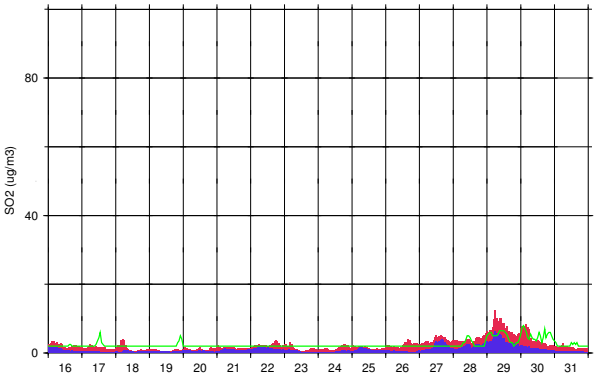

Hermannskogel SO2

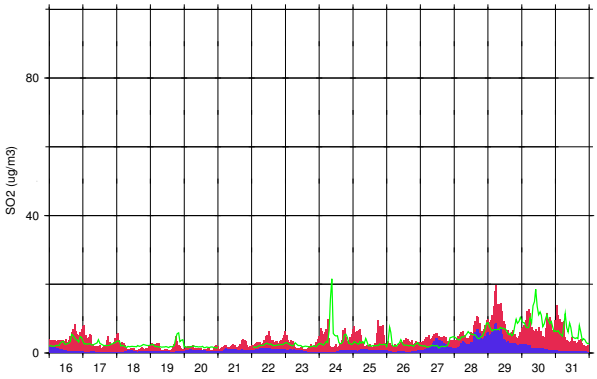

2003 Month 06 Part 1

Bad Vöslau NOx

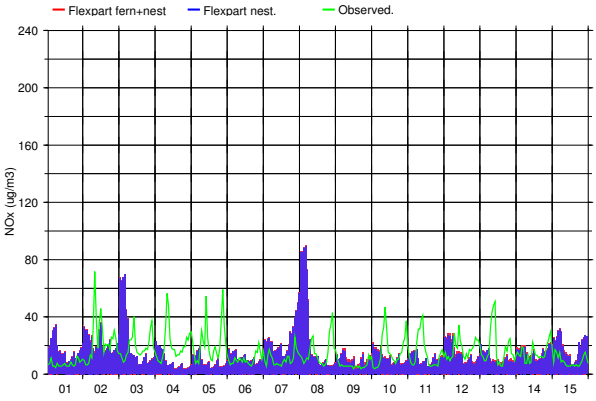

Streithofen NOx

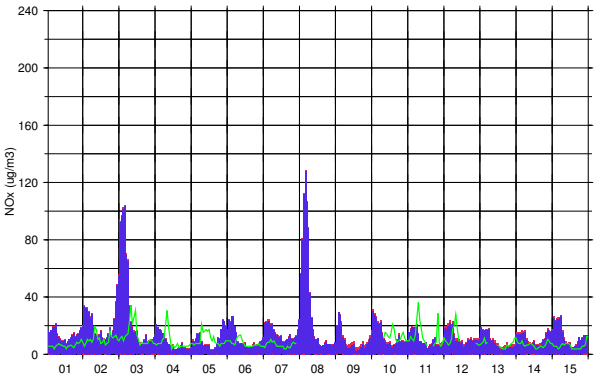

Tulbingerkogel NOx

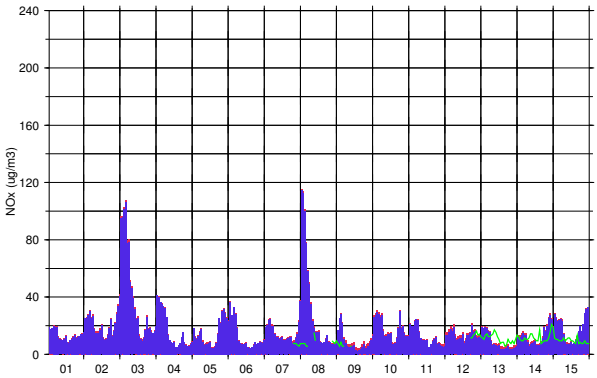

Forsthof NOx

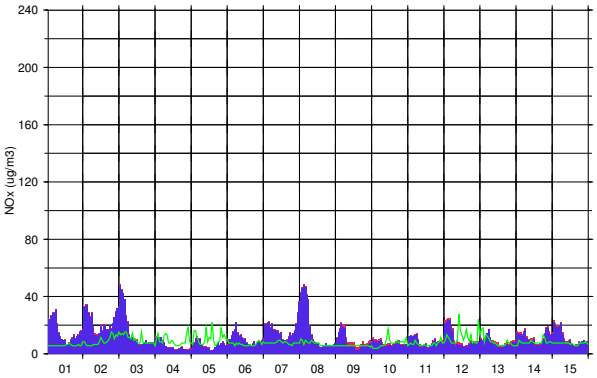

Hermannskogel NOx

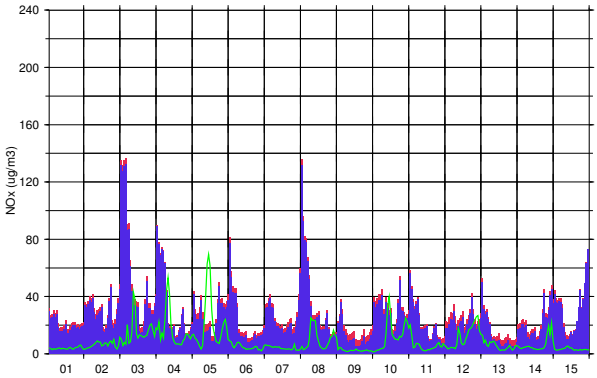

Forsthof SO2

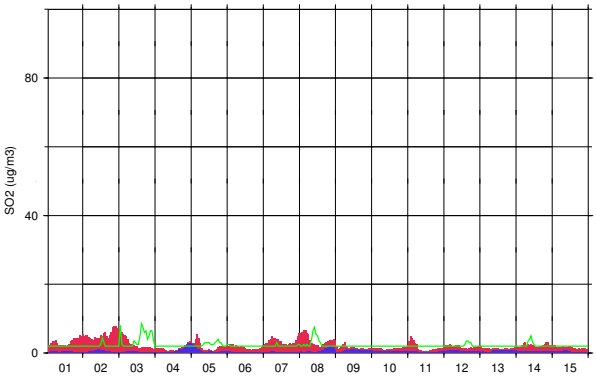

Hermannskogel SO2

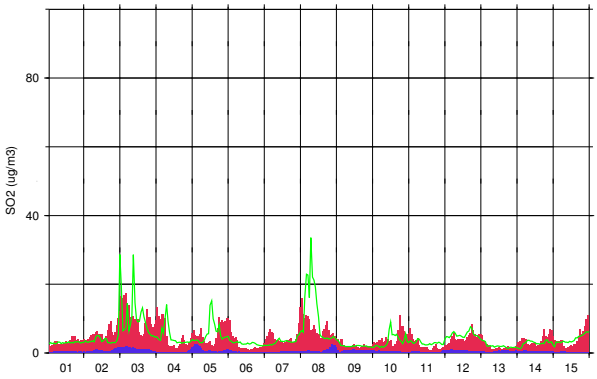

2003 Month 06 Part 2

Bad Vöslau NOx

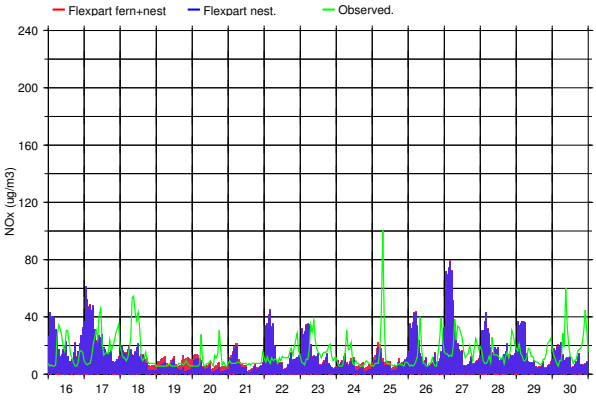

Streithofen NOx

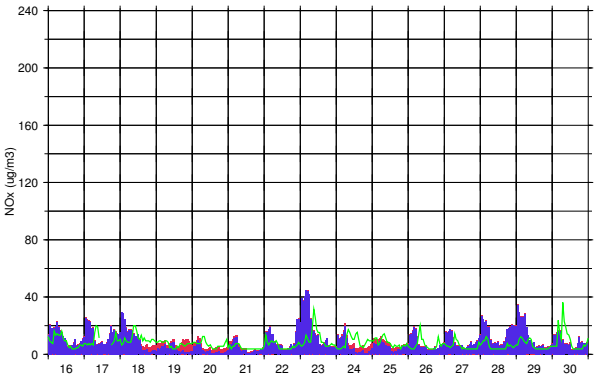

Tulbingerkogel NOx

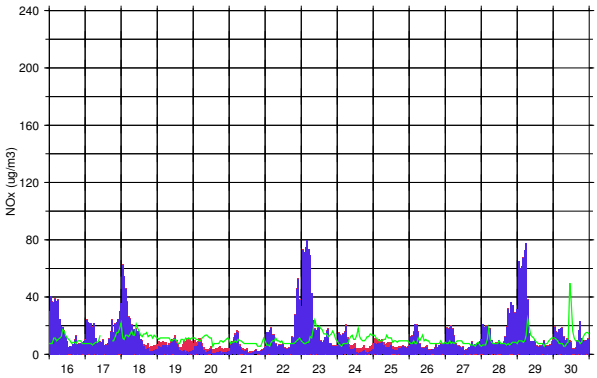

Forsthof NOx

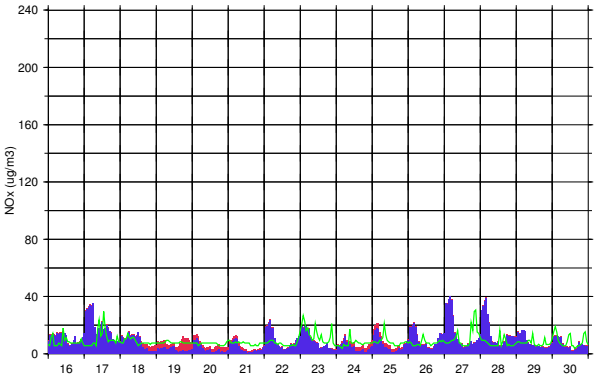

Hermannskogel NOx

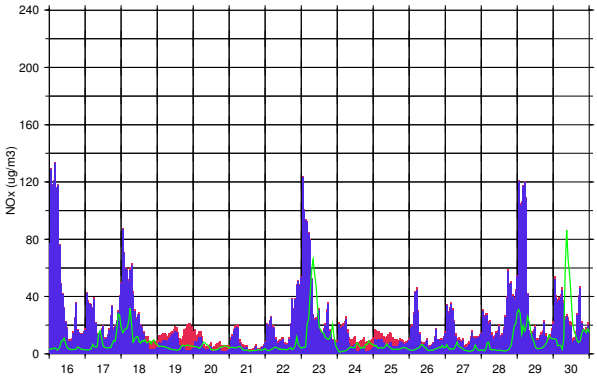

Forsthof SO2

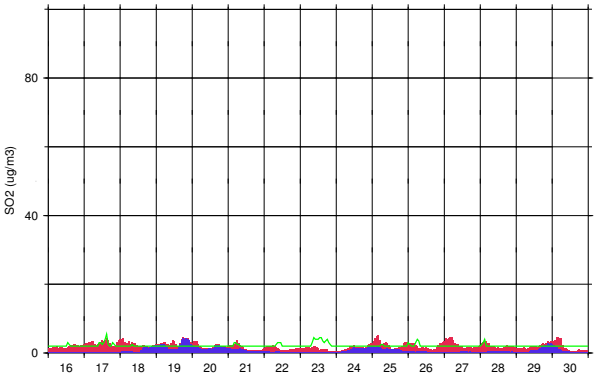

Hermannskogel SO2

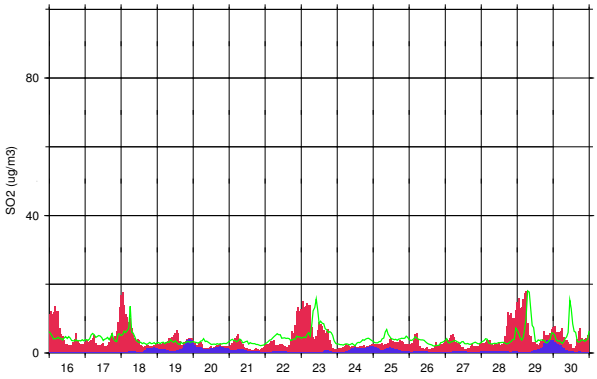

2003 Month 07 Part 1

Bad Vöslau NOx

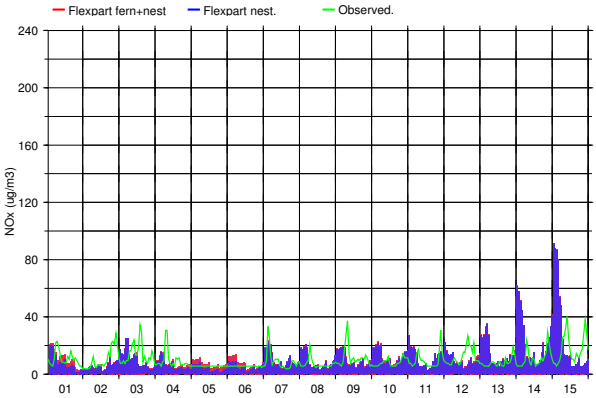

Streithofen NOx

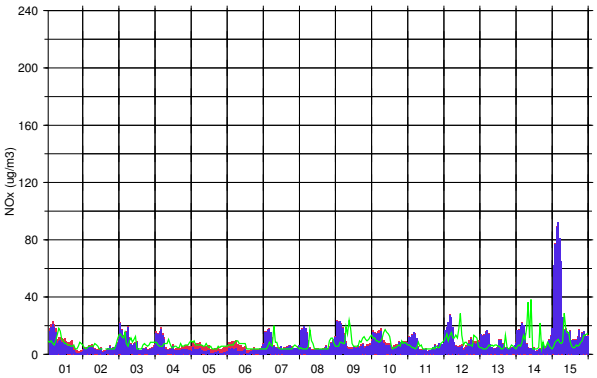

Tulbingerkogel NOx

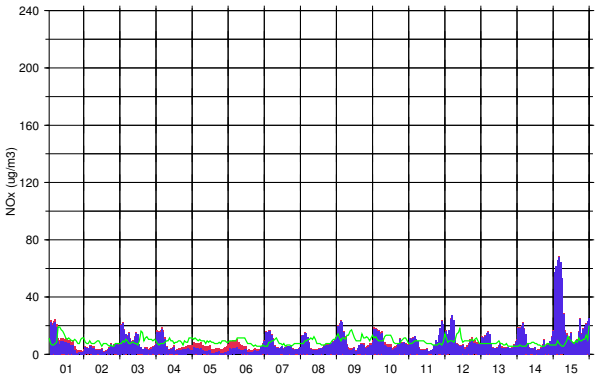

Forsthof NOx

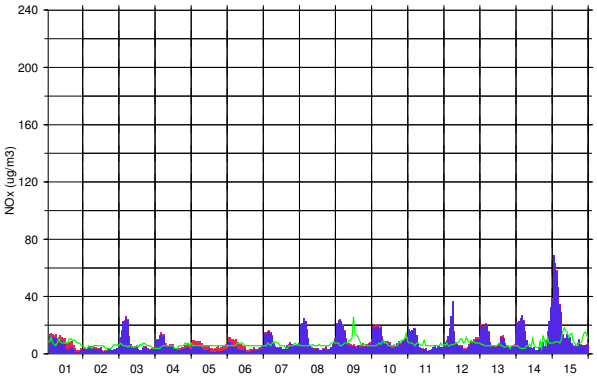

Hermannskogel NOx

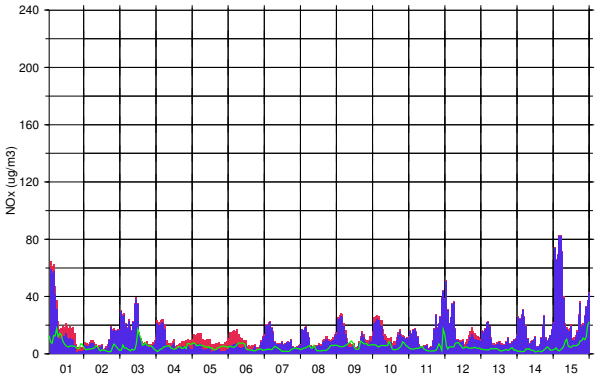

Forsthof SO2

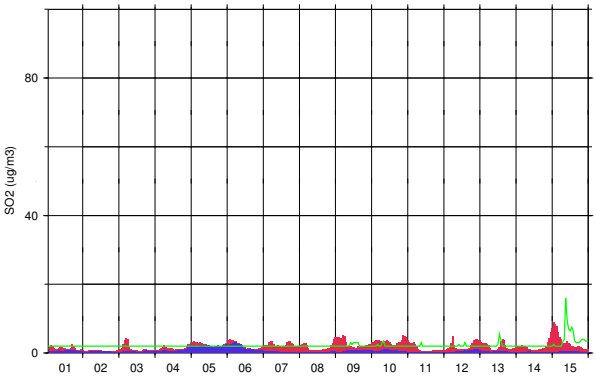

Hermannskogel SO2

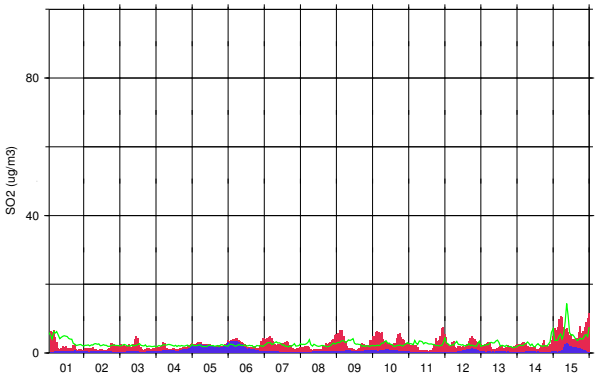

2003 Month 07 Part 2

Bad Vöslau NOx

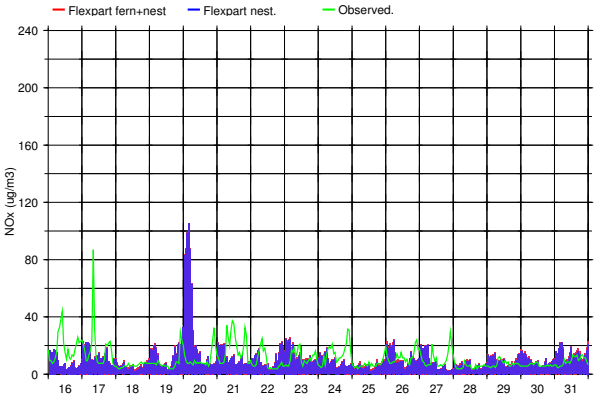

Streithofen NOx

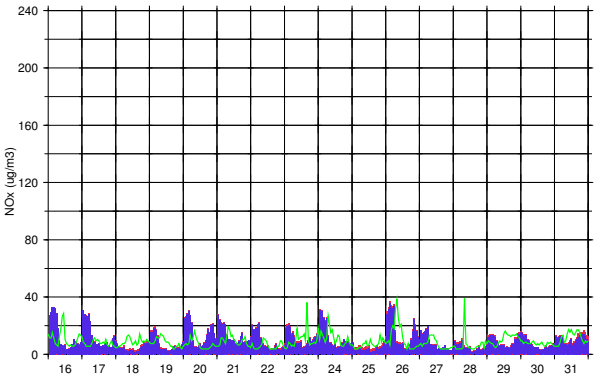

Tulbingerkogel NOx

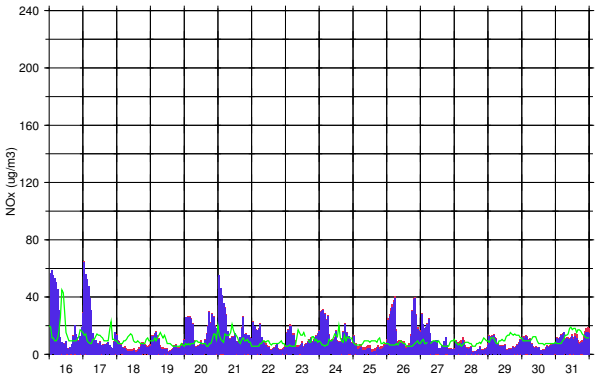

Forsthof NOx

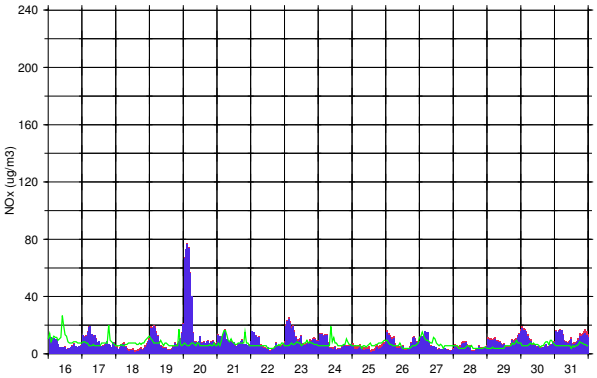

Hermannskogel NOx

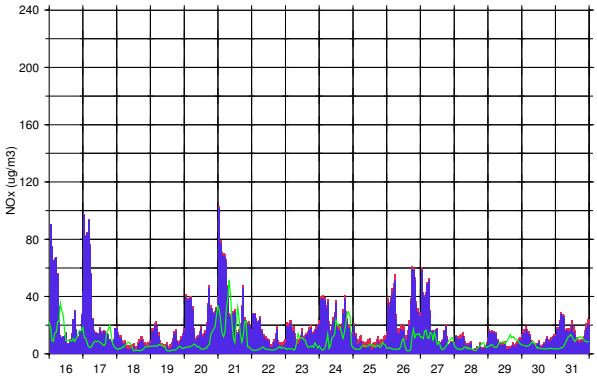

Forsthof SO2

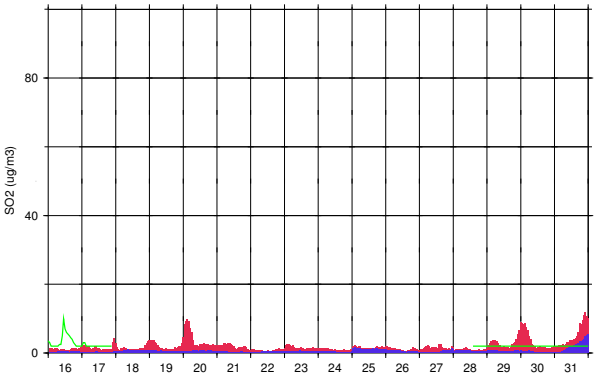

Hermannskogel SO2

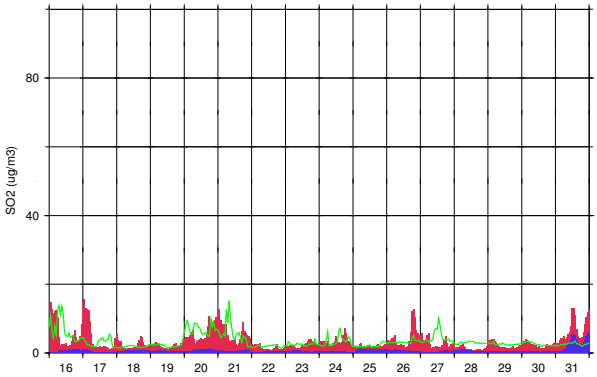

2003 Month 08 Part 1

Bad Vöslau NOx

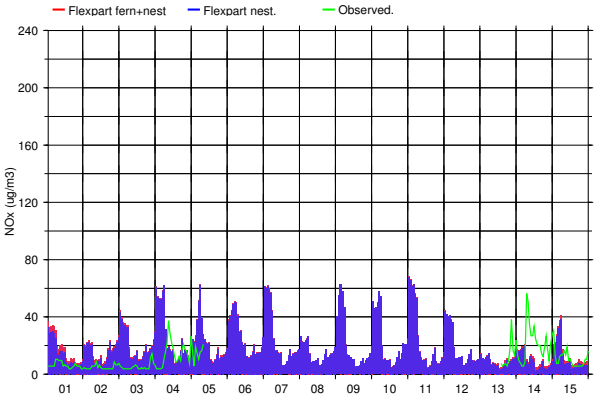

Streithofen NOx

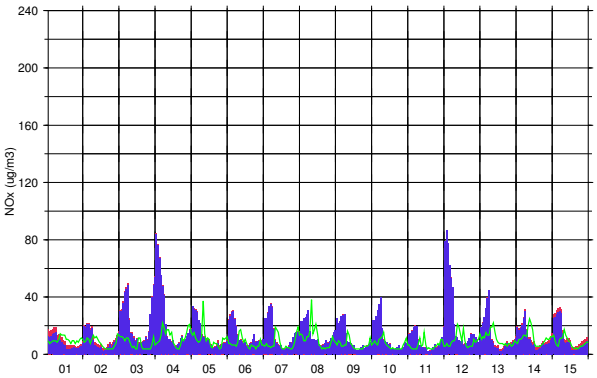

Tulbingerkogel NOx

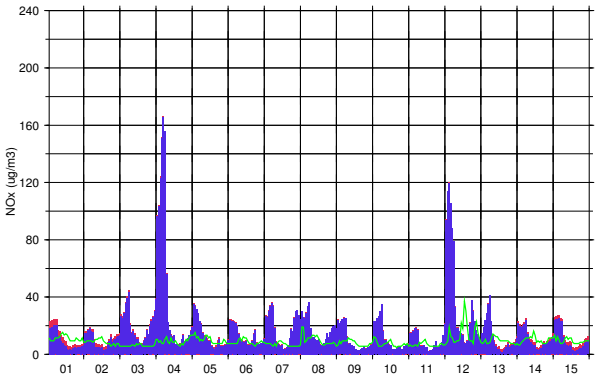

Forsthof NOx

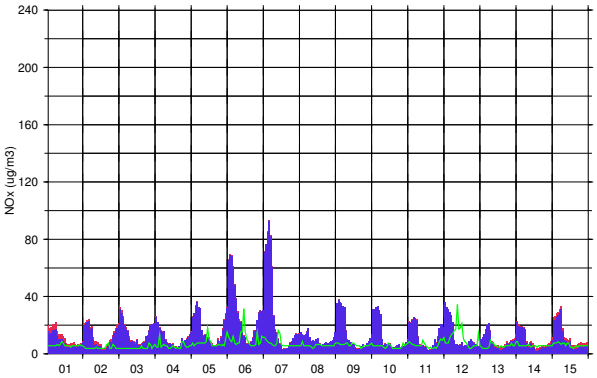

Hermannskogel NOx

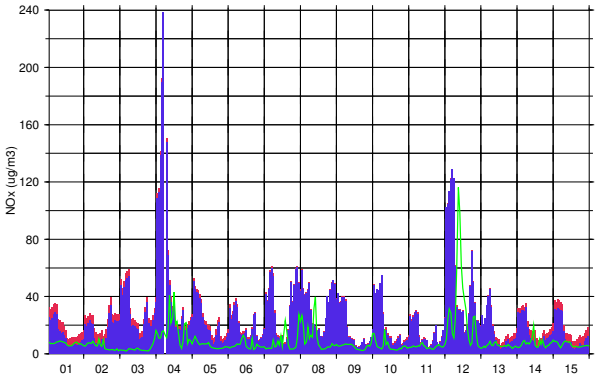

Forsthof SO2

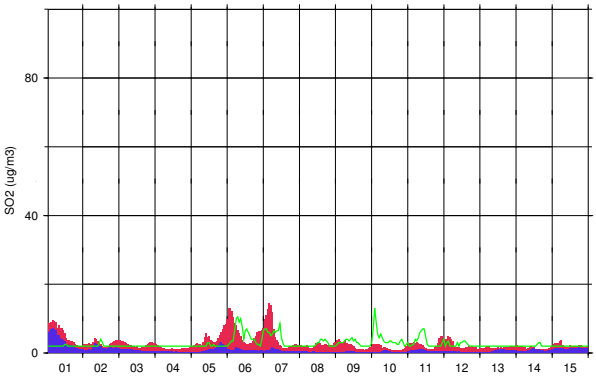

Hermannskogel SO2

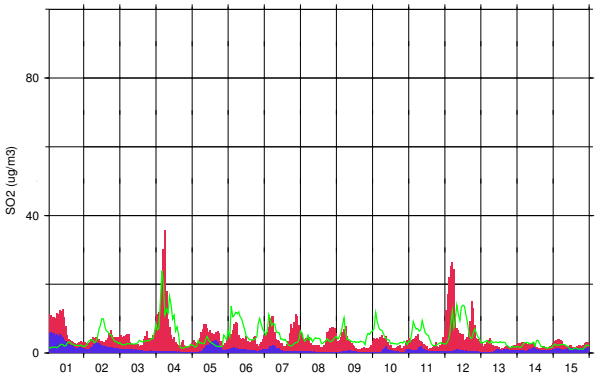

2003 Month 08 Part 2

Bad Vöslau NOx

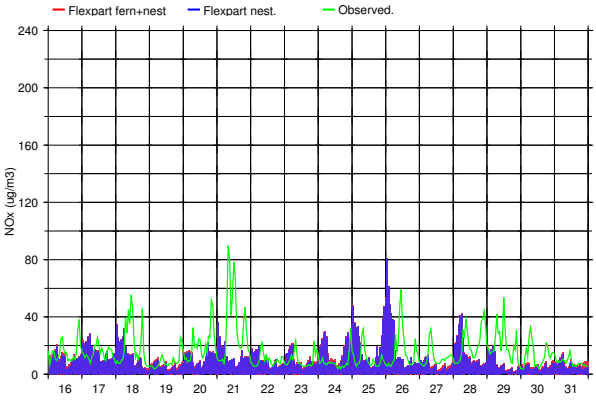

Streithofen NOx

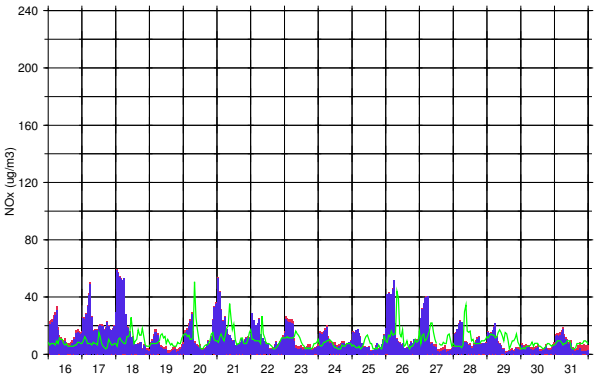

Tulbingerkogel NOx

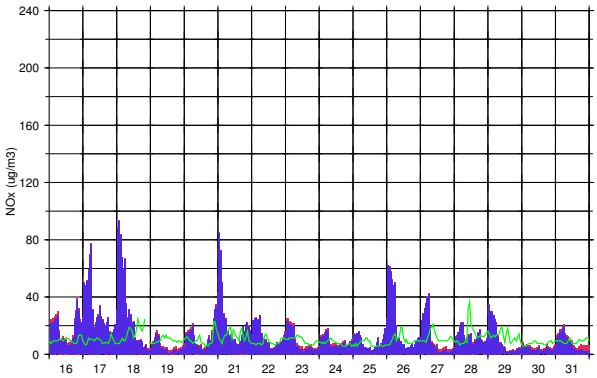

Forsthof NOx

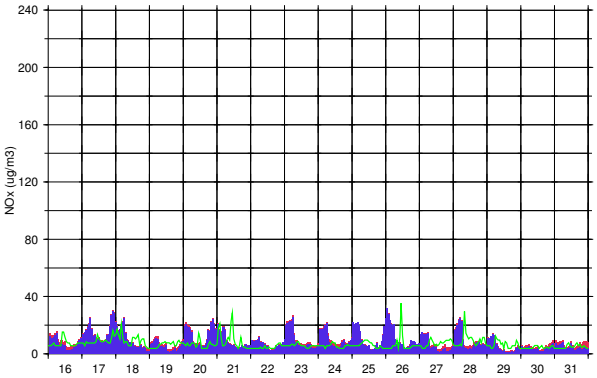

Hermannskogel NOx

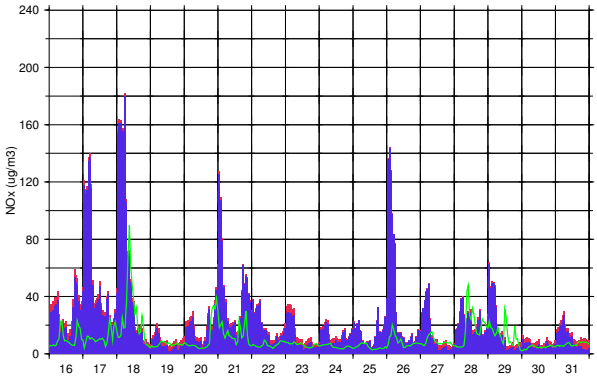

Forsthof SO2

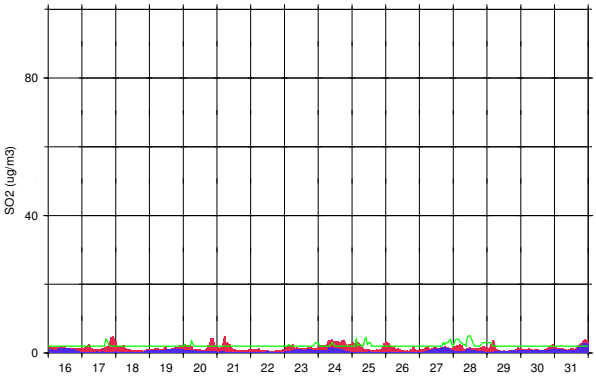

Hermannskogel SO2

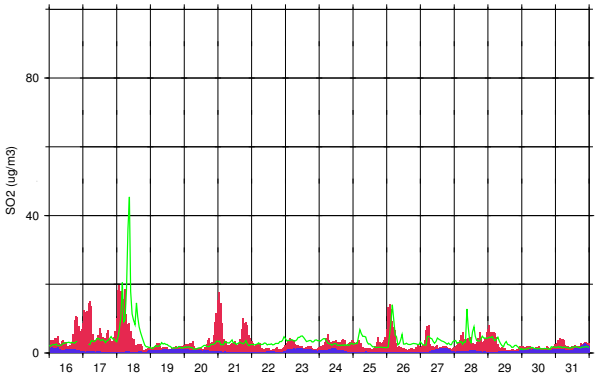

2003 Month 09 Part 1

Bad Vöslau NOx

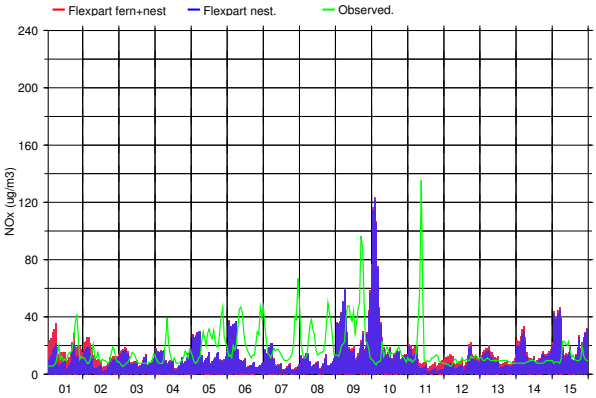

Streithofen NOx

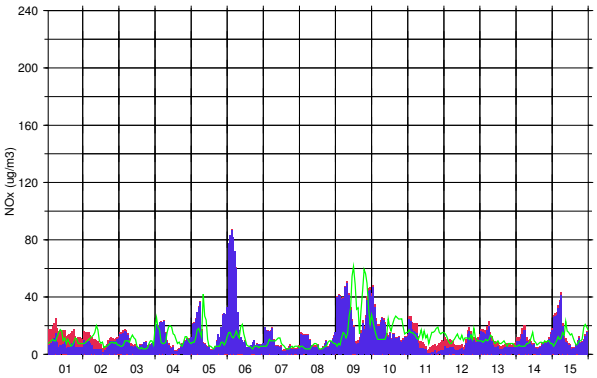

Tulbingerkogel NOx

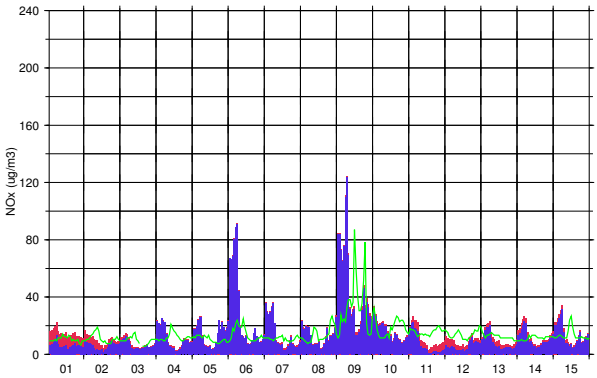

Forsthof NOx

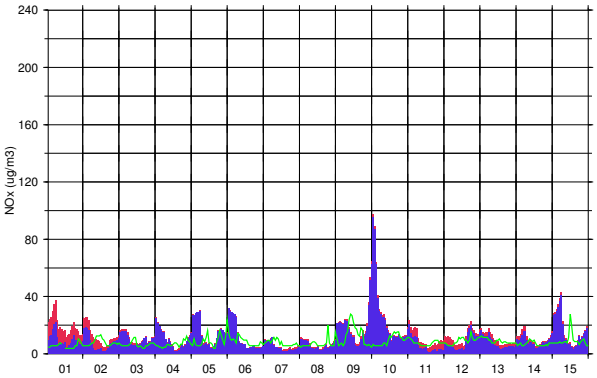

Hermannskogel NOx

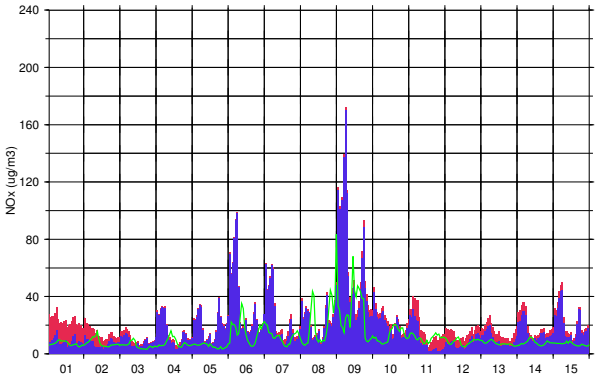

Forsthof SO2

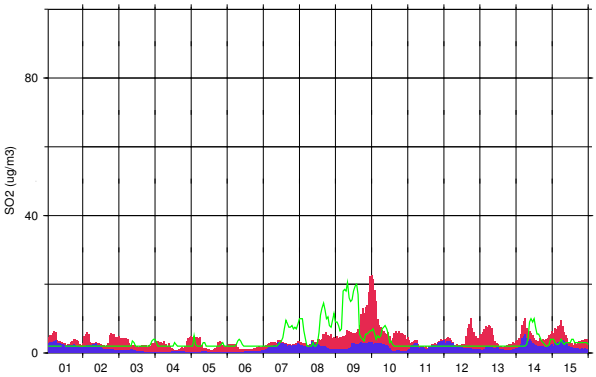

Hermannskogel SO2

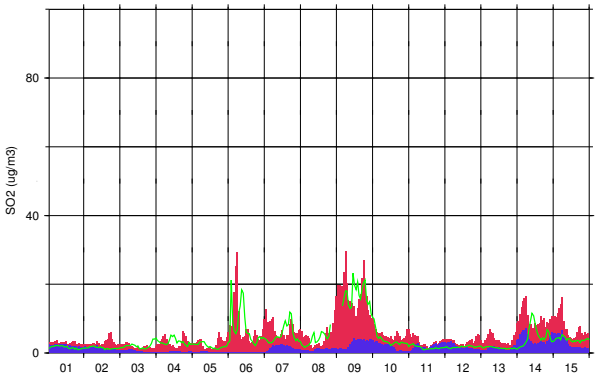

2003 Month 09 Part 2

Bad Vöslau NOx

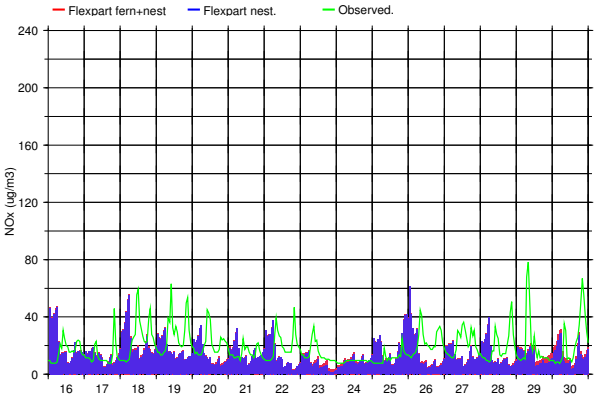

Streithofen NOx

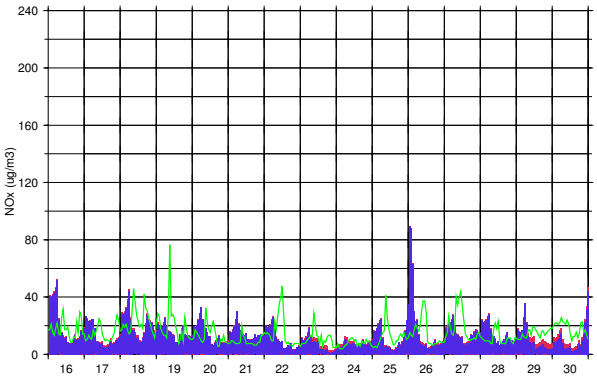

Tulbingerkogel NOx

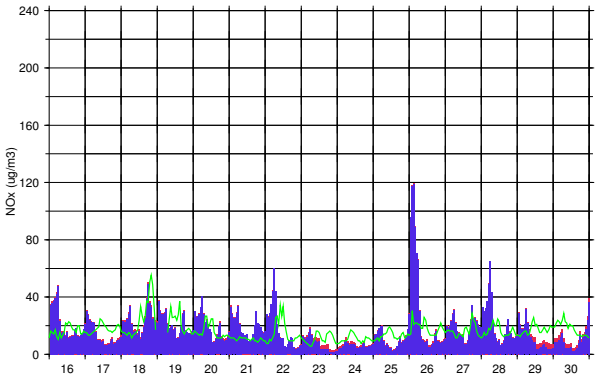

Forsthof NOx

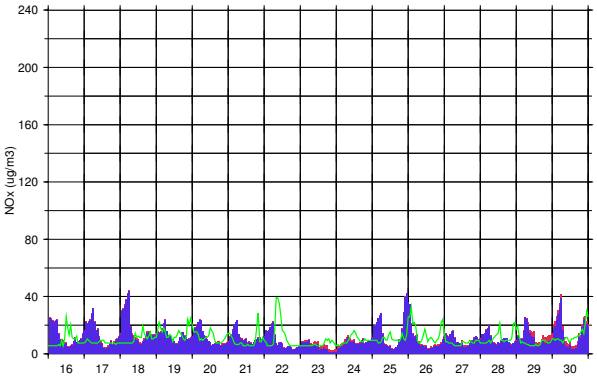

Hermannskogel NOx

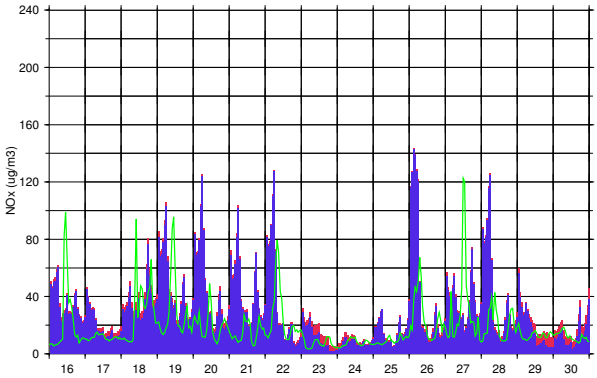

Forsthof SO2

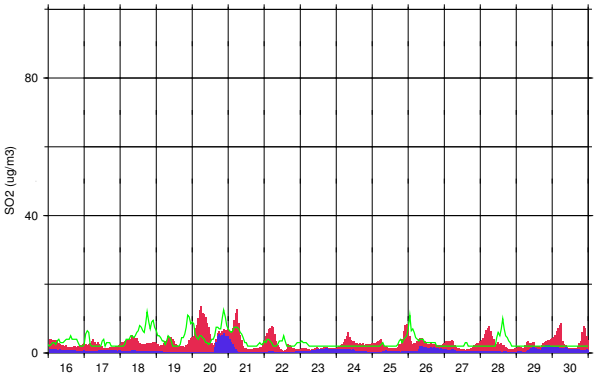

Hermannskogel SO2

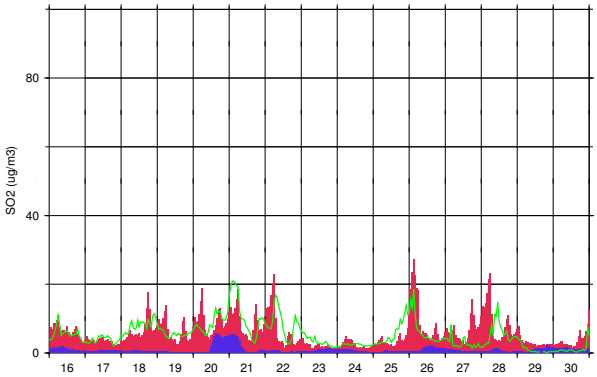

2003 Month 10 Part 1

Bad Vöslau NOx

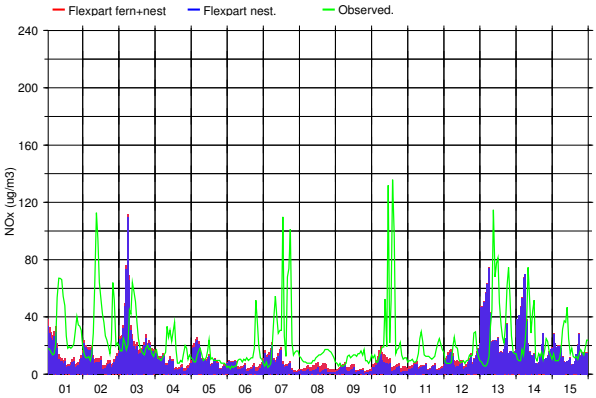

Streithofen NOx

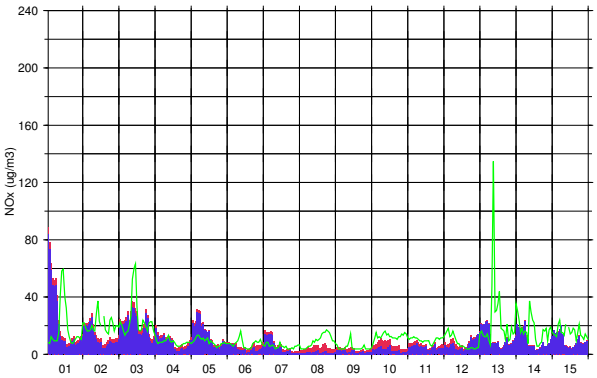

Tulbingerkogel NOx

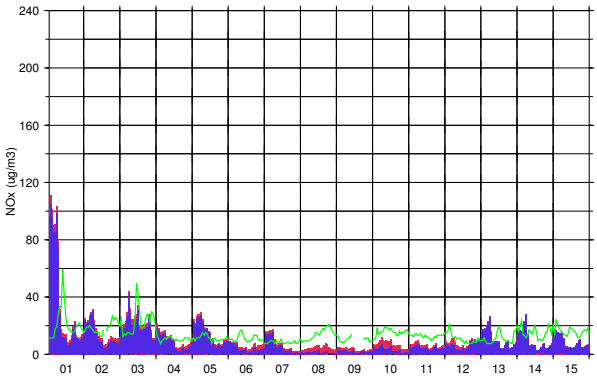

Forsthof NOx

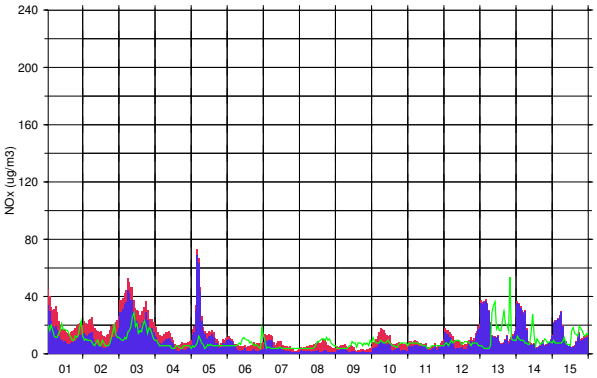

Hermannskogel NOx

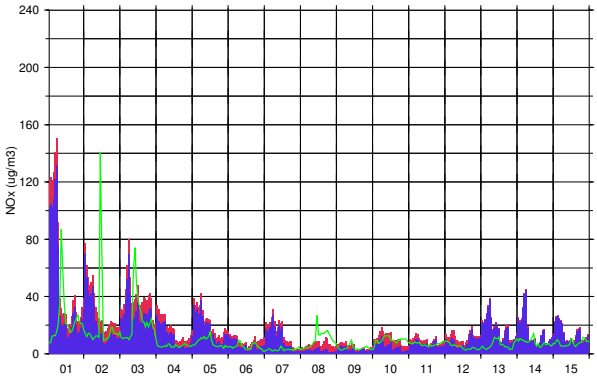

Forsthof SO2

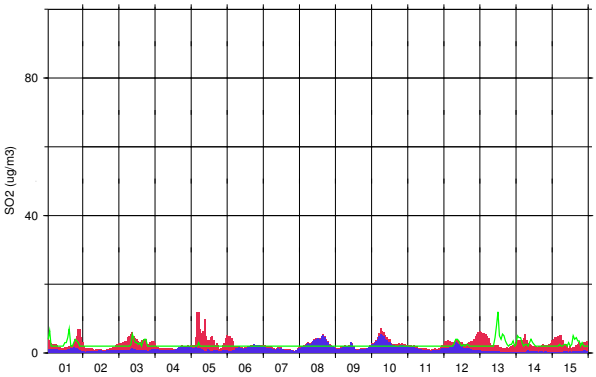

Hermannskogel SO2

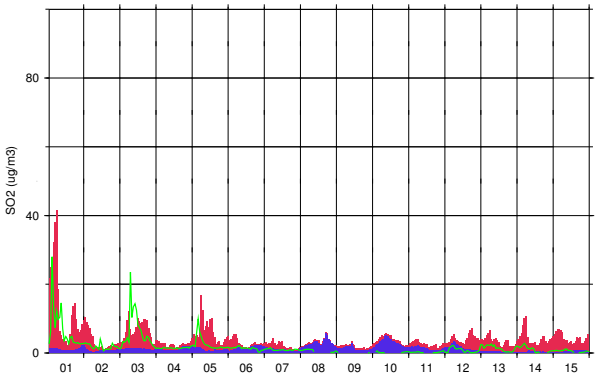

2003 Month 10 Part 2

Bad Vöslau NOx

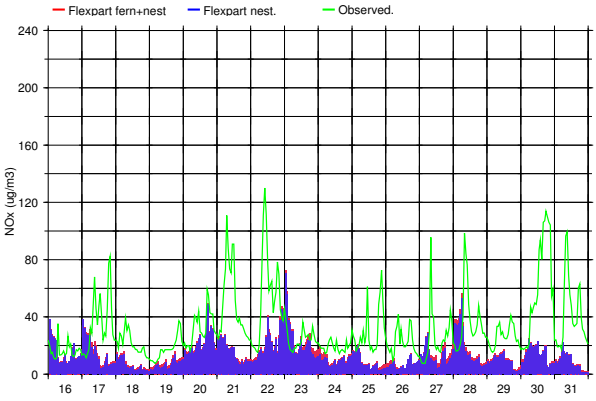

Streithofen NOx

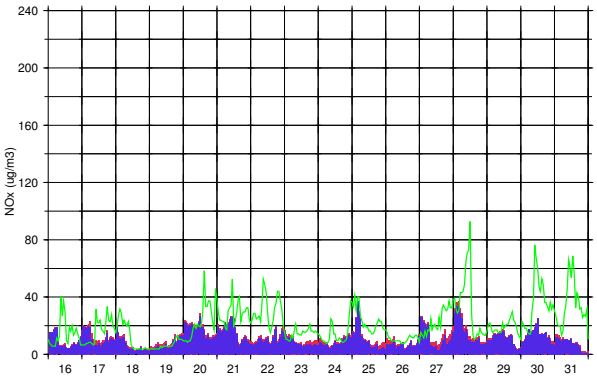

Tulbingerkogel NOx

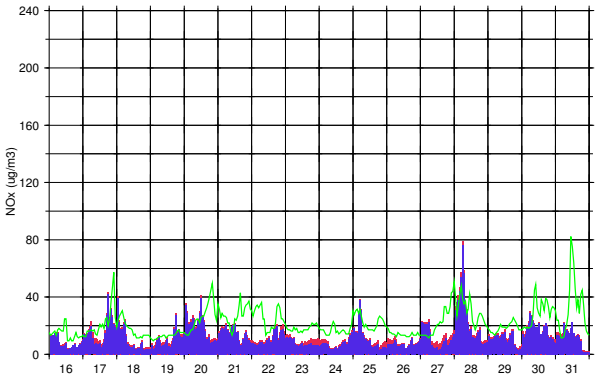

Forsthof NOx

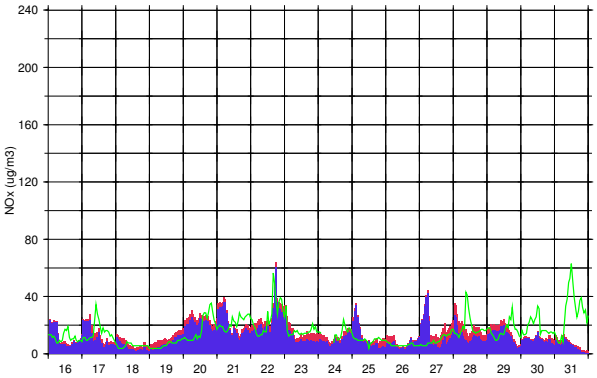

Hermannskogel NOx

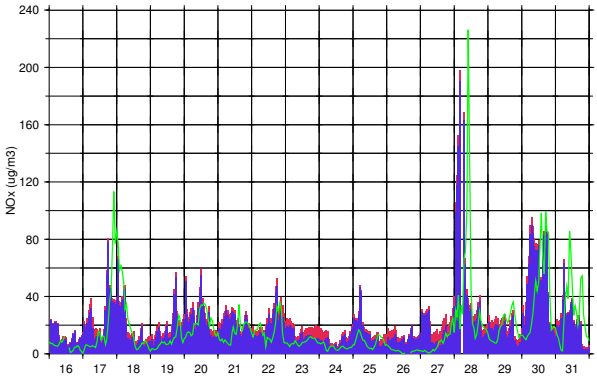

Forsthof SO2

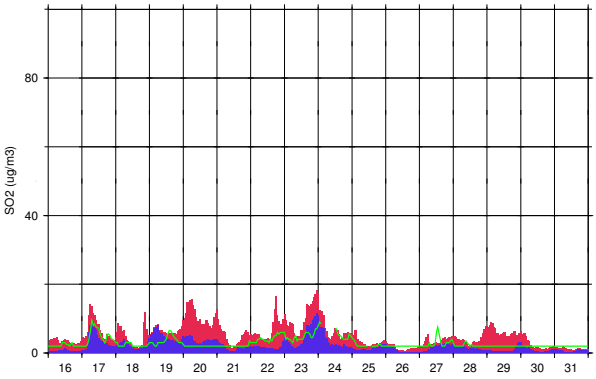

Hermannskogel SO2

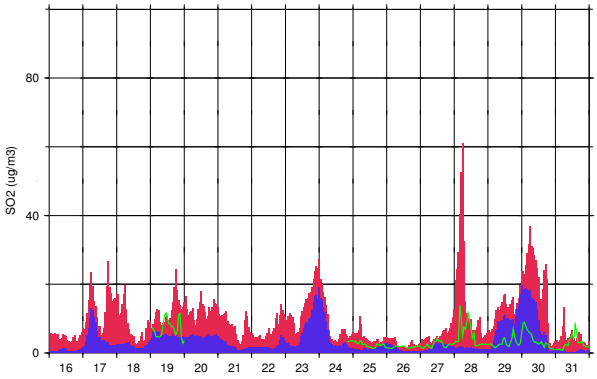

2003 Month 11 Part 1

Bad Vöslau NOx

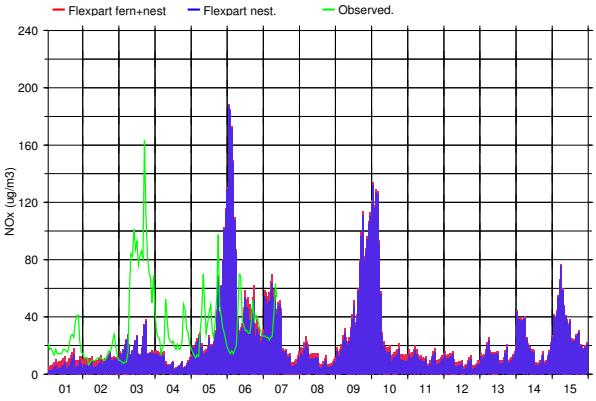

Streithofen NOx

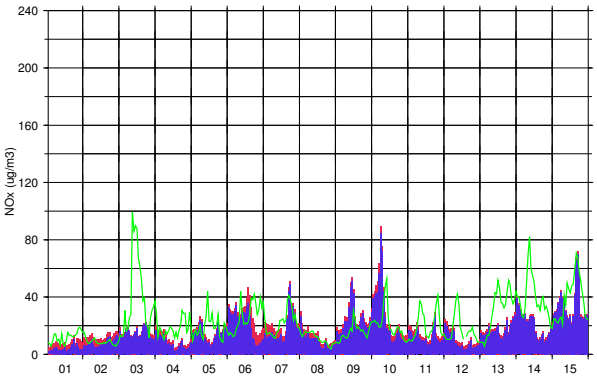

Tulbingerkogel NOx

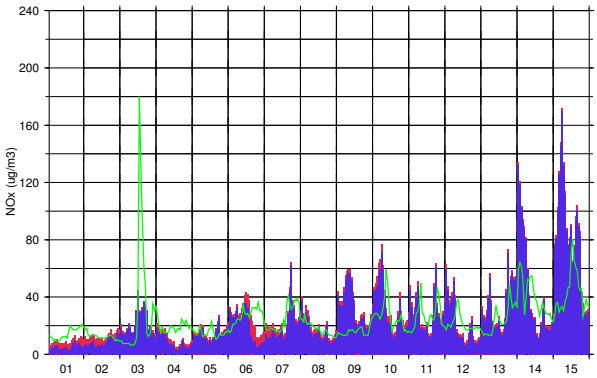

Forsthof NOx

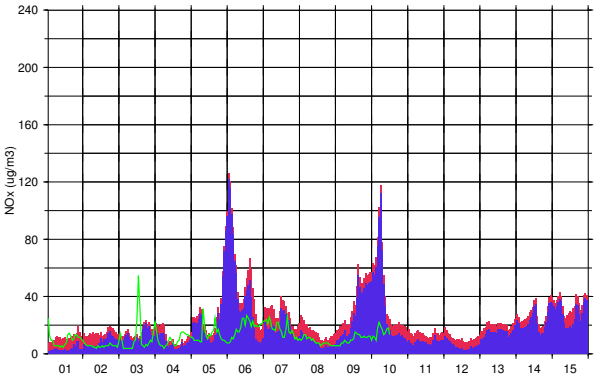

Hermannskogel NOx

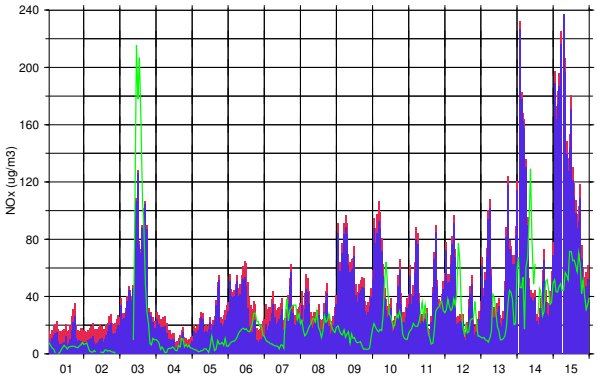

Forsthof SO2

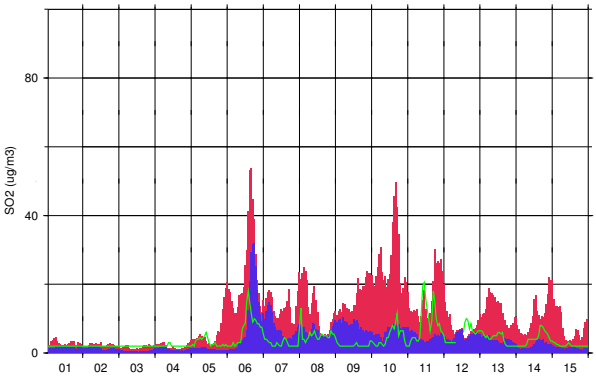

Hermannskogel SO2

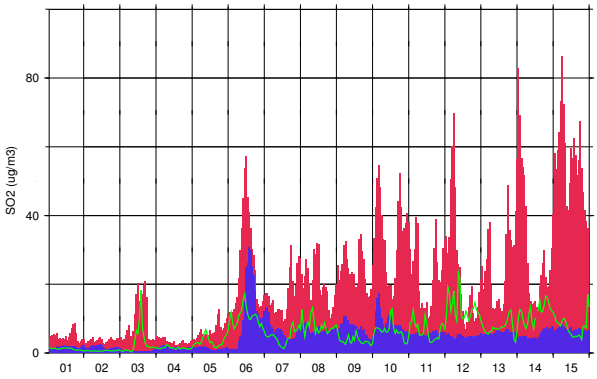

2003 Month 11 Part 2

Bad Vöslau NOx

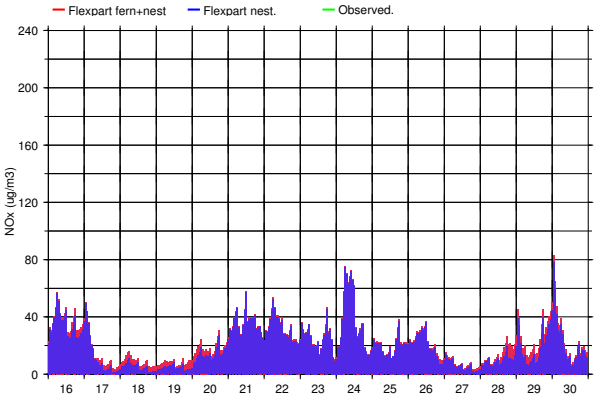

Streithofen NOx

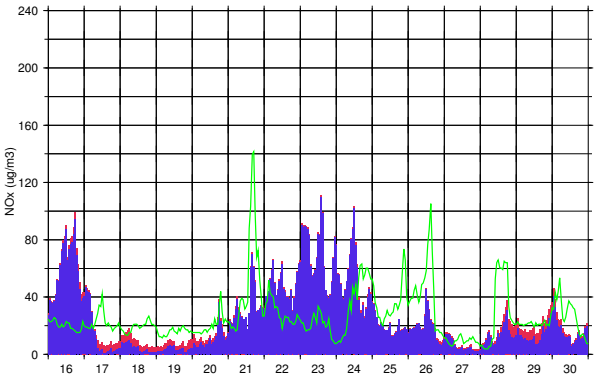

Tulbingerkogel NOx

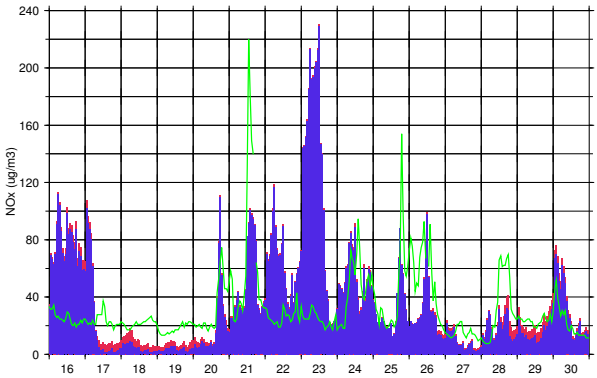

Forsthof NOx

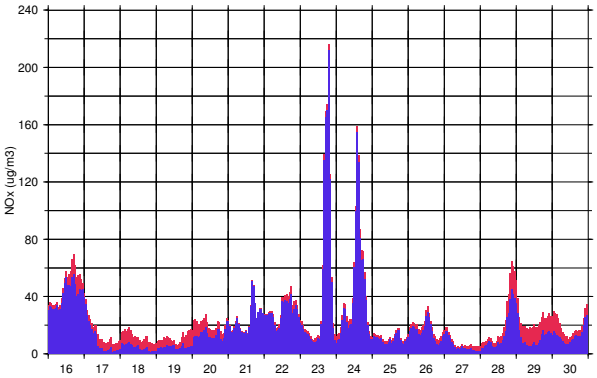

Hermannskogel NOx

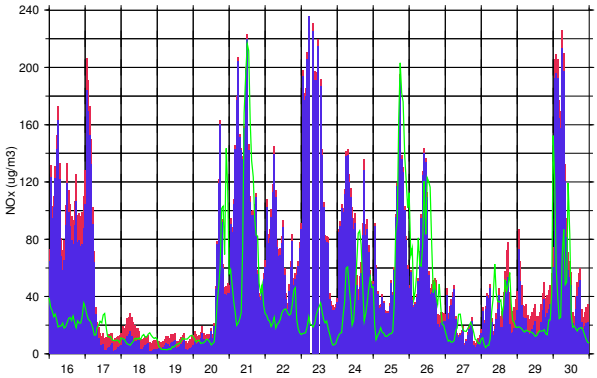

Forsthof SO2

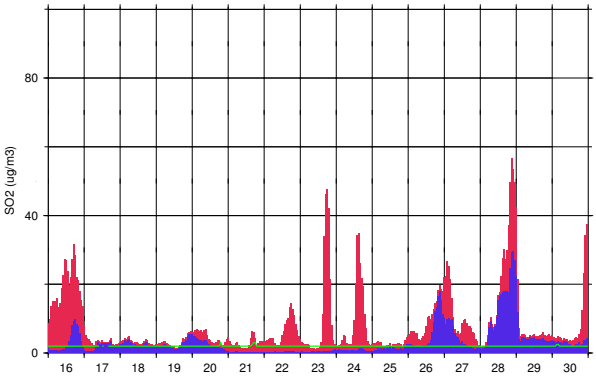

Hermannskogel SO2

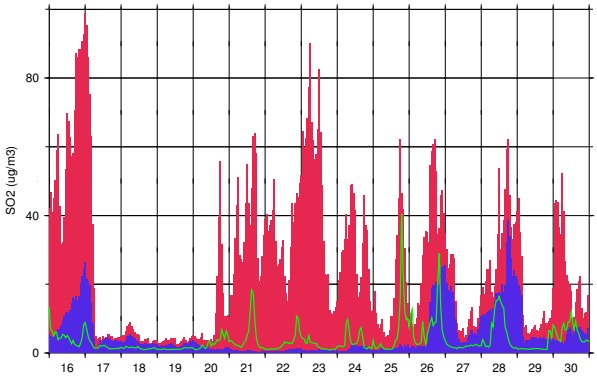

2003 Month 12 Part 1

Bad Vöslau NOx

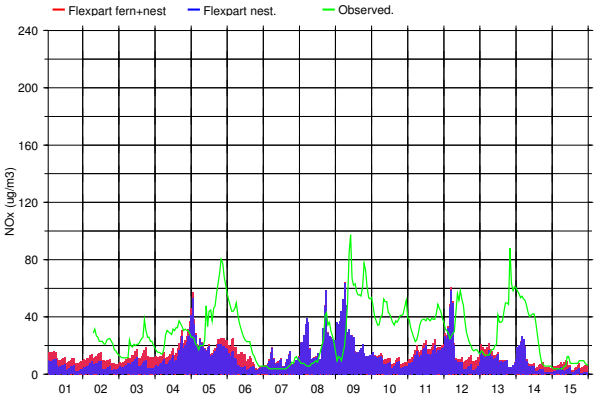

Streithofen NOx

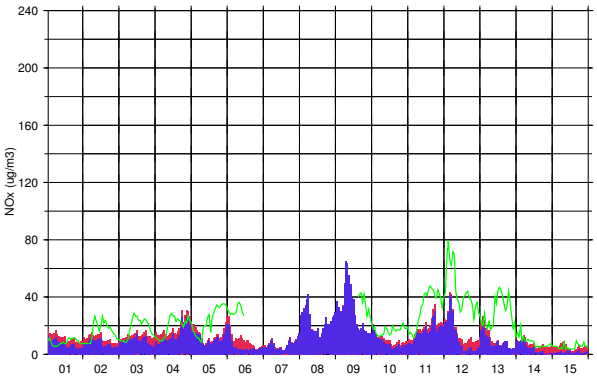

Tulbingerkogel NOx

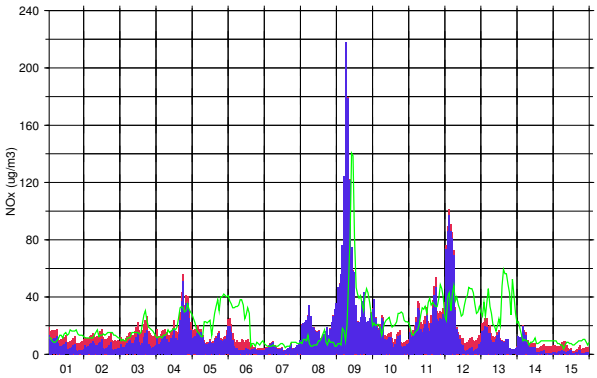

Forsthof NOx

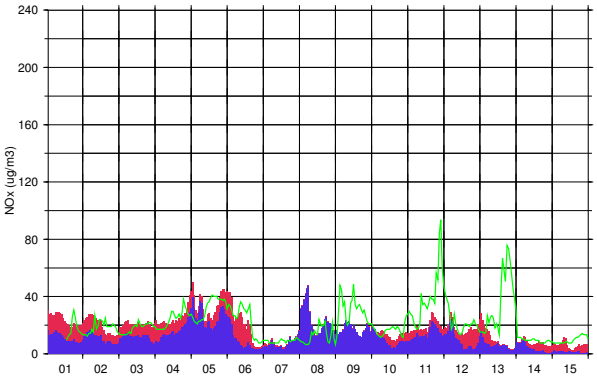

Hermannskogel NOx

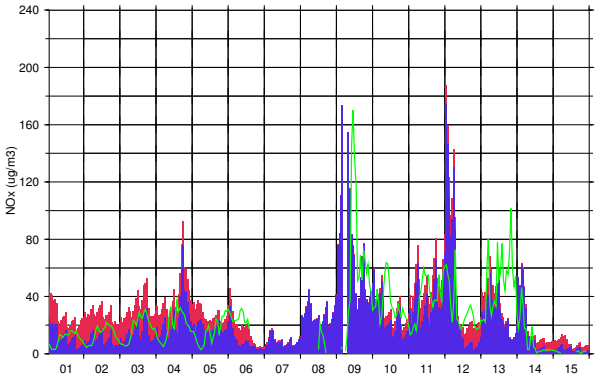

Forsthof SO2

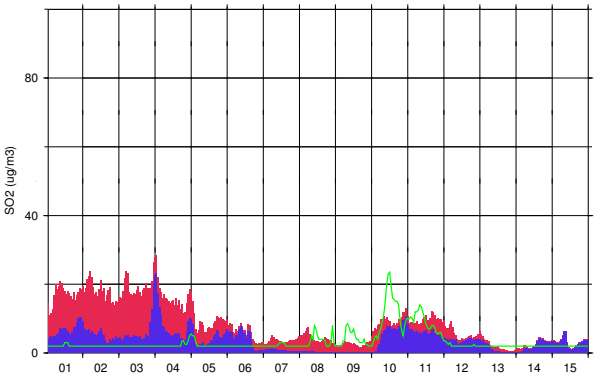

Hermannskogel SO2

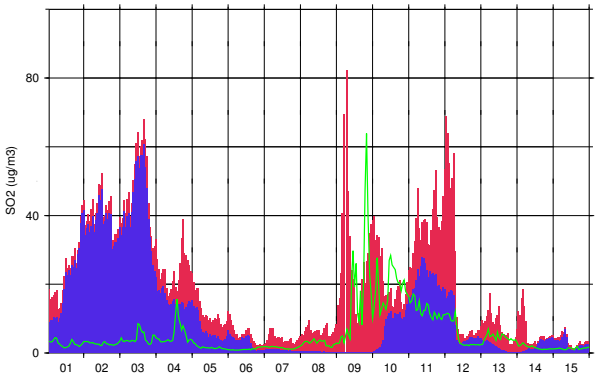

2003 Month 12 Part 2

Bad Vöslau NOx

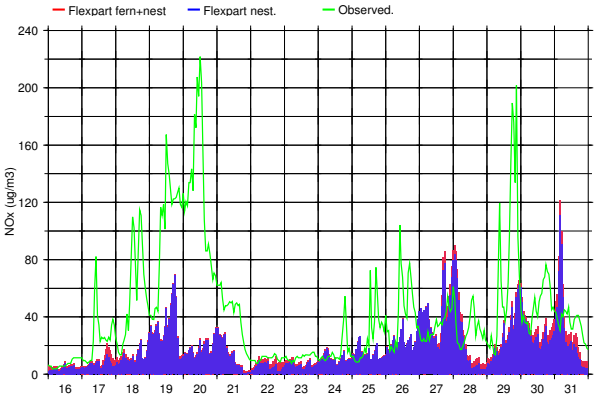

Streithofen NOx

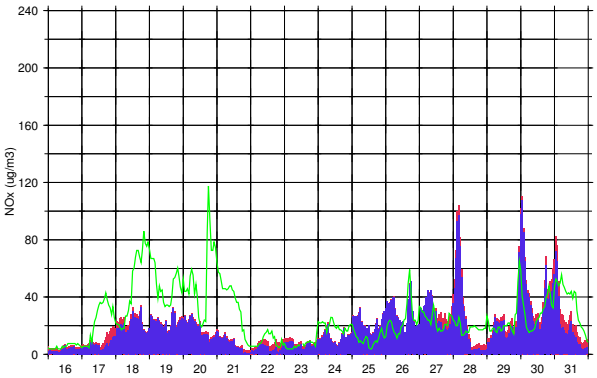

Tulbingerkogel NOx

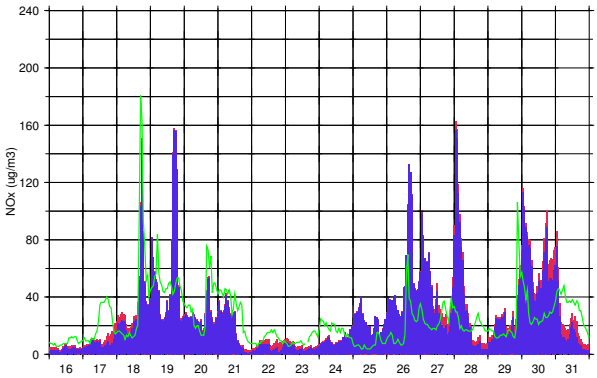

Forsthof NOx

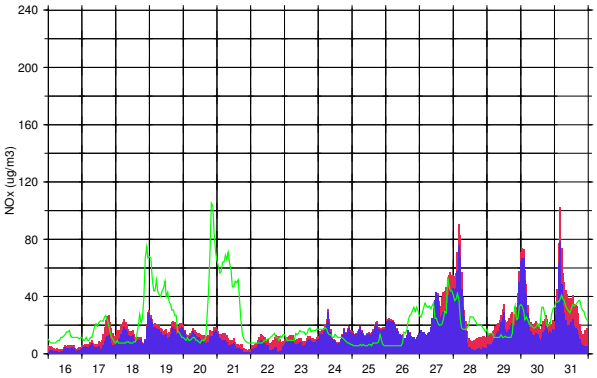

Hermannskogel NOx

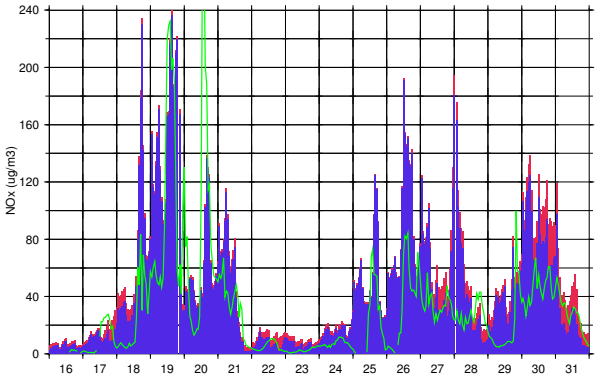

Forsthof SO2

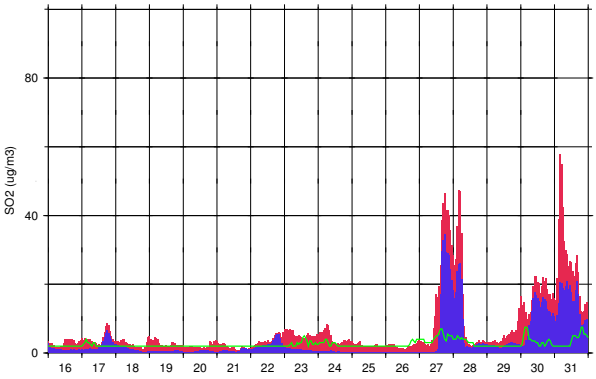

Hermannskogel SO2

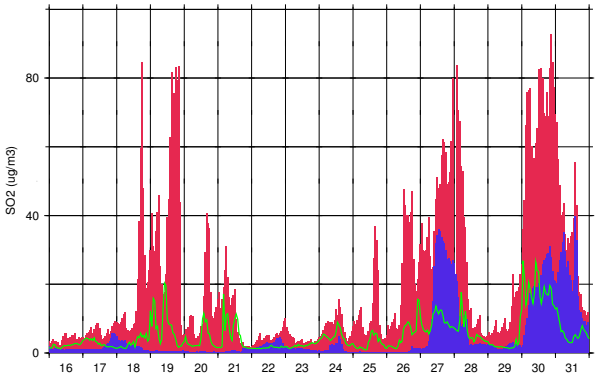

B Monthly residence times derived from FLEXTRA trajectories for station Auhof

Auhof 2003 Month 01

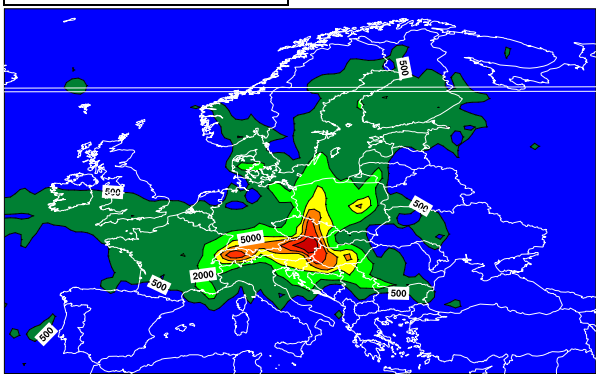

Auhof 2003 Month 04

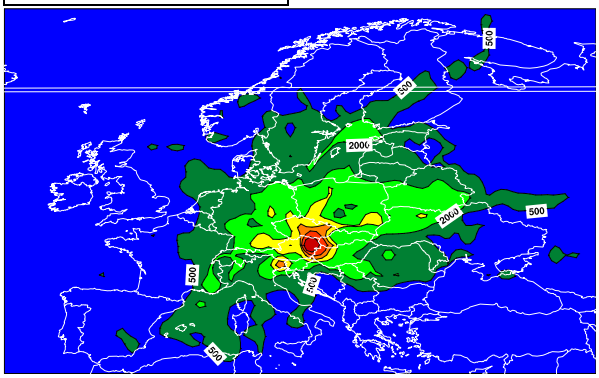

Auhof 2003 Month 02

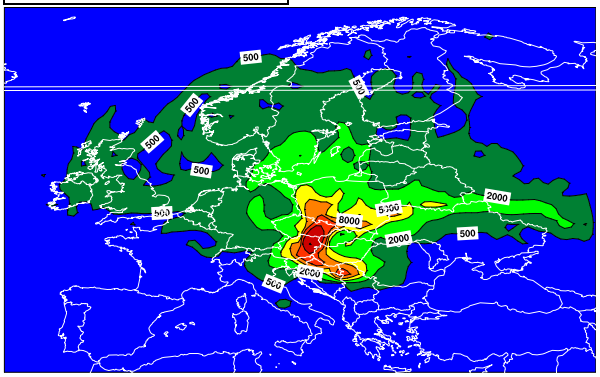

Auhof 2003 Month 05

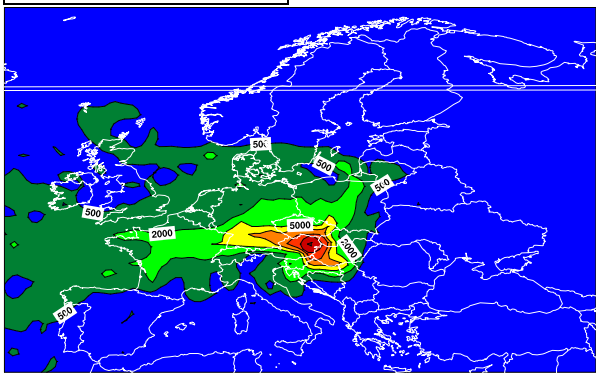

Auhof 2003 Month 03

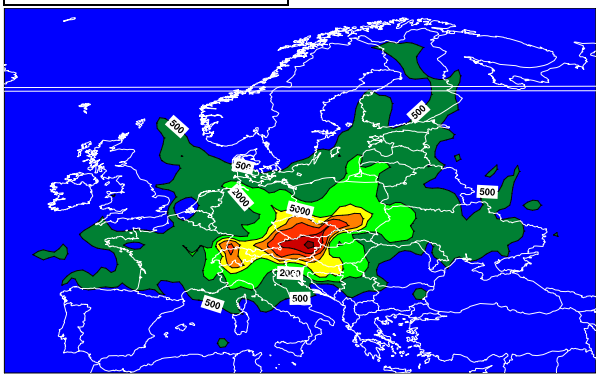

Auhof 2003 Month 06

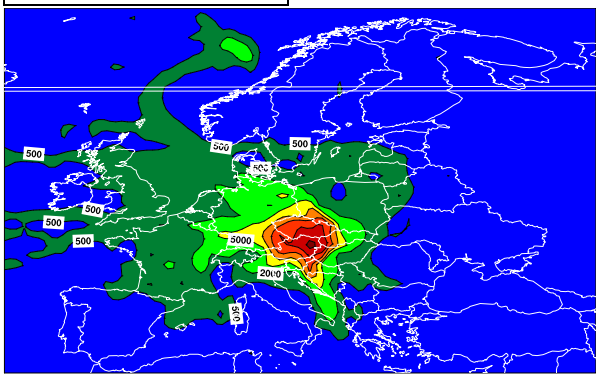

Auhof 2003 Month 07

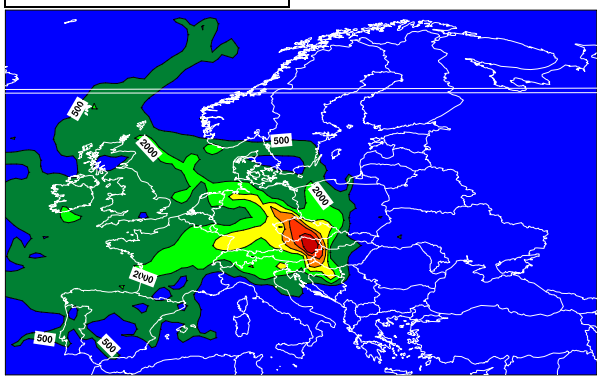

Auhof 2003 Month 10

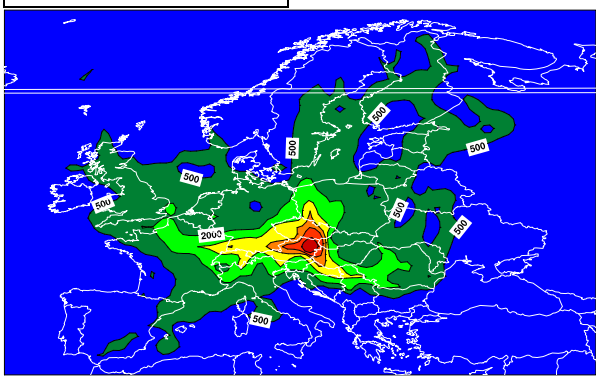

Auhof 2003 Month 08

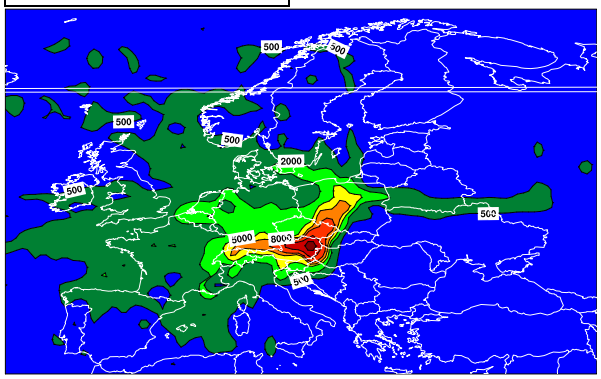

Auhof 2003 Month 11

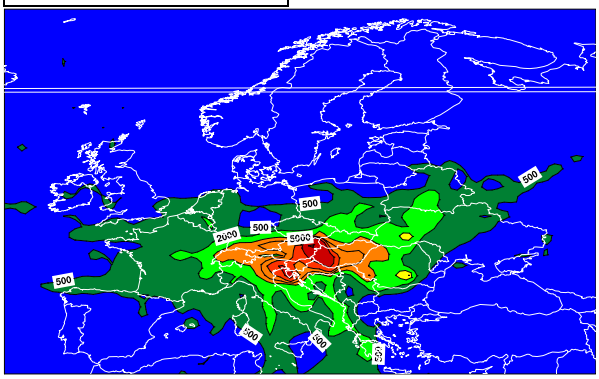

Auhof 2003 Month 09

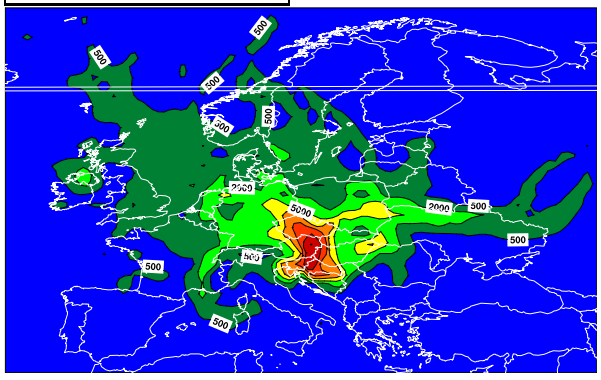

Auhof 2003 Month 12

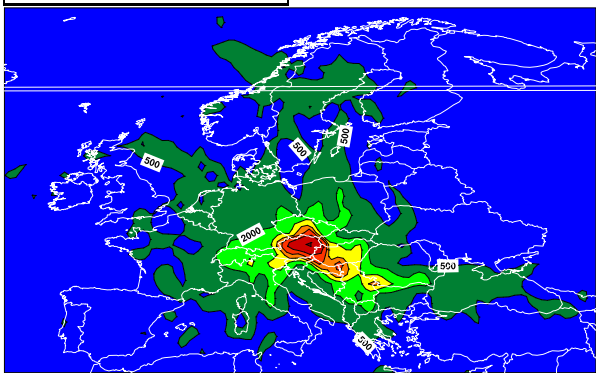

Bisher erschienen in der Reihe BOKU-Met Report:

Berichte von 2003 – 2008

1 Eitzinger, J., Kubu, G., Formayer, H., Haas, P., Gerersdorfer, T., Kromp-Kolb, H. (2009): **Auswirkungen einer Klimaänderung auf den Wasserhaushalt des Neusiedlersees** (Endbericht im Auftrag der Burgenländischen Landesregierung vom 15. Juli 2005).

2 Frank, A., Seibert, P. (2009): **Diagnose von Extremereignissen aus großräumigen meteorologischen Feldern** (Endbericht StartClim.4, November 2003).

3 Formayer, H., Matulla, C., Haas, P., Groll, N. (2009): **Statistische Downscalingverfahren zur Ableitung von Extremereignissen in Österreich aus GCM-Feldern** (Endbericht StartClim.5, November 2003).

4 Schwarzl, I., Haas, W. (2009): **Kommunikation an der Schnittstelle Wissenschaft und Bildung** (Endbericht StartClim.11, November 2003).

5 Formayer, H., Haas, P., Matulla, C., Frank, A., Seibert, P. (2009): **Untersuchungen regionaler Klimaänderungsszenarien hinsichtlich Hitze- und Trockenperioden in Österreich** (Endbericht StartClim2004.B, November 2003).

6 Schwarzl, I., Lang, E. (2009): **"Hängen Hitze und Leistungsfähigkeit zusammen?"** Ein Projekt an der Schnittstelle Wissenschaft und Bildung (Endbericht StartClim2004.G, Jänner 2005).

7 Formayer, H., Kromp-Kolb, H. (2009): **Hochwasser und Klimawandel**. Auswirkungen des Klimawandels auf Hochwasserereignisse in Österreich (Endbericht WWF 2006).

8 Gerersdorfer, T., Frank, A., Formayer, H., Haas, P., Moshammer, H. (2009): **Untersuchung zur nächtlichen Abkühlung in einem sich ändernden Klima** (Endbericht StartClim2005.A1b, November 2006).

9 Krüger, B. C., Schicker, I., Formayer, H., Moshammer, H. (2009): **Feinstaub und Klimawandel – Gibt es Zusammenhänge in Nordostösterreich?** (Endbericht StartClim2006.A, Juli 2007).

10 Rössler, M., Laube, W., Weihs, P. (2009): **Avoiding bird collisions with glass surfaces**. Experimental investigations of the efficacy of markings on glass panes under natural light conditions in Flight Tunnel II (Final report, March 2007).

11 Formayer, H., Hofstätter, M., Haas, P. (2009): **Untersuchung der Schneesicherheit und der potenziellen Beschneiungszeiten in Schladming und Ramsau** (Endbericht STRATEGE, Oktober 2007).

12 Kromp-Kolb, H., Formayer, H., Haas, P., Hofstätter, M., Schwarzl, I. (2009): **Beobachtete Veränderung der Hitzeperioden in Oberösterreich und Abschätzung der möglichen zukünftigen Entwicklungen** (Endbericht Band 1 der Forschungsreihe „Auswirkungen des Klimawandels auf Oberösterreich“, Februar 2007).

13 Moshammer, H., Gerersdorfer, T., Hutter, H.-P., Formayer, H., Kromp-Kolb, H., Schwarzl, I. (2009): **Abschätzung der Auswirkungen von Hitze auf die Sterblichkeit in Oberösterreich** (Endbericht Band 3 der Forschungsreihe „Auswirkungen des Klimawandels auf Oberösterreich“, Juli 2007).

14 Formayer, H., Kromp-Kolb, H., Schwarzl, I. (2009): **Auswirkungen des Klimawandels auf Hochwasserereignisse in Oberösterreich** (Endbericht Band 2 der Forschungsreihe „Auswirkungen des Klimawandels auf Oberösterreich“, Mai 2007).

15 Simic, S., Schmalwieser, A.W., Moshammer, H. (2009): **Gesundheitsrisiken für die österreichische Bevölkerung durch die Abnahme des stratosphärischen Ozons** (Endbericht StartClim2007.B, Juni 2008).

16 Formayer, H., Clementschitsch, L., Hofstätter, M., Kromp-Kolb, H. (2009): **Vor Sicht Klima! Klimawandel in Österreich, regional betrachtet** (Endbericht Global 2000, Mai 2008).

Berichte ab 2009

17 Eitzinger, J., Kubu, G. (eds.) (2009): **Impact of Climate Change and Adaptation in Agriculture** (Extended Abstracts of the International Symosium, University of Natural Resources and Applied Life Sciences (BOKU), Vienna, June 22-23 2009).

18 Formayer, H., Kromp-Kolb, H. (2009): **Klimawandel und Tourismus in Oberösterreich.**

19 Fleischhacker V., Formayer H., Seisser O., Wolf-Eberl S., Kromp-Kolb, H. (2009): **Auswirkungen des Klimawandels auf das künftige Reiseverhalten im österreichischen Tourismus.** (Forschungsbericht im Auftrag des Bundesministeriums für Wirtschaft, Familie und Jugend).

20 Seibert, P., Radanovics, R., Krüger, B. C. (2010): **Sources of Air Pollution Relevant for the Austrian Biosphere Reserve Wienerwald.** Final Report for the Project "Sources of Air Pollution Relevant for Austrian Biosphere Reserves: Quantification, Trends, Scenarios", Man and Biosphere Programme (MaB), Austrian Academy of Sciences (ÖAW).

Alle Berichte sind unter http://www.boku.ac.at/met/report/ online verfügbar.